USING THE ZEBRAFISH MODEL TO DETERMINE THE ROLE OF THE *HACE1* TUMOUR SUPPRESSOR IN NORMAL DEVELOPMENT AND TUMOURIGENESIS

by

Lindsay McDonald

Submitted in partial fulfillment of the requirements

for the degree of Master of Science

at

Dalhousie University

Halifax, Nova Scotia

June 2011

DALHOUSIE UNIVERSITY

MEDICAL SCIENCE GRADUATE PROGRAM

The undersigned hereby certify that they have read and recommend to the Faculty of Graduate Studies for acceptance a thesis entitled "USING THE ZEBRAFISH MODEL TO DETERMINE THE ROLE OF THE *HACE1* TUMOUR SUPPRESSOR IN NORMAL DEVELOPMENT AND TUMOURIGENESIS" by Lindsay McDonald in partial fulfillment of the requirements for the degree of Master of Science.

Dated: June 27, 2011

Supervisor: _____

Readers: _____

_____

_____

_____

Departmental Representative: _____

DALHOUSIE UNIVERSITY

DATE: June 27, 2011

AUTHOR: Lindsay McDonald

TITLE: USING THE ZEBRAFISH MODEL TO DETERMINE THE ROLE OF THE *HACE1* TUMOUR SUPPRESSOR IN NORMAL DEVELOPMENT AND TUMOURIGENESIS

DEPARTMENT OR SCHOOL: Medical Science Graduate Program

DEGREE: MSc CONVOCATION: May YEAR: 2012

_____

Signature of Author

TABLE OF CONTENTS

LIST OF TABLES vi
LIST OF FIGURES vii
ABSTRACT ix
LIST OF ABBREVIATIONS USED x
ACKNOWLEDGEMENTS xii
CHAPTER 1 INTRODUCTION 1
1.1 Pathogenesis of Cancer 1
1.2 Oncogenes and Tumour Suppressors 4
1.3 Cell Cycle 7
1.4 Apoptosis 11
1.5 Ubiquitin Ligases in Cancer 14
1.6 Wilms' Tumours 18
1.7 *HACE1* Tumour Suppressor 20
1.8 Zebrafish as a Model for Studying Human Cancers 22
1.9 Rationale 24
CHAPTER 2 MATERIALS AND METHODS 26
2.1 Zebrafish Maintenance and Embryo Staging 26
2.2 Generation of RNA Antisense Probes 26
2.3 Whole Mount RNA *in situ* Hybridization (WISH) 28
2.4 Morpholino Knockdown 29
2.5 RNA Extraction and Micro-Array 30
2.6 Generation of Transgenic Zebrafish Lines 31
2.6.1 Gateway Cloning 31
2.6.2 Establishment of Germline Integration 37
2.7 Apoptosis Assays 39
2.7.1 Acridine Orange Assay 39
2.7.2 Caspase 3 Assay 39
2.8 Cell Cycle Assays 40
2.8.1 BrDU Incorporation Assay 40
2.8.2 Phosphohistone H3 Assay 41

2.9 Adult Zebrafish Maintenance and Monitoring 42
2.10 Statistical Analysis 42
CHAPTER 3 RESULTS 43
3.1 Zebrafish *hace1* Expression 43
3.2 Morpholino Knockdown of zebrafish *hace1* Results in Abnormal Cardiac Development 46
3.3 Zebrafsih *hace1* Morphants Exhibit Altered Vascular Structure 51
3.4 Micro-Array Analysis of zebrafish *hace1* Morphants reveals Changes in Gene Expression 53
3.5 Transgenic Zebrafish Under Control of the zebrafish Ubiquitous β-Actin Promoter 55
3.6 Dominant Negative (*β-actin::GFPC876S*) Transgenic Zebrafish Demonstrate Increased Apoptosis 62
3.7 Effects of Loss of *HACE1* Function on Cell Cycle Progression 64
3.8 Transgenic Zebrafish Display Changes in Gene Expression by Micro-Array Analysis. 66
3.9 *β-actin::GFPhHACE1* and *β-actin::GFPC876S* transgenic Zebrafish Develop Masses and have Increased Mortality 70
CHAPTER 4 DISCUSSION 77
4.1 *HACE1* Expression is Conserved in Zebrafish 77
4.2 *HACE1* is Required for Cardiac Development 80
4.3 *HACE1* Affects Vasculature Development 84
4.4 *HACE1* Transgenic Zebrafish Provide a Model for Studying Cancer 86
4.5 Micro-Array Analysis Reveals Changes in Cell Cycle Genes and Developmental Genes 90
4.6 Conclusions 92
4.7 Future Directions 93
REFERENCES 96

LIST OF TABLES

Table 1: Summary of sacrificed adult *β-actin::GFPhHACE1* transgenic fish 73

Table 2: Summary of sacrificed adult *β-actin::GFPC876S* transgenic fish 74

LIST OF FIGURES

Figure 1: The Cell Cycle 8

Figure 2: Apoptosis 12

Figure 3: Ubiquitination Cascade 15

Figure 4: peGFP-C3-hHACE1 and peGFP-C3-C876S plasmids .. 32

Figure 5: pEC2-eGFP-4-4-Spe1-Rev middle entry clone 34

Figure 6: Gateway cloning of destination vectors 36

Figure 7: Establishment of the *HACE1* transgenic zebrafish line 38

Figure 8: Human *HACE1* and zebrafish *hace1* homology 44

Figure 9: Expression pattern of zebrafish *hace1* using probe to the ankyrin repeat domain 45

Figure 10: Expression pattern of zebrafish *hace1* using probe to the HECT domain 47

Figure 11: Co-localization of zebrafish *hace1* with tissue specific probes 48

Figure 12: Colocalization of *hace1* with tissue specific probes by double fluorescence whole mount *in situ* hybridization (WISH) 49

Figure 13: *hace1* morphants display abnormal cardiac development 52

Figure 14: *hace1* morphants display disorganized vasculature .. 54

Figure 15: Micro-array analysis of *hace1* morphants 56

Figure 16: Agarose gels confirming creation of Gateway destination vectors 60

Figure 17: Stable *HACE1* and dominant negative *HACE1* transgenic zebrafish lines 61

Figure 18: Dominant negative transgenic zebrafish show increased apoptosis 63

Figure 19: C876S mutants exhibit increased caspase 3 activation 65

Figure 20: Dominant negative transgenic zebrafish show no difference in S phase cell proliferation 67

Figure 21: Dominant negative transgenic zebrafish show no difference in G2/M phase 69

Figure 22: Micro-array analysis of transgenic zebrafish embryos 71

Figure 23: Dominant negative transgenic zebrafish develop masses at an early age 76

Figure 24: *hace1* morphants display a cardiac "looping defect" 83

ABSTRACT

HACE1 is a tumour suppressor gene located at human chromosome 6q21. *HACE1* is downregulated in Wilms' tumour as well as several other human cancers. Its role in normal development remains unknown. The zebrafish has established itself as a robust model for studying vertebrate development and human cancers. A zebrafish *hace1* homologue has been identified. Whole mount in situ hybridization (WISH) assays and colocalization studies demonstrate conserved *hace1* expression. Moreover, morpholino knockdown of *hace1* reveals perturbed cardiac development and function. Transgenic zebrafish harboring either wild type or dominant negative mutated C876S (C876S DN) human *HACE1* genes have been generated. DN zebrafish display increased apoptosis, both untreated and following irradiation-induced cellular damage. There was no difference in cell cycle progression between wild type embryos and C876S DN. Further characterization of the *HACE1* transgenic zebrafish model will serve to better our understanding of the role of human *HACE1* in normal development and tumourigenesis.

LIST OF ABBREVIATIONS USED

amhc	Atrial myosin heavy chain
APC	Adenomatous polyposis coli
BCIP	5-Bromo-4-chloro-3-indolyl phosphate, toluidine salt
BMB	Boehringer Mannheim Blocking Reagent
BRAF	Serine/threonine-protein kinase
BrDU	5-Bromo-2'-deoxyuridine
cdh17	Cadherin-17
CDK	Cyclin dependent kinase
CDKI	Cyclin dependent kinase inhibitor
CIP	CDK interacting protein
cmlc2	Cardiac myosin light chain 2
CNS	Central nervous system
CoDA	Context-dependent assembly
COG	Children's Oncology Group
cpa5	carboxypeptidase A5
DIG	Digoxigenin
DISC	Death inducing signaling complex
DMSO	Dimethyl sulfoxide
DN	Dominant negative
dpf	Days post fertilization
DN	Dominant negative
EDTA	Ethylenediaminetetraacetic acid
EMT	Epithelial-mesenchymal-transition
ER	Endoplasmic reticulum
FADD	Fas associated death domain
Fas-L	Fas ligand
FBS	Fetal bovine serum
FGF	Fibroblast growth factor
FITC	Fluorescein isothiocyanate
fli1	Friend leukemia integration 1 transcription factor
gamt	Guanidinoacetate N-methyltransferase
GFP	Green fluorescent protein
Gy	Gray
H&E	Hematoxylin and eosin stain
HACE1	HECT domain and ankyrin repeat containing E3 ubiquitin protein ligase
HECT	Homologous to the E6-AP carboxyl terminus
HGF	Hepatocyte growth factor
hpf	Hours post fertilization
HPV	Human papilloma virus
IGF	Insulin-like growth factor
JNK	c-Jun NH_2-terminal kinase
KIP	Kinase inhibitory protein
krox20	Early growth response 2

MAPK	Mitogen-activated protein kinase
NBT	Nitro blue tetrazolium chloride
NIH	National Institutes of health
nppa	natriuretic peptide precursor A
NWTS	National Wilms Tumour Study
P53	Protein 53
PBS	Phosphate buffered saline
PBST	PBS with Tween 20
PDGF	Platelet-derived growth factor
PDT	1% DMSO, 0.3% Triton X in PBST
PFA	Paraformaldehyde
PH3	Phosphohistone H3
PTEN	Phosphatase and tensin homolog
PTU	Phenylthiouracil
R	Restriction point
RB	Retinoblastoma protein
RLD	Ring-finger-like domain
RQI	RNA quality indices
SSCT	Saline sodium citrate buffer with Tween 20
tbx2b	T-box 2b
TGF-β	Transforming growth factor beta
TNF	Tumour necrosis factor
TSP-1	Thrombospondin 1
Tyr	Tyrosine
UPR	Unfolded protein response
VEGF	Vascular endothelial growth factor
vmhc	Ventricular myosin heavy chain
WISH	Whole mount *in situ* hybridization
WT1	Wilms tumour 1
WTX	Wilms tumour suppressor X
WW	tryptophan-tryptophan
ywhag1	3-monooxygenase/tryptophan 5-monooxygenase activation protein
ZFN	Zinc finger
ZV8	Zebrafish genome 8th Assembly
ZV9	Zebrafish genome 9th Assembly

ACKNOWLEDGEMENTS

First and foremost, I would like to thank Dr. Jason Berman for his direction and knowledge over the past two years. His daily enthusiasm and encouragement were extremely valuable throughout the completion of this Master's thesis. I wish to express my gratitude to my co-supervisor, Dr. Mark Walsh, for his continuous support and guidance. I would like to thank the members of my committee, Dr. David Hoskin, Dr. Craig McCormick, and Dr. Poul Sorensen for their advice and assistance throughout this research project.

I would especially like to express my appreciation to Sahar Da'as for her continued patience and assistance. Thank you to Andrew Coombs and Angela Young for the excellent fish care and husbandry. Thank you to the members of the Berman Laboratory, who have contributed immensely to my personal and professional experience.

I would like to thank Dr. Ian Scott from the University of Toronto for his collaboration with the morpholino studies, as well as Dr. Stephen Lewis for performing the micro-array experiments.

CHAPTER 1 INTRODUCTION

1.1 PATHOGENESIS OF CANCER

Cancer is a group of diseases characterized by uncontrolled cell proliferation, invasion into adjacent tissue, and the ability to metastasize to distant locations in the body. In 2000, Hanahan and Weinberg proposed six hallmarks of cancer that contribute to the transformation of normal cells into malignant cells[1]. These include sustaining proliferative signaling, resisting cell death, evading growth suppressors, activating invasion and metastasis, enabling replicative immortality, and inducing angiogenesis. Recently, avoiding immune destruction and deregulating cellular energetics have been suggested as two new hallmarks involved in the development of cancer[2]. Critical to the hallmarks described by Hanahan and Weinberg is the underlying concept of genomic instability, which refers to the tendency of acquiring alterations in the genome during the life of a cell. Recently, there has been a large interest in the tumour microenvironment and its interaction with cancer cells. This highly specific relationship between tumours and their supporting tissue is crucial for cancer phenotypes and growth. These cancer hallmarks serve as a framework by which research is targeted, as they represent mechanisms that evade normal cellular growth signaling and proliferation. Furthermore, these biological pathways may provide specific targets for therapies. Although many advances have been made in the past decade in cancer research, there remain many unanswered questions.

Fundamental to the maintenance of cancer cells and tumour growth is the ability of cells to display increased proliferation. Normally, cells are tightly regulated by growth

factors, providing stimulatory signaling, and apoptosis or programmed cell death, thereby providing a proper balance of cell number. During malignant transformation, this regulation is lost, and cancer cells receive continued proliferative signaling[3].

Cancer is a multistep disease process that usually occurs over decades. In pediatric cancers, this timeline is usually shorter, and genetic mutations may arise *in utero.* It is possible that fewer mutations in key genes are required to develop tumours. The incidence of some childhood cancers have been shown to follow a two mutation hypothesis[4]. The underlying basis of cell transformation lies in the accumulation of genetic alterations that lead to the dysregulated cell proliferation and increased cell survival. These genetic mutations may be familial and passed on from generation to generation, or may be accumulated in a sporadic manner. DNA sequencing has identified numerous somatic mutations that lead to activation of signaling pathways, for example, the MAP-kinase and PI3 kinase pathways[2]. Genetic modifications in a multitude of cancers, including lung cancer, esophageal cancer and cholangiocarcinoma, occur through epigenetic switches that result in alterations in gene expression, rather than a mutation in the DNA sequence[5-7].

Cells and tissue require adequate blood supply and nutrients for survival and proliferation. Angiogenesis is the physiologic process by which new blood vessels are generated from old blood vessels. This tightly regulated process is essential during development, as it provides the framework of vessels that are required to supply normal tissue. However, during tumour growth, a pro-angiogenic signal is activated and persists, leading to continued formation of new vasculature. This activation of angiogenesis occurs very early in the development of malignancy, as histologic examination of tissues

with dysplasia and carcinoma *in situ* have shown evidence of angiogenesis. This is an integral part of tumour progression, as newly formed blood vessels provide essential blood flow to the expanding neoplasm[8]. The newly formed blood vessels display abnormal morphology, marked by excessive irregular branching[9]. Key mediators of angiogenesis include vascular endothelial growth factor (VEGF), platelet derived growth factor (PDGF), fibroblast growth factor (FGF), and their receptor tyrosine kinases[2,10,11]. Intrinsic anti-angiogenic factors include thrombospondin-1 (TSP-1)[2]. During tumour maintenance, there is a shift in this pro- and anti-angiogenic signaling, allowing for persistent angiogenesis. Angiogenesis has been studied as a potential target of chemotherapeutic agents, with the first anti-VEGF antibody Bevacizumab being approved for use in metastatic colorectal cancer, breast cancer, lung cancer and gliomas[12].

Ultimately, tumours invade adjacent tissue, and malignant cells disseminate to distant organs throughout the body. This multistep process has been termed the invasion-metastasis cascade, and consists of local invasion, intravasation of tumour cells into blood vessels and lymphatics, escape of cancer cells from lymphatic and blood vessels, and formation of micrometastases[13]. It is through the process of epithelial-mesenchymal transition (EMT) that transformed cells acquire the ability to invade and metastasize. A critical component of EMT involves the loss of the cell-cell adhesion molecule E-cadherin, which may occur via gene mutations, transcriptional repression and hypermethylation of E-cadherin[14]. There are a number of transcription factors that lead to loss of E-cadherin, including transcription growth factor β (TGF−β), hepatocyte growth factor (HGF) and insulin-like growth factor (IGF)[15-17].

Cancer causes a significant burden on patients and families. When diagnosed at an early stage, some cancers may be resected with a resultant cure of disease. However, more advanced cancers may metastasize to distant sites within the body. A diagnosis of metastatic cancer is often followed by palliative treatment, and cure of disease is unlikely. Metastases account for approximately 90% of cancer deaths[18]. Chemotherapeutic agents are commonly used as an adjunct to surgery in the treatment of solid tumours, either as neoadjuvant or adjuvant therapy. An understanding of the genetic basis, and modulation of signaling pathways involved in specific cancers allows for the generation of targeted therapies that will ultimately improve survival outcomes.

1.2 Oncogenes and Tumour Suppressors

Cancer is a genetic disease, regulated by oncogenes and tumour suppressor genes. Proto-oncogenes are genes, that when mutated, result in the formation of oncogenes that have the ability to cause cellular transformation. Activation of a proto-oncogene into an oncogene usually results from a gain of function mutation, which may occur by a point mutation, gene overexpression, or a chromosome translocation. It has been 100 years since Peyton Rous suggested that it as possible induce solid tumours by a transferable agent[19]. This led to the discovery of the first oncogene, *src*, in a chicken retrovirus, sparking an area of research that had led to the identification of many other oncogenes involved in the development of cancer, as well as a heightened understanding of cancer biology[20].

Alternatively, tumour suppressor genes are those genes that, when normally expressed, act to inhibit cell proliferation. Unlike oncogenes where a single allele mutation is necessary for cellular transformation, it was thought that tumour suppressor genes generally required a mutation in both gene alleles for a resultant malignant effect. However, more recently, it has been shown that this is not always required. In diploid organisms, other than genes located on the X and Y chromosome, there are two functional alleles. For many genes, a single allele is sufficient for normal gene function. However, other genes require two functional gene alleles. Haploinsuffiency is when a single gene copy is insufficient to carry out the normal activity of the gene. p27 is a cyclin-dependent kinase involved in the progression from G1 to S phase of the cell cycle. Murine studies established p27 as a tumour suppressor protein[21]. In 1998, Fero *et al.* demonstrated that the cyclin-dependent kinase p27 is haploinsufficient for tumour suppression[22]. Since 1998, other tumour suppressor genes have been identified which function in a similar haploinsuffient fashion. For example, *E-cadherin* (involved in familial gastric cancer) and *APC* (mutated in familial adenomatous polyposis) are implicated in familial cancer syndromes as well as sporadic malignancies[23]. Tumour suppressors also result in cancer in the presence of a dominant negative mutation. Dominant negative mutations occur when a mutated allele acts antagonistically on the wildtype allele, thereby resulting in a loss of function. The *WT1* tumour suppressor, when present as a germline mutation, can lead to Denys-Drash syndrome, characterized by severe abnormalities in renal and sexual differentiation, as well as an increased incidence of Wilms' tumours. A dominant negative mutation at codon 394 is responsible for this phenotype[24]. Two other important tumour suppressors in human cancers are

retinoblastoma (RB), and TP53. The RB protein functions at the G1 to S phase checkpoint of the cell cycle. Cells with defects in the RB pathway lose this critical function, resulting in aberrant persistent progression through the cell cycle. Ultimately, this dysregulated proliferation results in tumour formation. The p53 tumour suppressor is mutated in approximately 50% of human cancers[25]. Human p53 is 393 amino acids long and possesses five domains[26]. It is regulated at the protein level by ubiquitination by MDM2, which targets p53 for degradation by the proteasome[27]. This tight regulation keeps p53 levels low in normal, unstressed cells, allowing for normal cell cycle progression. p53 normally functions to initiate apoptosis, senescence and cell cycle arrest in response to a number of stimuli. These include, but are not limited to, oncogene activation, DNA damage (induced by ultraviolet radiation, ionizing radiation, or chemical agents), and oxidative stress[27]. The majority of the mutations affecting p53 result from missense mutations located within its DNA binding domain[28]. These mutations can confer dominant negative effects on wild type p53, as has been shown using a mouse model of pancreatic adenocarcinoma[29]. Furthermore, mutant p53 results in gain of function properties. Transfection of mutant p53 into cell lines lacking endogenous p53 resulted in increased agar colony formation, as well as increased tumourigenicity in nude mice[30]. Mutations in p53 alter the fine balance required to maintain normal cell cycle progression, giving rise to dysregulated cell proliferation. *HACE1* is a novel tumour suppressor that was identified in a Wilms' tumour (see below)[31]. It has been associated with a variety of human cancers, and thus represents a potential target in cancer research. The accumulation of genetic mutations in oncogenes and tumour suppressor genes lead to

malignant transformation and tumour maintenance. Understanding how these mutations result in malignancy is crucial in developing potential cancer therapies.

1.3 CELL CYCLE

Normally, proliferating cells undergo a regulated series of events that include DNA synthesis, mitosis, and gap phases. Collectively, these events are referred to as the cell cycle (Figure 1). It is important to understand the molecular mechanisms that result in cell progression through the cell cycle, and how these signals are altered in malignant cells. The cell cycle consists of four distinct phases: G1 phase, S phase, G2 phase and mitosis. Many cells that are not actively dividing enter a senescent/quiescent state termed Go. When exposed to mitogenic signaling, senescent cells may enter back into G1, and progress through the cell cycle. In order to maintain normal cell cycle progression, there are a number of checkpoints. The primary checkpoint occurs at the G1/S phase transition, and is termed the restriction point (R). Once cells have passed the restriction point, they are committed to complete the cell cycle, and undergo mitotic cell division[32]. Additional checkpoints occur during S phase to ensure that DNA is properly replicated, and initiate DNA repair mechanisms, if necessary. There exists a checkpoint at the G2/M phase transition, which confirms that DNA replication has been completed, as well as further checkpoint mechanisms that occur during mitosis. Progression through each phase of the cell cycle depends on an intricate network of signaling by cyclins, cyclin-dependent kinases (CDKs) and CDK inhibitors[33]. Cyclins are a family of proteins that control progression through the cell cycle by binding and activating CDKs. They were

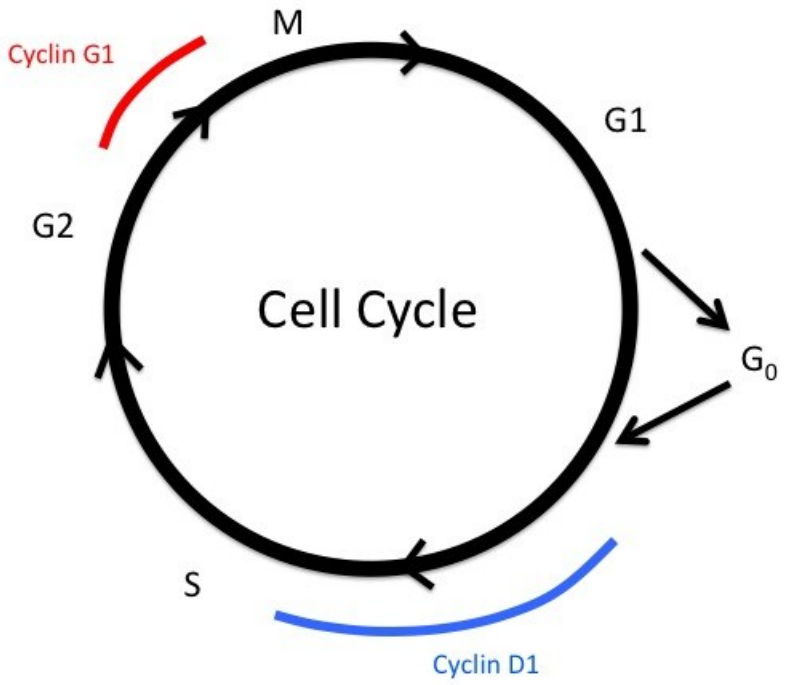

Figure 1: The Cell Cycle.
Cells progress through a cycle consisting of four phases of growth and division: G1, S, G2, and M phase. Cells may temporarily enter a quiescent phase (Go). Cell cycle progression is tightly controlled by numerous cyclins, cyclin dependent kinases, and cyclin dependent kinase inhibitors. Cyclin D1 is involved in progression from G1 to S phase. Cyclin G1 may be involved in G2/M phase arrest.

first identified by R. Timothy Hunt in 1982 while studying sea urchins[34]. To date, eight cyclins have been identified that act on various points throughout the cell cycle. Cyclins A through H share an approximately 150 amino acid conserved domain named the cyclin box, which is responsible for binding the N terminus of CDKs. Cyclin levels are altered through a balance of gene expression and proteolysis, thereby coordinating essential cell cycle signaling. CDKs are serine-threonine protein kinases, which when associated with cyclins, phosphorylate target proteins and allow progression through the cell cycle. Unlike cyclins, CDK levels remain relatively constant throughout the cell cycle[35].

Specific cyclin-CDK complexes are required for appropriate transition from one phase of the cell cycle to the next. For example, cyclin D associated with CDK4 or CDK6 and the cyclin E–CDK2 complex regulate the G1/S phase transition. These kinases phosphorylate members of the retinoblastoma family of proteins (Rb). In its hypophosphorylated state, Rb is bound to and inhibits transcription factors in the E2F family, which results in G1 phase arrest[36]. Once Rb is phosphorylated, liberation of E2F leads to transcription of cyclin E and CDC25A, which is essential for progression through the restriction point and entry into S phase of the cell cycle[37,38]. The Ras / mitogen activated protein kinase (MAPK) pathway is tightly involved with G1/S phase transition, as it has been shown to directly influence expression of cyclin D[39]. During DNA replication in S phase, there are a variety of checkpoints inhibit DNA replication in response to DNA damage. This allows the cell to repair the damage prior to proceeding to the G2 phase. Several proteins are thought to be involved in the DNA damage response, including ATM, ATR, DNA-PK, and the downstream target p53[35]. G2/M phase transition is regulated by the cyclin B – CDK1 complex. This complex remains in

its inactive phosphorylated form by phosphorylation of CDK1 at tyrosine (Tyr) 14 and Tyr 15. This important complex is activated by dephosphorylation by CDC25C[40,41].

Stimulatory cell cycle signaling by cyclins and CDKs is opposed by CDK inhibitors. These CDK inhibitors belong to two distinct families: the INK4 (inhibitor of CDK4) and CIP (CDK-interacting protein)/KIP (kinase inhibitor protein) families[42]. The INK4 family consists of p14, p15 (INK4B), p16 (INK4A), p18 (INK4C), and p19 (INK4D), which specifically inhibit G1 cyclin/CDK complexes. The CIP/KIP family includes p21 (CIP1/WAF1/SDI1), p27 (KIP1), and p57 (KIP2) proteins. Additional inhibitory signaling can be provided by the tumour suppressor p53. In response to DNA damage, p53 can upregulate expression of p21, thus inhibiting cyclin – CDK complexes and resulting in G1 arrest[43].

With the complex signaling required for cells to divide normally, there are multiple opportunities for the cell cycle to become dysregulated. A number of the important genes required for correct cell cycle checkpoint control are mutated or have altered expression in various human cancers. For example, there is decreased expression of p27 and increased expression of cyclin D1 in some breast cancers[44]. Both intrinsic and extrinsic stimuli are involved in the transformation of normal cells to malignant cells via DNA damage. Normally, the DNA damage response initiates programmed cell death, inhibiting the replication of abnormal cells. However, in the face of a mutated gene involved in apoptosis or cell cycle checkpoint control, cells with genetic abnormalities survive and proliferate.

1.4 APOPTOSIS

Apoptosis is an evolutionarily conserved process resulting in programmed cell death (Figure 2). The word apoptosis is derived from the Greek word that suggests "leaves falling off a tree". It was first reported by Kerr in 1972, and has since been recognized as a key component of malignancy[45]. In contrast to cell death by necrosis, which is characterized by increased cell volume, swelling of organelles, and ultimately cell lysis with associated inflammation, apoptosis results in a controlled non-inflammatory form of cell death[46]. Cell death by apoptosis is essential during organogenesis, and is a means by which the adult organism selectively kills cells to maintain cellular homeostasis.

There are three major pathways that mediate apoptosis: the extrinsic pathway, the intrinsic pathway and the endoplasmic reticulum stress response. The intrinsic and extrinsic pathways converge with the common effectors of apoptosis: the caspases. Caspases are a family of cysteine-aspartic proteases that are executors of apoptosis. Caspases are translated in an inactive precursor form, and are activated by cleavage in the cytoplasm or nucleus or by dimerization by an adaptor molecule[47,48]. Caspases are subclassified into initiator caspases-2, -8, -9, 10, and apoptosis executor caspases-3, -6, -7[49].

The extrinsic pathway, also called the death receptor pathway, functions through members of the tumour necrosis factor (TNF) superfamily. For example, a complex forms between Fas and Fas ligand (Fas-L), which in turn recruits Fas associated death domain (FADD) and procaspase-8, generating the death inducing signaling complex

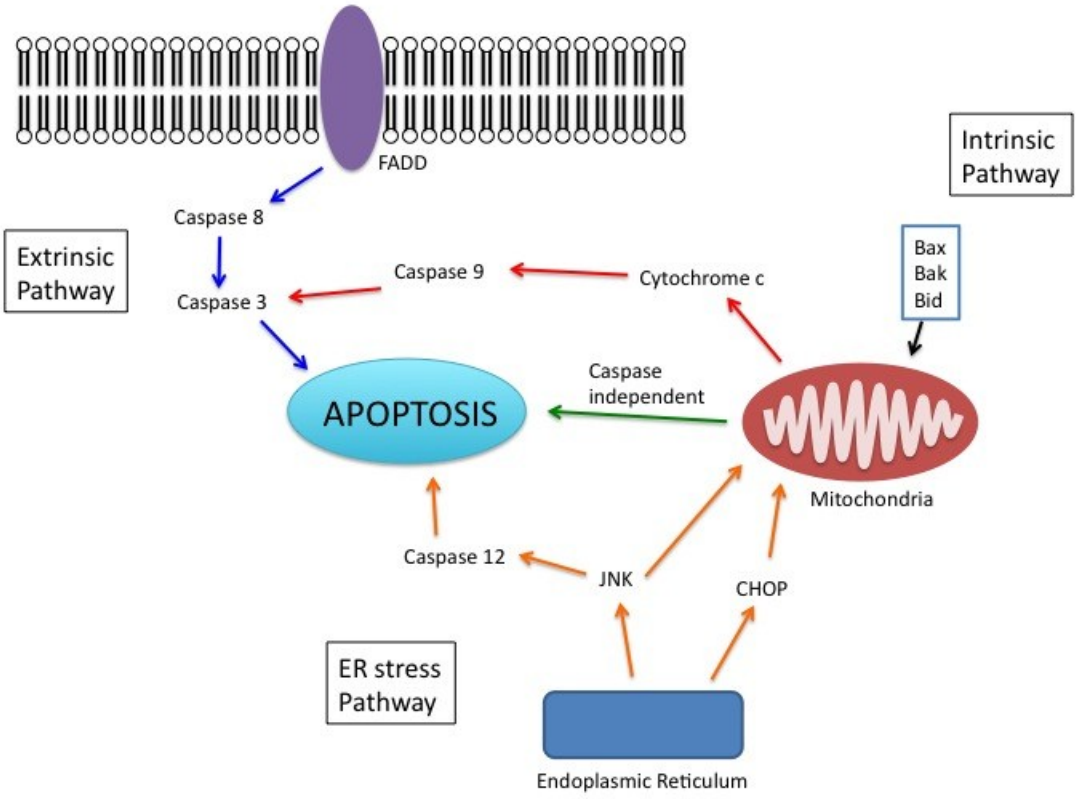

Figure 2: Apoptosis.
Schematic representation of the molecular mechanisms of apoptosis. Apoptosis is initiated via the intrinsic pathway, the extrinsic pathway or the endoplasmic reticulum (ER) stress pathway. The extrinsic pathway (death receptor pathway) commences when the Fas associated death domain (FADD) is recruited by a complex formed between Fas and Fas ligand (Fas-L). This initiates a cascade ultimately culminating in activation of effector caspases 8 and 3, leading to cell death. The intrinsic pathway involves release of cytochrome-c from the mitochondrion, occurring in response to stimulation by pro-apoptotic members of the Bcl-2 family (Bax, Bak, Bid). Cytochrome-c results in activation of caspase-9 and caspase-3. The intrinsic pathway also results in apoptosis through a caspase-independent mechanism. The ER stress pathway leads to apoptosis via accumulation of misfolded proteins in the ER. The unfolded protein response activates JNK and CHOP. The ER stress pathway functions in combination with the mitochondrial pathway, or by activation of caspase-12. Programmed cell death via these three pathways occurs following chromatin condensation, nuclear fragmentation, membrane blebbing, or cytoskeletal rearrangement.

(DISC)[50]. Subsequently, caspase-3 is activated and results in DNA fragmentation, nuclear fragmentation and membrane blebbing[51].

The intrinsic apoptotic pathway is regulated by the mitochondrion. When exposed to a stress, members of the Bcl-2 family, such as Bax, Bak, and Bid, act on the mitochondria, causing its membrane to become permeable and release cytochrome-c[51-53]. The release of cytochrome-c recruits Apaf-1 and procaspase-9, forming the apoptosome and initiating a signaling cascade by which caspase-9 and caspase-3 activation results in apoptotic cell death[49].

The endoplasmic reticulum (ER) is an intracellular organelle involved in calcium storage, protein folding and secretion, and lipid biogenesis[54]. Misfolded proteins can accumulate in the ER for a variety of reasons (i.e. point mutations). This results in activation of the unfolded protein response (UPR), mediated by three transmembrane proteins: IRE1α, PERK and ATF6, in the attempt of restoring cellular homeostasis[54]. When the ER stress is such that the UPR is overwhelmed, the UPR promotes apoptosis. Apoptosis initiated by the ER stress pathway occurs in conjunction with the mitochondrial pathway, as well as independently. PERK signaling induces the CHOP transcription factor, which inhibits the anti-apoptotic Bcl-2, and induces ER oxidation[55]. Phosphorylation of JNK by IRE1α leads to activation of the pro-apoptotic protein Bim, and inhibition of the anti-apoptotic Bcl-2[54]. JNK can also initiate apoptosis by activation of caspase 12[56].

The initiation of apoptosis is highly regulated, and activation of apoptotic pathways occurs only when cell death is indicated. There are multiple stimuli, both internal and environmental that lead to apoptosis. Apoptosis can be triggered by DNA damage,

oxidative stress, treatment with cytotoxic drugs, and irradiation. One of the hallmarks of cancer is the cell's ability to evade apoptosis. The crucial regulation of apoptosis is maintained by pro-apoptotic and anti-apoptotic signaling. This signaling occurs throughmembers of the Bcl-2 family of proteins. There is normally a balance between pro-apoptotic proteins (Bax and Bak) and anti-apoptotic proteins (Bcl-X_L, Bcl-w, Mcl-1, A1)[57]. During malignant transformation, there exist many mechanisms by which tumour cells resist apoptosis, and thereby increase cell survival. This may occur by upregulation of anti-apoptotic regulators, or downregulation of pro-apoptotic proteins. Examination of these key molecules in the apoptotic pathways will provide an understanding of how genetic alterations in specific cancers lead to increased cell survival. The highly specific pathway of ubiquitination is one mechanism by which apoptosis can be triggered.

1.5 Ubiquitin Ligases in Cancer

Ubiquitination is the ordered cascade by which an isopeptide bond is formed between the C terminal glycine of ubiquitin and a lysine residue of the substrate. Protein ubiquitination leads to numerous outcomes, including protein degradation, endocytosis, and apoptosis[58]. The sequence of events involved in ubiquitination begins with the ATP dependent activation of an E1 ubiquitin-activating enzyme that binds to ubiquitin through a thioester bond. Ubiquitin is then transferred to an E2 ubiquitin-conjugating enzyme. Ultimately, the E3 ubiquitin ligase facilitates the transfer of ubiquitin to the final substrate lysine residue (Figure 3). There are approximately 30-50 E2 enzymes and greater than 1000 E3 enzymes identified in the human genome[59]. Therefore, it is E3

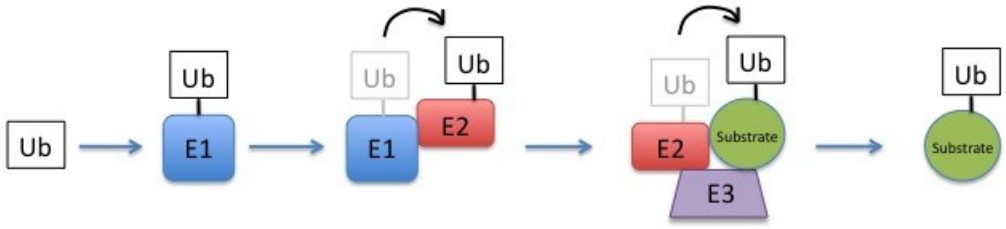

Figure 3: Ubiquitination Cascade.
Schematic representation of the ubiquitination cascade. Ubiquitin is transferred to a protein substrate through a multistep process involving the formation of a thioester bond between ubiquitin and an ubiquitin-activating enzyme (E1). The activated ubiquitin is then transferred to an ubiquitin-conjugating enzyme (E2). Ubiquitin is then transferred to a lysine residue on the protein substrate via an ubiquitin ligase (E3).

ubiquitin ligases that are responsible for the high degree of specificity within the ubiquitination process. E3 ubiquitin ligases are subdivided by their functional catalytic domains, of which there exist two major classes. The RING type of E3 ubiquitin ligase features a scaffold that brings the partner E2 near the substrate, and facilitates transfer of the ubiquitin molecule. HECT domains on the other hand possess a conserved cysteine residue that is required to form an intermediate thioester bond prior to catalyzing the transfer of ubiquitin to its substrate. The majority of the ubiquitin ligases belong to the RING type, leaving only 28 identified ubiquitin ligases with HECT domains[60].

The specificity of E3 ubiquitin ligases depends on protein-protein interaction domains, which classifies them into three subfamilies. These domains include the RCC1-like domain (RLDs), the tryptophan-tryptophan (WW) domain, and those proteins lacking either RLDs or WW domains[61]. The HECT family of ubiquitin ligases has been associated with the development of human malignancy. For example, E6-AP is the most studied HECT domain ubiquitin ligase. It exerts its oncogenic potential through binding with the adaptor human papillomavirus (HPV) viral oncoprotein E6 and with the tumour suppressor p53. E6-AP catalyzes ubiquitination of p53, leading to its degradation by the 26S proteasome[62]. Increased degradation of p53 results in loss of growth regulation, thereby leading to increased proliferative signaling. The E6-AP E3 ubiquitin ligase is involved in the development of approximately 90% of human cervical carcinomas [63]. *Huwe1* is involved with cellular transformation by ubiquitination of Cdc6, histones, c-Myc and p53[63]. There has been some controversy surrounding this E3 ubiquitin ligase and the onset of cancer, as it has been suggested that *Huwe1*-dependent ubiquitination of Mcl-1 or p53 results in either increased survival or increased apoptosis[64,65]. *Huwe1* is

highly expressed in lung and breast carcinomas. Its overexpression has also been linked to colorectal carcinoma[63]. Another important E3 ubiquitin ligase thought to be involved in malignant phenotypes is NEDD4. The NEDD4 E3 ubiquitin ligase interacts with the phosphatase and tensin homologue (PTEN) tumour suppressor, leading to its ubiquitination. The *PTEN* protein acts as a phosphatase that dephosphorylates phosphatidylinositol (3,4,5)-triphosphate. This dephosphorylation results in inhibition of the AKT survival signaling. There remains controversy regarding the mechanism by which NEDD4 results in increased cell survival, as its effect on PTEN failed to be replicated in *in vivo* studies[66]. NEDD4, however, is still thought to act as a proto-oncogene and has been found to be overexpressed in many human bladder and prostate carcinomas[67].

One of the end results of ubiquitination is protein degradation by the 26S proteasome. The ubiquitin-proteasome system is crucial for proper cell cycle control. As such, the proteasome has been pursued as a potential chemotherapeutic target in the treatment of cancer. Proteasome inhibitors tend to induce apoptosis in proliferating cells, thereby selectively inducing cell death signaling in transformed cells compared to quiescent cells. There are a variety of mechanisms by which these inhibitors function. For example, in HPV-related cancers, p53 is inactivated by proteasomal degradation. By inhibiting the proteasome, p53 levels are restored and growth arrest or apoptosis ensues[68]. Additional mechanisms include accumulation of p21 and p27, both of which regulate cell cycle progression at G1. Proteasome inhibitors are currently used as chemotherapeutic agents, with Bortezomib being the first of this category of drugs to be approved by the Food and Drug Administration for use in multiple myeloma (Millenium Pharmaceuticals,

2008). Because the 26S proteasome is the end effector in the ubiquitin-proteasome system, its inhibition may result in off target effects. More precise inhibition could be accomplished by generating molecules that are directed towards ubiquitin ligases, as they provide a high degree of specificity in the ubiquitination process.

1.6 WILMS' TUMOURS

Wilms' tumours (nephroblastoma) are childhood embryonic tumours of the kidney. Wilms' tumours account for greater than 90% of pediatric kidney tumours, and 6% of all pediatric cancers[69]. In the United States, it is estimated that there are approximately 500 new cases diagnosed each year[70]. Wilm's tumour is commonly a disease of early childhood with 75% of cases being diagnosed in children younger than five years of age, with a peak incidence at 2-3 years of age[71]. The most common presentation is a palpable abdominal mass. Survival rates of children diagnosed with Wilms' tumours was previously dismal, reaching approximately 30% . However, Wilms' tumours are now much more treatable, with survival rates reaching 90%[71]. The treatment of Wilms' tumours is multidisciplinary. Surgery is paramount in the management of Wilms' tumours. In addition, the use of chemotherapeutic agents, as well as radiation therapy has greatly improved survival. Because Wilms' tumours are relatively rare, information regarding appropriate treatment regimens was limited until the formation of the National Wilms' Tumour Study (NWTS). The NWTS was amalgamated with a number of other clinical trial groups, including the Pediatric Oncology Group and the Children's Cancer Group into the Children's Oncology Group (COG) in 2001. The COG currently

recommends nephrectomy followed by histologic diagnosis prior to initiation of therapy. Although a tremendous amount of information has been gained about the biology of Wilms' tumours, the staging of Wilms' tumours continues to rely on the anatomic extension of disease with unilateral disease classified as stage I-IV and bilateral disease as stage V[72]. In North America, chemotherapy regimens are commenced following tissue diagnosis. Through the efforts of the NWTS, five studies have been published and have contributed to current chemotherapy and radiation regimens[73-79].

The histology of Wilm's tumours suggests a disorganized and incomplete development of the kidney[80]. It has been suggested that Wilms' tumours arise from a transformation event in renal stem cells[81,82]. This concept is supported by micro-array analyses, which have identified gene profiles in Wilms' tumours that are similar to those gene profiles found in fetal kidneys, and more specifically the earliest commited stage in the metanephric mesencymal-epithelial transition[83,84].

Molecular analysis of Wilms' tumours has led to the discovery of genes that are involved in its development. Four genes in which mutations are associated with onset of Wilms' tumours include Wilms' tumour 1 (*WT1*), Wilms' tumour gene on the X chromosome (*WTX*), β-catenin, and *TP53*. The *WT1* gene encodes a zinc finger transcription factor that is involved in normal renal development. *WT1* is expressed early in nephrogenesis, and shows continued expression in the mature kidney[85]. The *WT1* gene functions as a tumour suppressor, and transformation of normal kidney cells to malignant Wilms' tumours has been observed with deletions, insertions, and missense mutations[86,87]. The *WTX* gene is mutated in approximately 20% of Wilms' tumours, and encodes a protein that negatively regulates the Wnt pathway. Missense mutations in the

tumour suppressor p53 have also been reported in anaplastic Wilms' tumours and confer a poor prognosis[80]. The *HACE1* tumour suppressor recently joined this list of genes that are associated with the development of Wilms' tumours.

1.7 *HACE1* TUMOUR SUPPRESSOR

HACE1 is a novel tumour suppressor gene located at human chromosome 6q21 that was originally identified by the Sorensen lab at the University of British Columbia in a Wilms' tumour from a 5 month old male diagnosed and treated at the IWK Health Centre in Halifax[31,88]. *HACE1* was discovered by mapping a t(6;15)(q21;q21) translocation in the index Wilms' tumour. The *HACE1* gene encodes a 909 amino acid protein that possesses two important domains. The first domain of interest is an ankyrin repeat domain containing 6 ankyrin repeats. The catalytically active HECT domain is located at the C-terminal end of the protein. *HACE1* possesses ubiquitin ligase activity *in vitro* and *in vivo. In vitro* studies have identified UbcH7 as a partner E2 enzyme[31]. HECT family E3 ligases contain a critical cysteine residue necessary for thioester bond formation. The *HACE1* critical cysteine residue is located at amino acid 876. A mutation at this critical cysteine residue abolishes ubiquitin ligase activity *in* vitro[31]. *HACE1* appears to localize predominantly to the cytoplasm and, more specifically, the outer endoplasmic reticulum, and is thought to be involved in both ubiquitination and protein degradation itself [31].

When comparing Wilms' tumour samples to patient-matched normal kidney tissue, the level of *HACE1* expression at both mRNA and protein levels was downregulated in

>75% of Wilms' tumours[89]. *HACE1* is widely expressed in human tissues. In particular, there is strong expression of *HACE1* in heart, brain and kidney[89].

HACE1 is downregulated in a variety of human cancers, including Wilms' tumours[89], melanoma, breast cancer, lung cancer, lymphoma and colon cancer, and thus represents an exciting and potentially broadly applicable genetic target[89-91]. There are no identified mutations or deletions in *HACE1* that lead to its loss of function, rather it appears that there is an epigenetic inactivation of the gene resulting in significant downregulation of its expression. CpG islands are regions within DNA sequence that contain a high proportion of cytosine next to a guanosine nucleotides. CpG islands have a tendency to occur near the start site of a gene. Hyper- or hypo-methylation of CpG islands may alter gene expression levels. There are three upstream CpG islands associated with *HACE1*. There are two located approximately 50 kb upstream of the transcriptional start site (CpG-177 and CpG29). The third is CpG-88 which is located within the *HACE1* promoter and extends into the first exon. When comparing Wilms' tumour tissue to normal kidney tissue, there is increased methylation at CpG-177[89].

Hace1-/- mice spontaneously develop a similar multitude of tumour types at rates higher than their littermate controls. This tumour development can be accelerated by DNA damaging agents or other environmental stressors, suggesting that the absence of *HACE1* protein predisposes cells to future genetic oncogenic "hits"[89].

p53 is a well known tumour suppressor that is mutated in approximately 50% of human cancers[92]. Mouse studies have implicated mutant p53 in *HACE1*-dependent tumour formation. In *Hace1-/-* mice, tumour incidence was greatly increased with a heterozygous loss of p53. Moreover, the size of tumours was significantly larger.

Although loss of p53 on its own increases tumour incidence, these tumours were primarily thymic lymphomas. Loss of *HACE1* resulted in a wider array of malignancies, suggesting a collaborating role between *HACE1* and p53[89].

The role of *HACE1* in cell cycle progression and cellular proliferation remains currently unknown. *HACE1* overexpression in HEK293 cells results in a significant reduction in cyclin D1, which is a protein involved in the G1/S phase transition of the cell cycle. This decrease in cyclin D1 occurs through proteasomal degradation by the 26S proteasome. Therefore, *HACE1* may slow cell cycle progression via degredation of cyclin D1, supporting its role as a tumour suppressor [89]. A significant decrease in *HACE1* may therefore lead to overproliferation by loss of regulation at this cell cycle checkpoint.

1.8 Zebrafish as a Model for Studying Human Cancers

The zebrafish (*Danio rerio*) has been used as a model to study vertebrate developmental biology since the 1960s, and has more recently emerged as an important model in cancer research[93-96]. Advantages of the zebrafish include its high level of genetic conservation with mammals (approximately 85%), rapid embryonic development, and transparency of embryos allowing direct visualization of tissue formation and organogenesis[97]. As well, the entire zebrafish genome has been sequenced, and is now in its ninth assembly (ZV9, Sanger Institute, Hinxton, Cambridge, UK). Despite over 300 million years of species deviation between zebrafish and humans, many biochemical pathways are conserved. Furthermore, when examined histologically, there are many

similarities between tumours formed in fish and humans[98].

Cancer research using zebrafish as a model has expanded with technological advancements in the field. The zebrafish is an effective system for studies using forward genetics. Mutations can be introduced into the zebrafish genome by chemical mutagenesis, irradiation, or using viral vectors. Fish are then screened for abnormal phenotypes, and through sequence analysis, the mutated genes are identified[99]. This may detect new genes involved in malignant phenotypes and pathways. These screens would be very cost intensive and difficult to undertake using a mammalian system. Moreover, transgenic technology is well developed in the zebrafish and transgenic zebrafish models of human cancers can be easily subjected to chemical modifier screens[100-102]. External fertilization facilitates the ability to directly study vertebrate development from the one cell stage, which is more challenging and limited in mammalian model systems.

Zebrafish have been used as an *in vivo* model to study cellular processes, such as apoptosis and cell cycle regulation. Previous literature reports assessing apoptosis in zebrafish by acridine orange or Annexin V staining were accompanied by live embryo imaging[103,104]. Methods have been reported for studying the cell cycle in zebrafish embryos, including protocols to examine cell proliferation, DNA damage, and senescence[105].

Several cancer models have been developed in the zebrafish. For example, the zebrafish has become a robust model for investigating the p53 tumour suppressor pathway. Berghmans *et al.* performed mutagenesis studies and identified fish containing mutations in the p53 gene[106]. Some of these mutations localize to the DNA binding domain of the p53 protein, as is common in human mutated p53. Zebrafish with

homozygous p53 mutations develop tumours beginning at eight months of age, with the majority of these tumours being peripheral nerve sheath tumours[106]. Melanoma is an aggressive cancer, in which mutations of the RAS/RAF/MEK/ERK signaling cascade have been identified. Approximately two thirds of melanomas have mutations in BRAF[107]. Zebrafish are now an instrumental player in melanoma research. There are transgenic zebrafish lines expressing mutated *BRAF* in melanocytes. These fish develop large lesions of proliferating melanocytes[96].

The field of hematopoiesis and blood malignancies has expanded immensely with the introduction of zebrafish research. The Berman laboratory has contributed to this field with the discovery of carboxypeptidase A5 (cpa5) as a mast cell-specific enzyme, and its conserved function in zebrafish[108,109]. Ongoing projects are focused on other blood disease models, including systemic mastocytosis and acute myelogenous leukemia. Zebrafish offer many benefits for investigating solid tumours, and therefore, we hope to utilize the zebrafish to uncover how the *HACE1* tumour suppressor contributes to development and oncogenesis.

1.9 RATIONALE

This study will exploit the advantages of the zebrafish model to examine the role of the *HACE1* tumour suppressor in normal development and tumourigenesis. To date, research on *HACE1* has been limited to *in vitro* and murine studies. We believe that the zebrafish will provide important insight into the function of this gene, and will complement information gained from murine research. The transparency of zebrafish

embryos allows direct visualization of organogenesis, which is extremely difficult to study using mice. Therefore, we hope that using zebrafish as a model system, we will uncover how *HACE1* is involved in vertebrate development. With the ability to generate stable transgenic zebrafish lines, this research will set up a cancer model system, by which we can begin to dissect the effect of *HACE1* on cell proliferation and apoptosis. This will further the understanding of the mechanism by which decreased *HACE1* expression leads to malignancy. Ultimately, with a better understanding of the function of *HACE1,* and the signaling pathways in which it is involved, will provide potential targets for cancer therapeutics to improve patient outcomes.

CHAPTER 2 MATERIALS AND METHODS

2.1 ZEBRAFISH MAINTENANCE AND EMBRYO STAGING

Zebrafish were maintained, bred and developmentally staged according to Westerfield[110]. Use of zebrafish in this study was approved by the Dalhousie University Animal Care Committee. Zebrafish were maintained in 28.5° C water with a salinity of 1100 - 1300 us and a pH between 6-8. Fish were exposed to light for 14 hours. Zebrafish embryos were collected, and incubated at 28.5°C in either egg water (5mM NaCL, 0.17 mM KCl, 0.4 mM $CaCl_2$ and 0.16 mM $MgSO_4$) or 0.003% 1-phenyl-2-thiourea (PTU, Sigma-Aldrich, St. Louis, MO) water to inhibit pigmentation for optical clarity. Embryos were treated with Pronase (Roche, Indianapolis, IN, USA) (10 mg/mL) in PTU water and were removed from their chorions. They were then staged at desired developmental timepoints and fixed overnight in 4% paraformaldehyde in 1X phosphate buffered saline (PBS) at 4°C. Fixed embryos were stored at 4°C for up to 4-6 weeks.

2.2 GENERATION OF RNA ANTISENSE PROBES

cDNA constructs were linearized with the appropriate restriction enzyme for 2 hours at 37°C. The linearized DNA was purified with the QIAQUICK PCR purification kit (QIAGEN). Digoxegenin (DIG)- and fluorescein (FITC)- labeled probes were then transcribed with either T7 or SP6 polymerase for 4 hours at 37°C, according to manufacturer's protocol (Roche Molecular Biochemicals, Indianapolis, IN). Probes were

purified with Ambion NucAway spin colums (Ambion). RNA probes were stored at -80°C.

Generation of linearized DNA for the *hace1* ankyrin repeat probe was accomplished by PCR amplification from the plasmid clone ID 8158899 (Accession number DV598969) containing the sequence from the *hace1* ankyrin repeat domain (Open Biosystems, Huntsville, AL). This cDNA sequence is in the pME18S-FL3 vector, which lacks an RNA polymerase binding site. Therefore, PCR amplification of the ankyrin repeat domain utilized primers that incorporated a T7 site flanking the 5' end of the PCR product and an SP6 site flanking the 3' end of the PCR product. The following primers were used:

forward primer TAATACGACTCACTATAGGGGATGTTGCCTTTACTTCTA

reverse primer ATTTAGGTGACACTATAGTCTCTGACGTGACTGCAGCG.

The following PCR program was used:

94°C	3 minutes
94°C	30 seconds
60.8°C	30 seconds
72°C	30 seconds
72°C	7 minutes

The 900 bp PCR product was gel extracted using the QIAQuick gel extraction kit as per the manufacturer's protocol. The PCR product was eluted in 30 uL of DEPC water. The probe was generated using SP6.

The probe for the *hace1* HECT domain was generated from the zf_mu_184f12 clone (provided by the University of Sheffield). Zf_mu_184f12 was linearized with Pst1, and antisense probe was generated using SP6 RNA polymerase.

2.3 WHOLE MOUNT RNA *IN SITU* HYBRIDIZATION (WISH)

Dechrionated embryos were staged at desired timepoints (24 hours post fertilization – 7 days post fertilization) and fixed with 4% paraformaldehyde (PFA, Sigma-Aldrich, St. Louis, MO, USA). Fixed zebrafish embryos were washed in phosphate buffered saline with Tween (PBST). They were treated with hyb- (50% formamide in 5x saline sodium citrate buffer 0.1% Tween 20 (SSCT)) for 15 minutes followed by hyb+ (50% formamide in 5x saline sodium citrate buffer 0.1% Tween 20 (SSCT), 5 mg/mL torula (yeast) RNA type IV, and 50 µg/mL heparin) for 1 hour. Hybridization with antisense probes was performed at 65°C in hyb+ overnight. Embryos were washed in 2X SSCT-50%formamide for 15 minutes each, once in 2X SSCT for 15 minutes, and twice in 0.2 X SSCT for 15 minutes each. The embryos were then washed in MABT (100 mM Maleic acid, 150 mM NaCl, 10% Tris base and 0.1% Tween 20) thrice for 5 minutes, followed by 1 hour in blocking solution (10% FBS, 2% Blocking reagent (Roche, Indianapolis, IN, USA) and MABT). Either anti-DIG or anti-FITC antibody (Roche, Indianapolis, IN, USA) was added, and embryos were incubated overnight at 4°C. For double *in situ* hybridization, both antibodies were added simultaneously. Embryos were washed for 30 minutes at room temperature in 1X blocking solution, twice in MABT, and four washes for 5 minutes in 0.1 M Tris base pH

9.5 for BCIP/NBT stain or 0.1 M Tris base pH 8.2 for Fast Red stain. Colour staining was performed with either BCIP/NBT (Vector Laboratories, Inc. CA, USA) at room temperature for 2-4 hours, or Fast Red (Roche, Indianapolis, IN, USA) for 2 hours at 37°C, followed by overnight at 4°C. For double *in situ* experiments, staining was first performed with Fast Red, followed by BCIP/NBT. Staining of Fast Red was inactivated by incubating in MAB + 10mM EDTA (ethylenediaminetetraacetic acid) for 10 minutes at 60°C, twice in MABT at room temperature, and 1 hour in blocking solution. Double fluorescence *in situ* experiments were performed with Fast Red staining, and then imaged with a Zeiss Observer Z.1 microscope with a Colibri fluorescence source. Single WISH images were taken on a Leica MZ16F with a Leica DFC 490 camera at 5X magnification for whole embryo images and various magnifications for closer images.

2.4 MORPHOLINO KNOCKDOWN

The following morpholino and control morpholino were purchased from Genetools LLC (Philomath, OR): *hace1-HECT*: CCCTCGAACTGTTAGACAGAATAAA (splice site) and standard control: CCTCTTACCTCAGTTACAATTTATA.

Morpholinos were diluted to a working concentration (1.5, 1.6 and 1.9 mM) with 1% phenol red and were injected into live zebrafish embryos at the 1-4 cell stage. Dechrionated embryos were staged at desired timepoint and fixed with 4% PFA or were live imaged using the Leica MZ16F with brightfield or fluorescence.

2.5 RNA EXTRACTION AND MICRO-ARRAY

Zebrafish embryos were grown in PTU water and were staged at 48 hpf. Approximately 50 embryos were homogenized in 1mL of phenol. Samples were stored at room temperature for 5 minutes. Chloroform (200 uL) was added to samples, and they were vortexed for 15 seconds. Samples were centrifuged at 13 000 rpm for 15 minutes at 4°C. The aqueous phase was transferred to a new tube, and an equal volume of cold (-20°C) 70% ethanol was added. Samples were loaded into QIAGEN RNeasy columns and were purified following the manufacturer's protocol. Samples were eluted with 30uL of DEPC treated water (Ambion). Samples were stored at -80°C. Purified RNA concentration was quantified by UV spectrophotometry. Extracted RNA was sent to Dr. Stephen Lewis at the Atlantic Cancer Research Institute (Moncton, NB, Canada), where the micro-arrays were performed.

Micro-arrays were performed as follows. Prior to use in labelling, RNA quality was assessed using BIO-RAD Experion bioanalyzer capillary electrophoresis system and total RNA standard sense chips (cat#s 700-7104, 700-7154), according to manufacturer's instructions. All RNA samples used in these experiments had RNA quality indices (RQI) of 8 or higher (out of 10) with corresponding low levels of degradation. RNA (10 ug per sample) was used in labelling reactions as outlined in Invitrogen's Superscript III Direct Labeling kit (cat# L1015-04) (Invitrogen, Burlington, ON, Canada). First strand cDNA was synthesized using 10 ug of RNA, Anchored Oligo (dT)20 primer (5ug), random hexamers (0.5 ug), and nuclease free water. Reactions were incubated at 70°C for 10 minutes, and then were chilled on ice for 1 minute. A second reaction mixture was

prepared with 5X first-strand buffer, 0.1M DTT, 10X nucleotide mix with Alexa Fluor dye (555 or 647), RNaseOUT, and Superscript III reverse transcriptase (800 U). This second reaction was mixed in a 1:1 ratio with the first strand cDNA reaction mixture and was vortexed gently. Samples were incubated at 46°C for 3 hours, then 15uL of 0.1M NaOH was added to each reaction tube in order to degrade original RNA. Samples were incubated for 30 minutes at 70°C and 15uL of 0.1M HCl was added to each reaction tube in order to neutralize the pH. Labeled probe was purified using Invitrogen's Low Elution cDNA Purification module (cat# 46-6346), according to the manufacturer's instructions. Labeled probe was eluted in 25uL of nuclease-free water. Probe labelling yield and efficiency were assessed by Nano-Drop Spectrophotometer. Two samples were used per hybridization mixture, and were equalized for quantity (ug) of labelled cDNA added. Labeling efficiencies are controlled through the use of dye swaps. Hybridization mixtures were made up to 200uL with Ambion's SlideHyb mix #2 (cat# AM8862) Samples were hybridized to Agilent Zebrafish V3 slides using TECAN HS4800 Pro instrument. Slides were hybridized at 42°C for 16 hours.

2.6 GENERATION OF TRANSGENIC ZEBRAFISH LINES

2.6.1 Gateway Cloning

Plasmids (peGFP-C3-hHACE1 and peGFP-C3-C876S) possessing a green fluorescent protein (GFP) fusion human *HACE1* or dominant negative mutated (DN) *HACE1 (C876S)* gene were provided by Dr. Poul Sorensen's laboratory at the University of British Columbia (Figure 4). eGFP-HACE1 and eGFP-C876S fragments were ligated

A

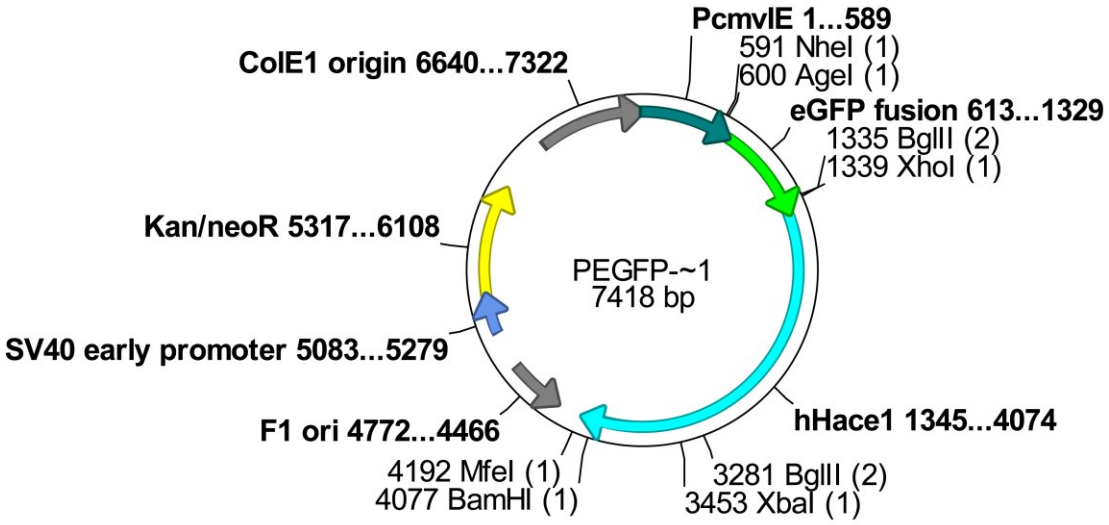
PcmvIE 1...589
591 NheI (1)
600 AgeI (1)
ColE1 origin 6640...7322
eGFP fusion 613...1329
1335 BglII (2)
1339 XhoI (1)
Kan/neoR 5317...6108
PEGFP-~1
7418 bp
SV40 early promoter 5083...5279
hHace1 1345...4074
F1 ori 4772...4466
4192 MfeI (1)
4077 BamHI (1)
3281 BglII (2)
3453 XbaI (1)

B

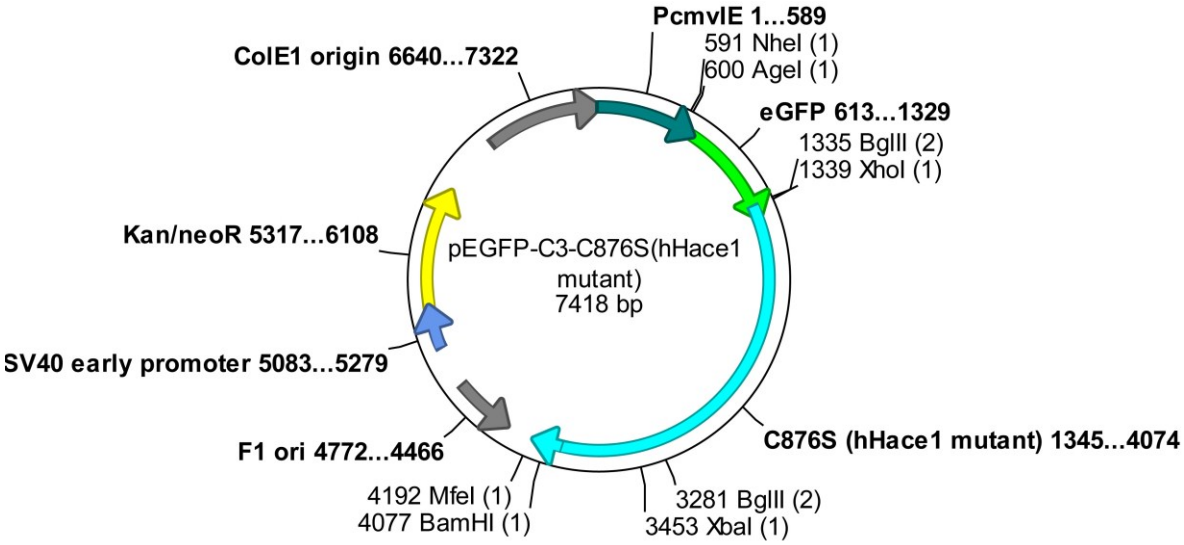
PcmvIE 1...589
591 NheI (1)
600 AgeI (1)
ColE1 origin 6640...7322
eGFP 613...1329
1335 BglII (2)
1339 XhoI (1)
Kan/neoR 5317...6108
pEGFP-C3-C876S(hHace1
mutant)
7418 bp
SV40 early promoter 5083...5279
C876S (hHace1 mutant) 1345...4074
F1 ori 4772...4466
4192 MfeI (1)
4077 BamHI (1)
3281 BglII (2)
3453 XbaI (1)

Figure 4: peGFP-C3-hHACE1 and peGFP-C3-C876S plasmids.
(A) Plasmid possessing a green fluorescent protein and wildtype human *HACE1* fusion gene.
(B) Plasmid possessing a green fluorescent protein and dominant negative mutated human *HACE1* gene. The dominant negative mutation is a serine substituted for the critical cysteine residue at amino acid position 876.
Cloned by Dieter Fink. Provided by Dr. Poul Sorensen, University of British Columbia.

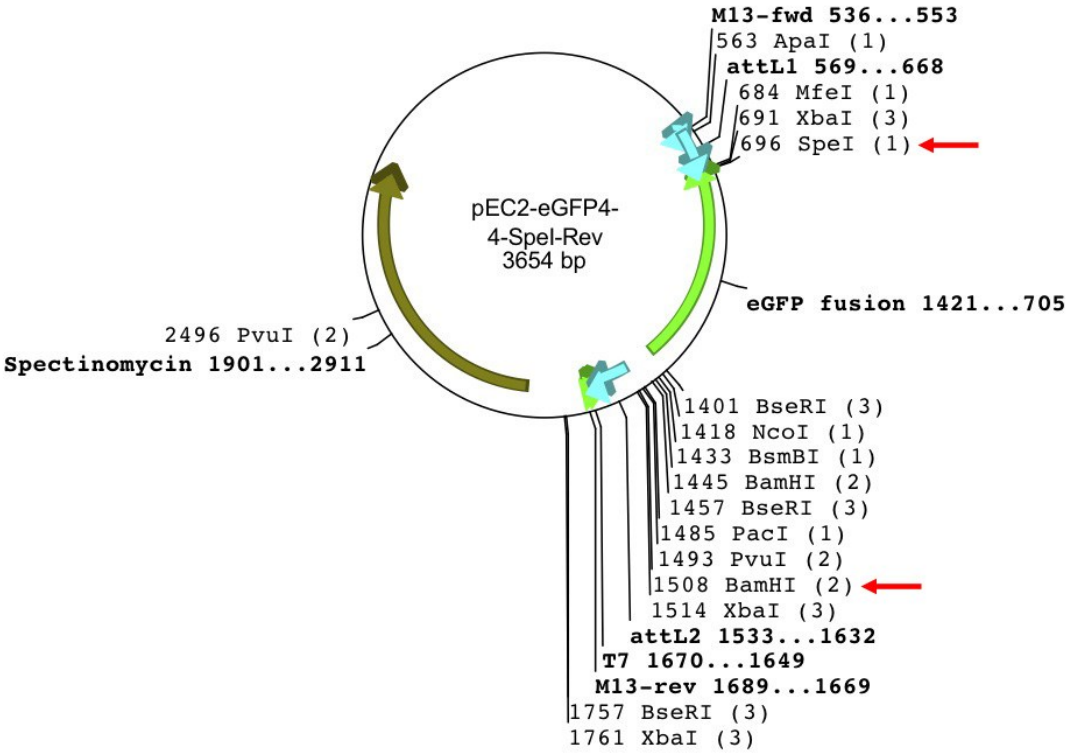

Figure 5: pEC2-eGFP-4-4-Spe1-Rev middle entry clone.
Map of Gateway middle entry clone pEC2-eGFP-4-4-Spe1-Rev. Wildtype human *HACE1* and dominant negative mutated human *HACE1 (C876S)* were ligated into this vector backbone at the Spe1 and BamHI restriction enzyme sites (indicated by red arrows).
Cloned by Martin Kleinheinz. Provided by Dr. Poul Sorensen, University of British Columbia.

into the Gateway middle entry clone pEC2-eGFP-4-4-Spe1-Rev (Figure 5). Both plasmids possessing either wildtype human *eGFP-HACE1* or *eGFP-C876S* (peGFP-C3-hHACE1 and peGFP-C3-C876S) were digested with Nhe1 and BamH1 restriction enzymes. pEC2-eGFP-4-4-Spe1-Rev was digested with Spe1 and BamH1. The 3.9 kb fragment from Nhe1/BamHI digested peGFP-C3-hHACE1 and peGFP-C3-C876S were gel extracted and purified using a QIAGEN QIAquick gel extraction kit (QIAGEN, Mississauga, ON, Canada). The 2.8 kb fragment from Spe1/BamHI digested pEC2-eGFP-4-4-Spe1-Rev was also gel extracted and purified using the QIAquick gel extraction kit. The 3.9 kb fragment with eGFP-hHACE1 was ligated to the 2.8 kb vector backbone (pEC2-eGFP-4-4-Spe1). The same was done with the eGFP-C876S and the 2.8 kb vector backbone. The resultant plasmids (pEC2-hHACE1 or pEC2-C876S) were transformed into Top 10 *E. coli* cells (Invitrogen, Burlington, ON, Canada) and were plated on Spectinomycin (75 ug/mL) agar plates. Correct clones were identified by restriction digests with Hind III, and were checked a second time with EcoRI.

A Gateway destination vector with either GFP fused to wildtype human *HACE1* or DN (C876S) human *HACE1* under the control of the zebrafish β – actin promoter was generated. An LR reaction (Invitrogen, Burlington, ON, Canada) was set up with an entry clone (p5E-βactin), middle entry clone (pEC2-hHACE1), and destination vector (pDestTol2pA-R2R4). A second LR reaction was set up with the same entry clone (p5E-β–actin), the middle entry clone (pEC2-C876S), and the same destination vector (pDestTol2pA-R2R4) (Figure 6). Reactions used LR Clonase II and were incubated at room temperature overnight. The following day, the reactions were transformed into Top 10 *E. coli* competent cells and were plated onto ampicillin (100 ug/mL) agar plates.

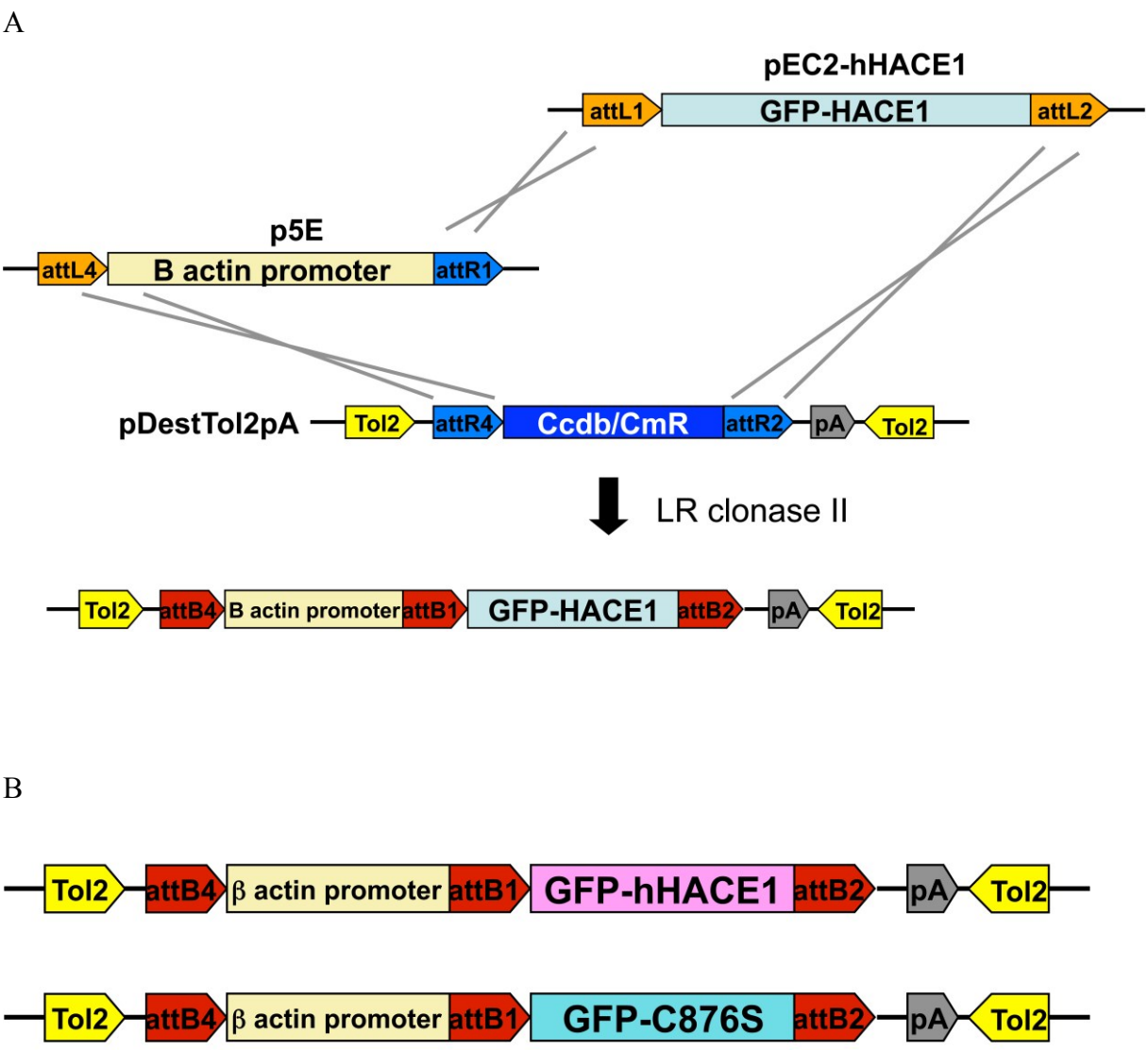

Figure 6: Gateway cloning of destination vectors.

(A) Cloning strategy using Gateway Tol2 platform to generate a destination vector with either a wildtype or dominant negative *GFP* human *HACE1* fusion gene under the control of the ubiquitous β–actin promoter. LR reaction (Invitrogen) was performed with p5E-βactin, pEC2-hHACE1 or pEC2-C876S and the destination vector pDestTol2pA-R2R4.

(B) Destination vectors with either a wildtype or dominant negative mutated (C876S) human *HACE1* gene.

Clones were screened by colony PCR. Colonies were boiled in 20 uL of sterile MQ water for 3 minutes, then 2 uL of the boiled colonies were used in the PCR reactions. Primers used for PCR designed within the human *HACE1* gene sequence were as follows: forward primer TGTCTGCAAACATGATGAAG and reverse primer GTCTTCTACAACTTCCCAG. The PCR program used was:

94°C	3 minutes
94°C	30 seconds
54°C	30 seconds
72°C	30 seconds
72°C	7 minutes

Following colony PCR, clones were verified by restriction digest with SacII.

2.6.2 Establishment of Germline Integration

Destination vectors harboring either a wildtype or DN human *HACE1* gene were injected into wild type zebrafish embryos at the one cell stage. Embryos were screened for green fluorescent protein (GFP) expression at 24 hpf. Zebrafish embryos with GFP labeling were grown until 3 months of age. They were outcrossed with wildtype fish and heterozygous F1 generation fish were identified by GFP labeling. The F1 generation was in-crossed to produce a stable transgenic F2 generation (Figure 7). F2 generation embryos from the A lines were used for all experiments (hHACE or C876S).

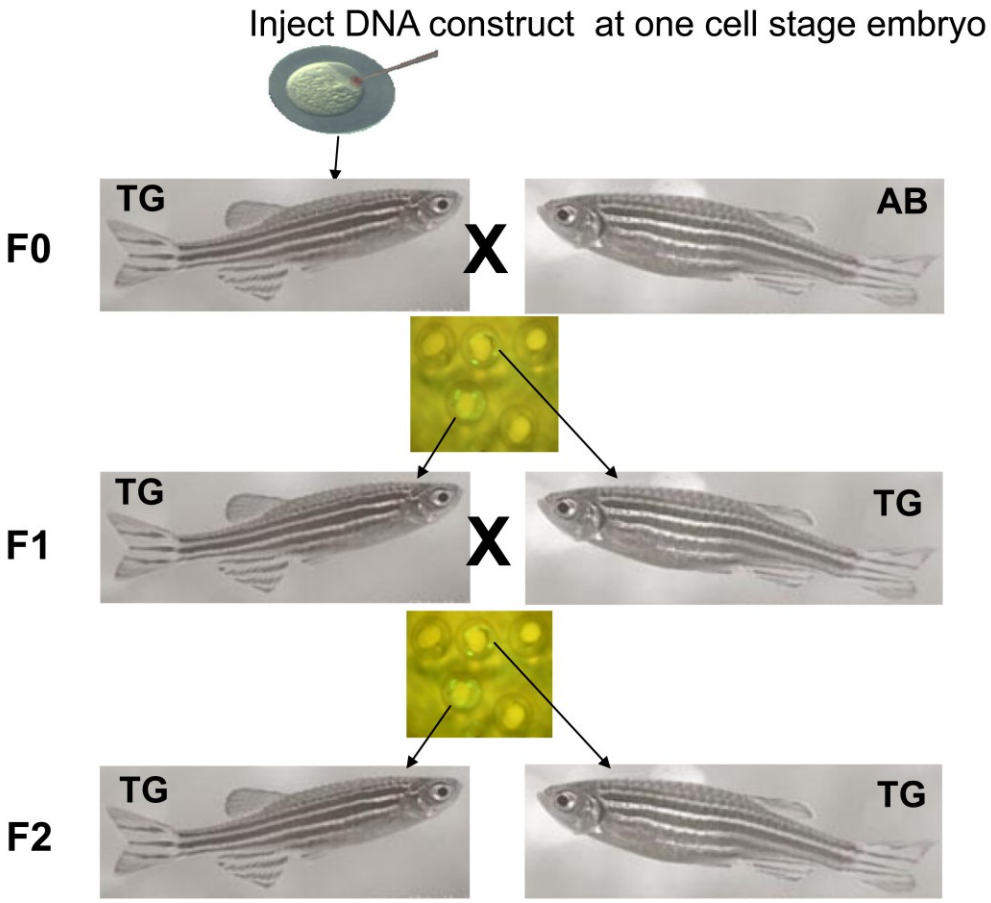

Figure 7: Establishment of the *HACE1* transgenic zebrafish line.
Gateway destination vectors harbouring either a wildtype or dominant negative mutated (C876S) copy of *HACE1* fused to *GFP* were injected into wildtype zebrafish embryos at the one cell stage. Embryos demonstrating GFP expression were grown to 3 months of age. They were then outcrossed to wildtype zebrafish to generate the F1 generation. Transgenic F1 zebrafish were incrossed at 3 months of age to generate the F2 generation.

2.7 Apoptosis Assays

2.7.1 Acridine Orange Assay

Wildtype and C876S (gfp+) zebrafish embryos were dechorionated with Pronase (1mg/mL) and were staged at 24hpf. One set of embryos were irradiated with 16 Gy of radiation for 3 minutes using a Gammacell GC3000 irradiator (MDS Nordion, Ottawa, ON, Canada). Following irradiation, all embryos were maintained at 28.5°C until 28hpf. Embryos (irradiated and non-irradiated) were stained with acridine orange (1 mg/mL) for 30 minutes at 28°C. Embryos were washed with egg water for twenty minutes thrice, and were imaged using the Leica MZ16 fluorescence microscope. Representative pictures were taken.

2.7.2 Caspase 3 Assay

Wildtype and C876S (gfp+) zebrafish embryos were collected and incubated at 28.5°C in PTU. Embryos were dechorionated with Pronase (1mg/mL), staged at 24 hpf and allowed to grow until 26 hpf. At 26 hpf one half of each group of embryos (approximately 12 embryos) were irradiated with 16 Gy of radiation for 3 minutes using the Gamma cell GC3000 irradiator. Irradiated and non-irradiated embryos were incubated until 28 hpf in PTU. Embryos were fixed at 28 hpf in 4% paraformaldehyde following a 10 minute incubation in 1% proteinase K. Embryos were stored up to one week at 4°C.

The zebrafish embryos were permeabilized for 20 minutes in PDT (1% DMSO, 0.3% Triton X in PBST). Embryos were then blocked for one hour with blocking

solution (PDT, 10% FBS, 2% BMB). Anti-activated caspase 3 antibody was then added at a 1:500 concentration, and embryos were incubated overnight at 4°C. Embryos were washed with PDT (1 quick wash, 1 x 20 min, 1 quick wash) at room temperature, followed by blocking solution for 30 minutes at 4°C. AlexaFluor-conjugated secondary antibody was then added (1:250) and embryos were incubated at 4°C for 2 hours. Embryos were washed 3 x 20 minutes in PDT at room temperature. Embryos were mounted in 1.5% low melting point agarose (Sigma-Aldrich, St. Louis, MO) and were visualized using the Zeiss Observer Z.1 microscope with a Colibri fluorescence source at 10X.

2.8 Cell Cycle Assays

2.8.1 BrDU Incorporation Assay

Wildtype and C876S zebrafish embryos were collected and grown in PTU water at 28.5°C. C876S (gfp+) zebrafish. Approximately 20 wildtype and C876S transgenic embryos were staged at 24 hpf. At 26 hpf, embryos were chilled for 15 minutes on ice. They were then incubated in bromodeoxyuridine (BrdU) (10 mM BrdU, 15% DMSO) for 20 minutes chilled on ice. Embryos were allowed to recover at 28.5°C in PTU water for 10 minutes. They were washed with PBST (1 quick wash, 1 x 5 minutes, 1 quick wash). Embryos were fixed in 4% paraformaldehyde for 2 hours at 4°C. They were then transferred to 100% methanol and were stored overnight at -20°C.

Zebrafish embryos were rehydrated in a graded fashion using a methanol:PBST series (3:1, 1:1, 1:3) for 5 minutes each. Embryos were washed 2 x 5 minutes in PBST, followed by digestion with 1% proteinase K for 10 minutes. After washing quickly with PBST twice, embryos were placed in 4% paraformaldehyde for 20 minutes. They were washed with 2N hydrochloric acid for 1 hour at room temperature. The embryos were blocked with blocking solution (FBS, BMB, PBST) for 30 minutes after washing 5 times quickly with PBST. Anti-BrdU antibody was added to the blocking solution at a 1:100 dilution. The embryos were incubated with primary antibody overnight at 4°C.

The following day, the embryos were washed 5 x 10 minutes in PBST at room temperature. Embryos were then incubated with AlexaFluor-conjugated secondary antibody at a 1:675 dilution. Samples were incubated overnight at 4°C.

Embryos were washed 5 x 10 minutes on the shaker at room temperature. They were then mounted in 1.5% low melting point agarose, and were visualized using the Zeiss Observer Z.1 microscope with a Colibri fluorescence source at 10X power. Representative pictures were taken of approximately 8 embryos. Images were quantified using ImageJ.

2.8.2 Phosphohistone H3 Assay

The protocol for the phosphohistone H3 assay is the same as described for the Caspase 3 assay (see above). Anti-phosphohistone H3 primary antibody was used at a 1:750 dilution. Embryos were incubated in primary antibody overnight at 4°C as described for the caspase 3 assay.

2.9 Adult Zebrafish Maintenance and Monitoring

Transgenic zebrafish (β−actin::GFPhHACE1 and (β−actin::GFPC876S) were grown to adulthood as per the fish husbandry protocols in 28.5°C water. Fish were monitored daily the development of neoplasms, or an unhealthy appearance. Fish with clinically apparent masses were sacrificed and sectioned. Sections were stained with hematoxylin and eosin (H&E). Fish that appeared ill, or were swimming with difficulty in the tank were also sacrificed and sectioned. They were again stained with H&E.

2.10 Statistical Analysis

Statistical analysis was performed by 2 sample test of proportions using STATA/IC11 (Statacorp LP, College Station, Texas, USA). A Student's t test was performed using GraphPad Calculator software. A p value <0.05 was considered significant.

CHAPTER 3 RESULTS

3.1 ZEBRAFISH *HACE1* EXPRESSION

HACE1 is widely expressed in human tissues, with particularly strong expression in heart, brain, kidney and pancreas. This has been demonstrated at the mRNA level by Northern blot analysis[31]. We have identified a *HACE1* homologue in zebrafish, which shares 74.7% DNA homology, and 88.9% protein identity with human HACE1 (Figure 8). Zebrafish *hace1* possesses the two functional domains that are found in human *HACE1;* there is an ankyrin repeat domain, which is involved in protein-protein-interactions, as well a domain sharing homology to the HECT domain. There is currently no zebrafish *hace1* antibody available in order to examine *hace1* protein expression; therefore, in order to determine expression patterns of zebrafish *hace1* we have to rely on RNA expression. Whole mount RNA *in situ* hybridization (WISH) was used to determine *hace1* RNA expression in zebrafish embryos at early developmental time points. Antisense digoxigenin (DIG) probes were made to RNA sequences within ankyrin repeat and HECT domains of zebrafish *hace1*.

WISH was performed using a probe to the ankyrin repeat domain of *hace1* and demonstrated widespread staining throughout the entire zebrafish embryo (Figure 9). There is evidence of staining in the head region, and in the somites of the tail, especially at the earlier timepoints (24 hpf). WISH studies were then undertaken using a probe to the HECT domain. Staining in the kidney was observed by 24 hpf, in cardiac structures by 48 hpf, and staining in the central nervous system (CNS) at both these time points,

A

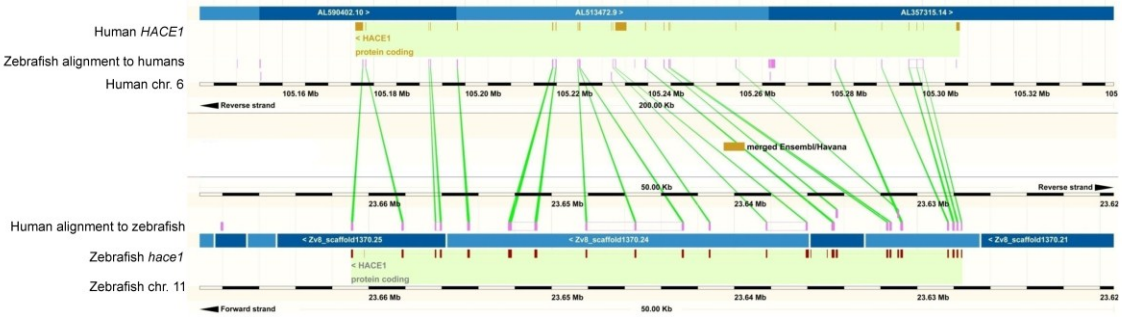

B

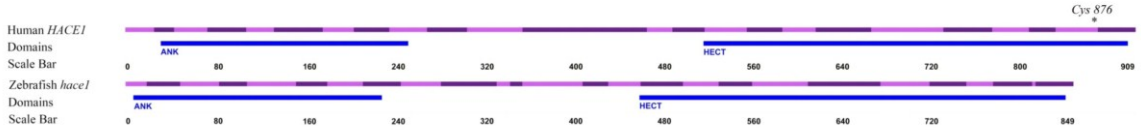

Figure 8: Human *HACE1* and zebrafish *hace1* homology.
(A) *HACE1* gene homology.
(B) Protein homology with ankyrin repeat and HECT domains (85% identity).
www.ensembl.org, EnsEMBL release 58, May 2010, WTSI / EBI

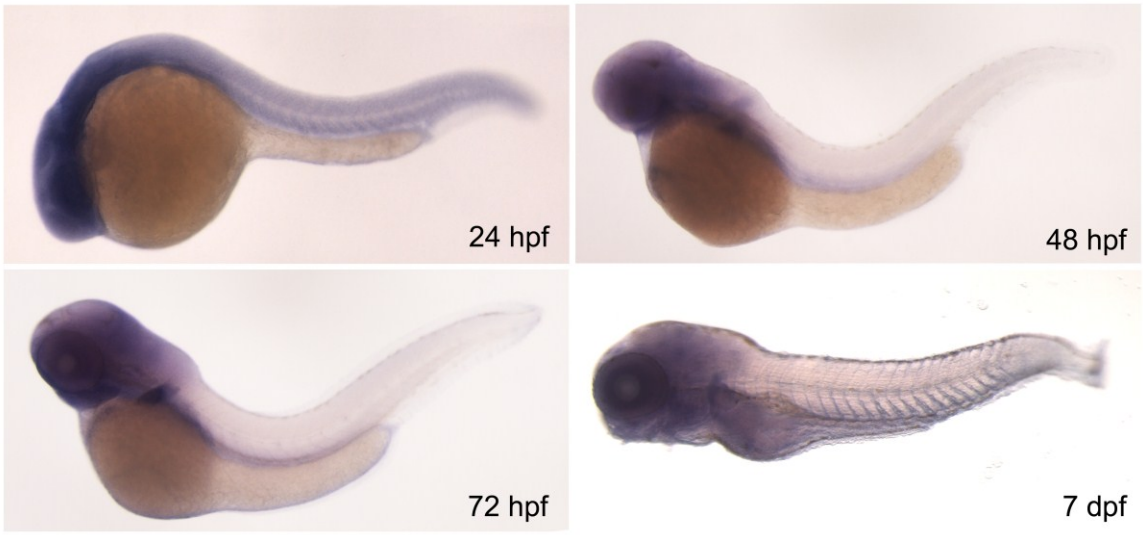

Figure 9: Expression pattern of zebrafish *hace1* using probe to the ankyrin repeat domain.
Whole mount *in situ* hybridization (WISH) of wild type zebrafish embryos using an antisense digoxigenin (DIG) labeled probe to the zebrafish *hace1* ankyrin repeat domain at 24 hours post fertilization (hpf) – 7 days post fertilization (dpf) demonstrates widespread expression throughout the embryo.
hpf = hours post fertilization, dpf = days post fertilization.
Lateral view, anterior to the left.

suggesting conserved tissue expression for *hace1* between zebrafish and mammals (Figure 10).

In order to validate these findings, double *in situ* hybridization studies were performed using the probe to the zebrafish *hace1* HECT domain and known renal, cardiac and CNS tissue-specific probes. *Cadherin 17 (cdh17)* is expressed in the embryonic kidney beginning at the 5-somite stage and has persistent expression throughout zebrafish development into adulthood[111]. At 48 hpf, by single fluorescence double *in situ* hybridization, there was co-localization of *hace1* HECT with *cdh17* (Figure 11). This was similarly demonstrated using double fluorescence *in situ* hybridization at 48 hpf (Figure 12). *Cardiac myosin light chain 2 (cmlc2)* is expressed in zebrafish cardiac tissue. Its expression is apparent throughout the entire lifespan of the zebrafish[112-114]. Zebrafish *hace1* HECT co-localized with *cmlc2* at 48 hpf by both single and double fluorescence WISH (Figure 11 and Figure 12, respectively). *Krox20* is expressed in rhombomeres 3 and 5 within the hindbrain of the zebrafish embryo starting at the 1-4 somite stage, with continued expression until 60 hpf. There was evidence for co-localization of zebrafish *hace1* with *krox20* at 48 hpf (Figure 11).

3.2 MORPHOLINO KNOCKDOWN OF ZEBRAFISH *HACE1* RESULTS IN ABNORMAL CARDIAC DEVELOPMENT

Human *HACE1* is expressed in fetal kidney tissue, suggesting that its early expression may be required for normal vertebrate development[31]. However, the contribution of *HACE1* to development is currently unknown. Development of stable

Figure 10: Expression pattern of zebrafish *hace1* using probe to the HECT domain. Whole mount *in situ* hybridization (WISH) of wild type zebrafish embryos using a probe to the zebrafish *hace1* HECT domain at 24 hours post fertilization (hpf) – 7 days post fertilization (dpf) demonstrates expression in kidney, heart and brain. Expression in brain and kidney is indicated by arrows at 24 hpf. Cardiac expression is indicated by the arrow at 48 hpf, and kidney expression by the arrow at 72 hpf.
hpf = hours post fertilization, dpf = days post fertilization.
Lateral view, anterior to the left.

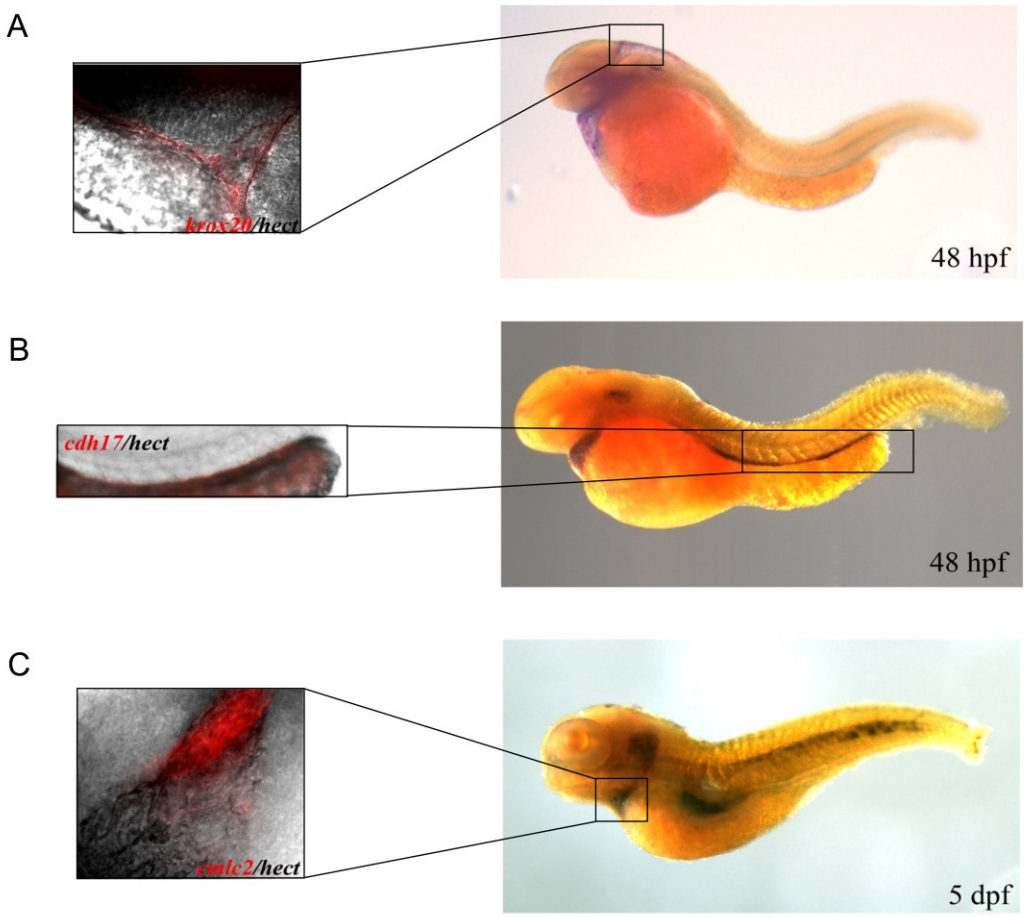

Figure 11: Co-localization of zebrafish *hace1* with tissue specific probes.

(A) Double WISH performed on wildtype zebrafish embryos at 48 hpf using a labeled RNA anti-sense probe to *krox20* (brain – red) and the zebrafish *hace1* HECT domain (black).

(B) Double WISH performed on wildtype zebrafish embryos at 48 hpf using a labeled RNA anti-sense probe to *cdh17* (kidney – red) and the zebrafish *hace1* HECT domain (black).

(C) Double WISH performed on wildtype zebrafish embryos at 5 dpf using a labeled RNA anti-sense probe to *cmlc2* (cardiac – red) and the zebrafish *hace1* HECT domain (black).

hpf = hours post fertilization, dpf = days post fertilization.

A

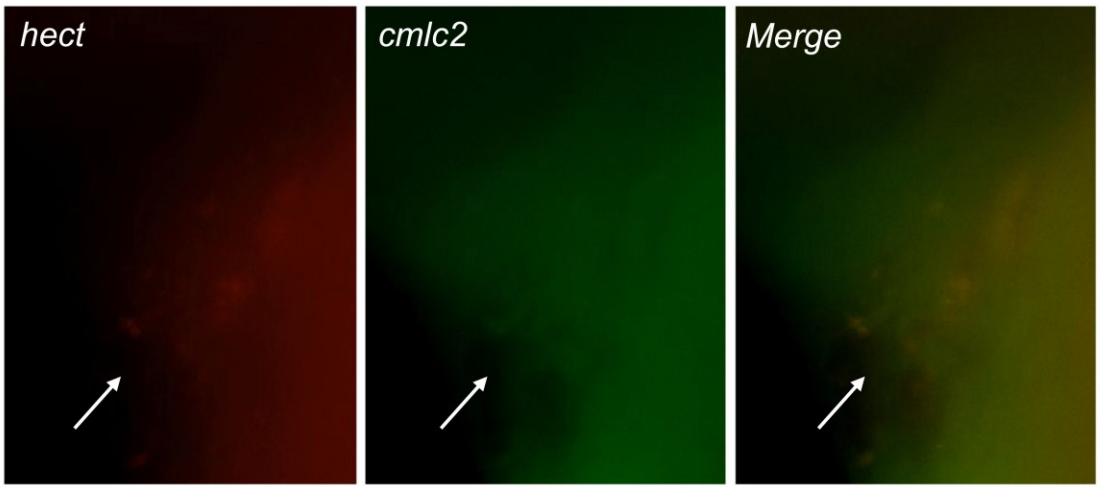

B

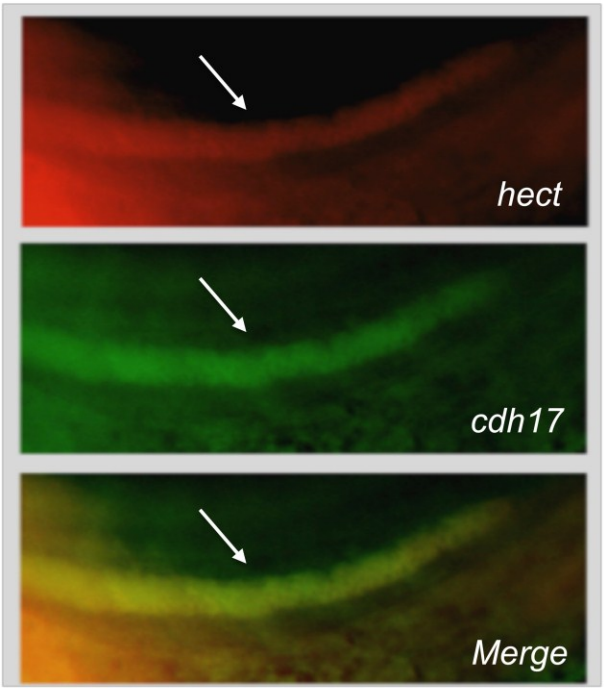

Figure 12: Colocalization of *hace1* with tissue specific probes by double fluorescence whole mount *in situ* hybridization (WISH).

(A) Image of zebrafish heart by double WISH performed on wildtype zebrafish embryos at 48 hpf using a labeled RNA anti-sense probe to *cmlc2* (FITC – green) and the zebrafish *hace1* HECT domain (Fast Red – red) (20X objective).

(B) Image of zebrafish kidney by double WISH performed on wildtype zebrafish embryos at 48 hpf using a labeled RNA anti-sense probe to *cd17* (FITC – green) and the zebrafish *hace1* HECT domain (Fast Red – red) (10X objective).
hpf = hours post fertilization, lateral view, anterior to the left.

knockout zebrafish lines through homologous recombination, as is common practice in mammalian research, has been challenging and until recently a limitation in the field[115] (see Future Directions). However, morpholino oligonucleotides (morpholinos), which inhibit mRNA translation, are in common use in zebrafish and are easily designed with the assistance of websites/companies such as GeneTools (Philomath, OR). Morpholinos result in a transient knockdown during the first three days post fertilization, which provides information about a gene's function early in development. In order to determine the potential function of *HACE1* in normal organism development, I designed a morpholino to knockdown *hace1* gene expression in the zebrafish embryo. This morpholino targets a splice site within the *hace1* HECT domain, and is located upstream of the critical cysteine residue (876). I designed a splice site morpholino instead of a translational start site morpholino, as there was some sequence discrepancy between 8th and 9th version of the whole genome assembly of the zebrafish genome (ZV8 and ZV9) at the translational start site in zebrafish *hace1*. Furthermore, a splice site morpholino allows the ability to confirm correct morpholino targeting by PCR, as the length of the mRNA transcript is altered by intron insertion or exon deletion. We do not currently know any downstream targets of *hace1,* and therefore we could not use WISH to validate morpholino knockdown. This morpholino was injected into wildtype embryos at the 1-4 cell stage. By 48 hpf, *hace1* morphants displayed abnormal cardiac structure and severely compromised function. To further investigate the effect of *hace1* knockdown on cardiac development, I injected the *hace1* morpholino into *cmlc2::GFP* transgenic zebrafish. Transgenic zebrafish lines that fluorescently label different organs allow for the ability to directly visualize organogenesis. *Cmlc2::GFP* is a transgenic zebrafish line

that was developed by Huang *et al.* and possesses heart specific green fluorescent protein expression[116]. It was generously provided by Dr. Ian Scott, Hospital for Sick Children, Toronto, ON. When injected into wildtype, and *cmlc2::GFP* embryos at the 1-4 cell stage, cardiac structure and function was severely perturbed by 48 hpf (Figure 13A). The normal zebrafish embryo possesses a heart with a single atrium and ventricle separated by a valve[117]. In contrast, *hace1* morphants lose this tightly regulated cardiac structure, resulting in the loss of defined cardiac chambers. This altered cardiac structure was observed both by fluorescence live imaging using transgenic zebrafish with a green fluorescent protein-labeled heart, as well as in fixed embyros by WISH. Enumeration of the cardiac abnormalities in embryos injected with *hace1* morpholino compared to control morpholino was performed to quantify this phenotype and revealed a statistically significant increase in the number of abnormal hearts ($p=0.0007$) (Figure 13B). Furthermore, there was a statistically significant increase in embryo mortality by 48 hpf in *hace1* morphants compared to control morpholino-injected embryos ($p<0.0001$) (Figure 13B). This experiment was performed in triplicate, totaling 179 control embryos and 363 *hace1* morphants.

3.3 ZEBRAFSIH *HACE1* MORPHANTS EXHIBIT ALTERED VASCULAR STRUCTURE

Friend leukemia integration 1 transcription factor (*fli1)* is a member of the ETS transcription factor family. *fli1a* is normally expressed in endothelial cells and shows

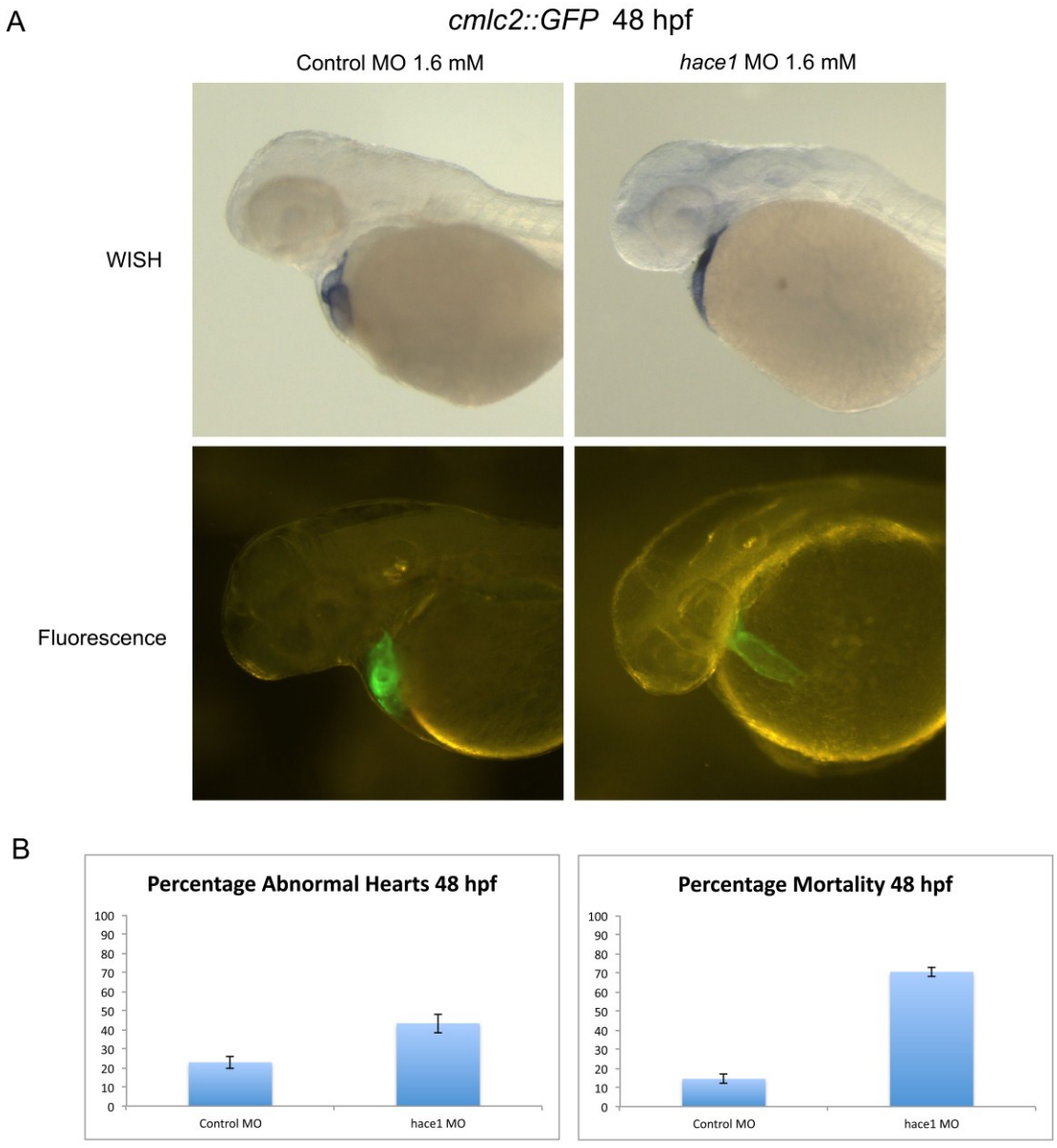

Figure 13: *hace1* morphants display abnormal cardiac development.
(A) *cmlc2::GFP* zebrafish embryos injected with a morpholino targeted to a *hace1* splice site within the HECT domain show abnormal cardiac development at 48 hpf.
(B) Quantification of *hace1* morphants compared to control morpholino show a significant increase in abnormal cardiac phenotype ($p=0.0007$) and a significant increase in mortality ($p<0.0001$). Control morpholino N = 179 embryos scored, *hace1* morphants N= 363 embryos scored. Error bars indicate standard error of the mean (SEM). Pooled triplicate experiment
hpf = hours post fertilization; WISH = whole mount *in situ* hybridization.

conserved expression in mammals and zebrafish. Therefore a *fli1* can be used to label zebrafish vasculature during embryogenesis[118]. The *fli1a::gfp* line was developed in the laboratory of Dr. Brent Weinstein (NIH, Bethesda, MD, USA)[119]. Given the effect on cardiac structure by knockdown of *hace1*, we hypothesized that *hace1* may play a more global role in vascular development. To assess this, the *hace1* morpholino designed to a splice site in the HECT domain was injected into *fli1a::gfp* zebrafish embryos at the 1-4 cell stage. By 48 hpf, there was evidence that vascular patterning was disrupted. There was loss of the organized structure of the intersomitic vessels in *hace1* morphants compared to the highly organized structure in control embyros (Figure 14). These findings suggest a potential role for hace1 in vascular development; however, this experiment was only performed once using approximately 50 embryos.

3.4 Micro-Array Analysis of zebrafish *hace1* Morphants reveals Changes in Gene Expression

Micro-array analysis was used to examine the changes in gene expression caused by loss of *hace1*. Zebrafish micro-array analysis chips are now commercially available, allowing this technology to be utilized with ease. Whole embryo RNA was extracted at 48 hpf from approximately 50 wildtype embryos and 50 *hace1* morphants. The RNA samples were labeled, and micro-arrays using Agilent zebrafish V3 slides were performed in collaboration with Dr. Stephen Lewis at the Atlantic Cancer Research Institute. Results were based on two RNA extractions and three micro-array analyses. A heat map of upregulated and downregulated genes identified by micro-array analysis are

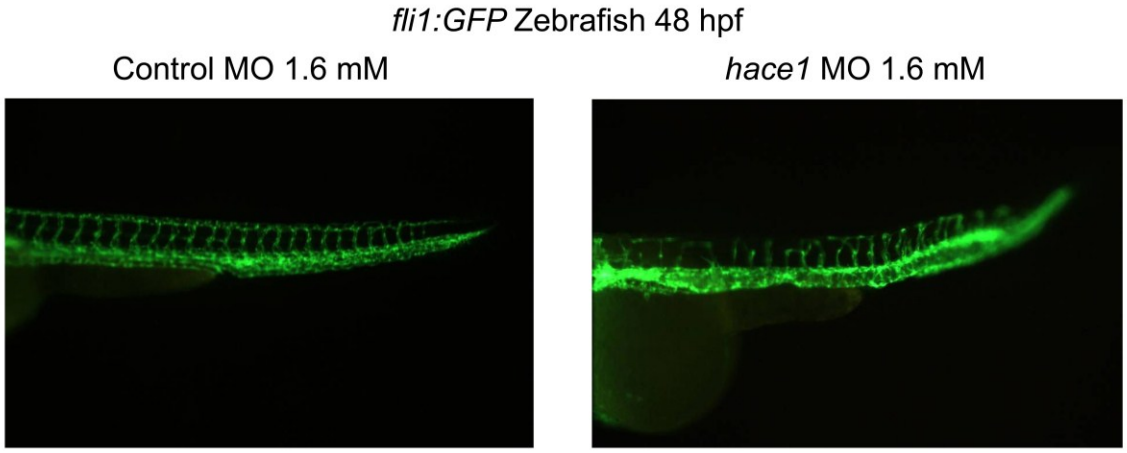

Figure 14: *hace1* morphants display disorganized vasculature.
fli1::GFP zebrafish injected with a morpholino targeted to a *hace1* splice site within the HECT domain show disruption in normal vascular development. The regular structure of the intersomitic vessels is interrupted at 48 hpf.
hpf = hours post fertilization.

shown in Figure 15. Interestingly, cyclin G1, which is involved in cell cycle regulation, is upregulated. In the third experiment, cyclin D1 (involved in G1/S phase transition) was upregulated. Other gene products identified by micro-array analysis include Sox3 and ELAV-like protein 3, which play a role in neural development. Guanidinoacetate N-methyltransferase (gamt), involved in creatine synthesis, was found to be downregulated in *hace1* morphants.

3.5 TRANSGENIC ZEBRAFISH UNDER CONTROL OF THE ZEBRAFISH UBIQUITOUS β-ACTIN PROMOTER

As mentioned above, generation of knockout zebrafish lines by homologous recombination has been a significant limitation of this model system compared to the ease of this approach in mammals. In murine research, it is possible to create mouse lines that are lacking a particular gene of interest. This has been possible largely in part because of the homologous recombination that occurs when DNA constructs are injected into mammalian cells[120]. Using a positive-negative selection technique, by which *neo*^{r} is used for positive selection, and HSV-tk for negative selection, chimeric mice can be generated that then pass the "knockout" gene to their progeny[121]. The advent of zinc finger nuclease (ZFN) technology in zebrafish has overcome this barrier[122]. This methodology has permitted the creation of zebrafish knockout lines, but until recently this has been challenging to undertake independently and was extremely costly when engaging commercial partners. However, recent adaptations have made this technology much more accessible, and the targeting of hace1 by ZFNs is currently underway (see

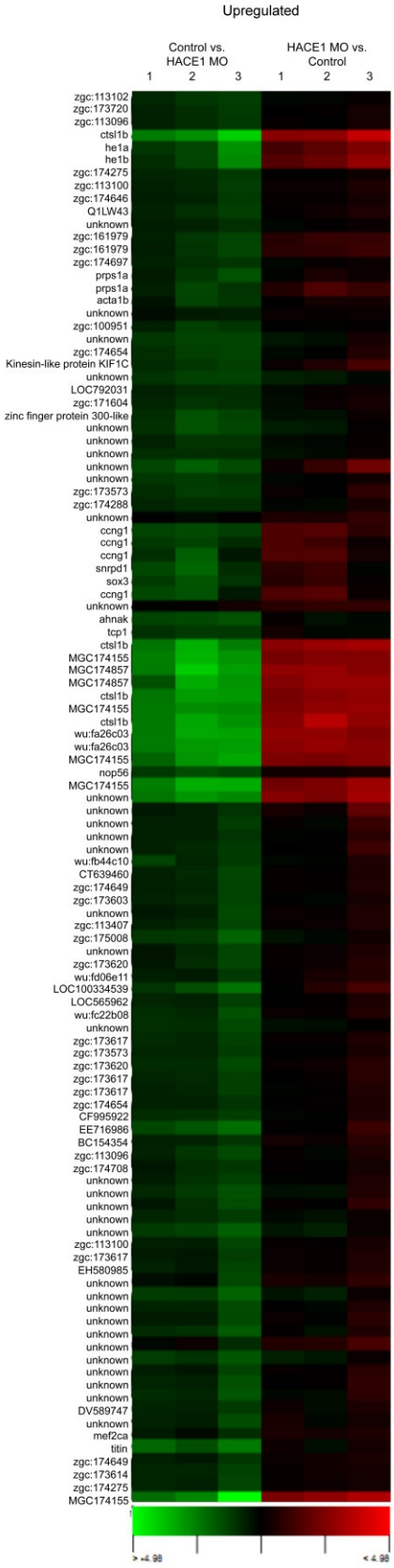
Upregulated
Control vs. HACE1 MO
HACE1 MO vs. Control
1 2 3 1 2 3
zgc:113102
zgc:173720
zgc:113096
ctsl1b
he1a
he1b
zgc:174275
zgc:113100
zgc:174646
Q1LW43
unknown
zgc:161979
zgc:161979
zgc:174697
prps1a
prps1a
acta1b
unknown
zgc:100951
unknown
zgc:174654
Kinesin-like protein KIF1C
unknown
LOC792031
zgc:171604
zinc finger protein 300-like
unknown
unknown
unknown
unknown
unknown
zgc:173573
zgc:174288
unknown
ccng1
ccng1
ccng1
snrpd1
sox3
ccng1
unknown
ahnak
tcp1
ctsl1b
MGC174155
MGC174857
MGC174857
ctsl1b
MGC174155
ctsl1b
wu:fa26c03
wu:fa26c03
MGC174155
nop56
MGC174155
unknown
unknown
unknown
unknown
unknown
wu:fb44c10
CT639460
zgc:174649
zgc:173603
unknown
zgc:113407
zgc:175008
unknown
zgc:173620
wu:fd06e11
LOC100334539
LOC565962
wu:fc22b08
unknown
zgc:173617
zgc:173573
zgc:173620
zgc:173617
zgc:173617
zgc:174654
CF995922
EE716986
BC154354
zgc:113096
zgc:174708
unknown
unknown
unknown
unknown
unknown
zgc:113100
zgc:173617
EH580985
unknown
unknown
unknown
unknown
unknown
unknown
unknown
unknown
unknown
unknown
unknown
DV589747
unknown
mef2ca
titin
zgc:174649
zgc:173614
zgc:174275
MGC174155
> +4.98
< 4.98

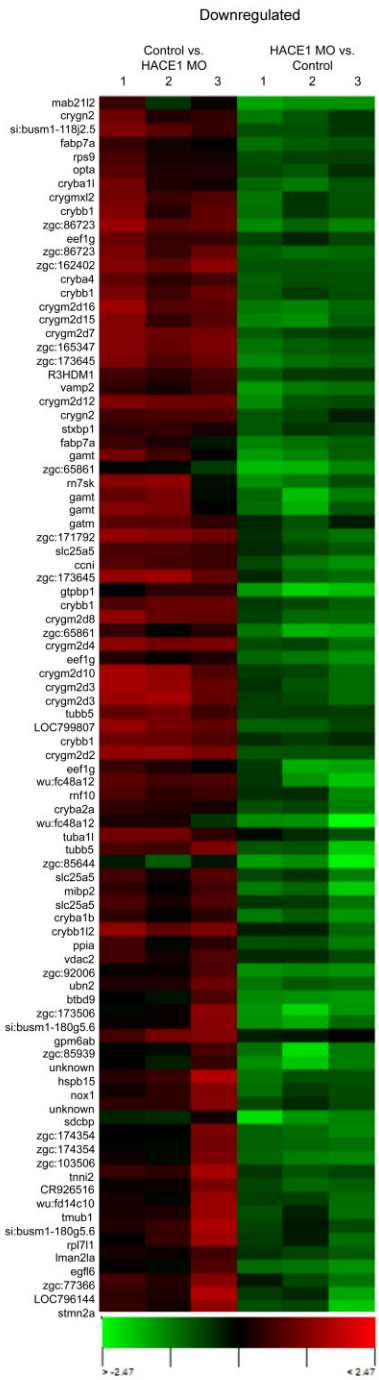
Downregulated
Control vs. HACE1 MO
HACE1 MO vs. Control
1 2 3 1 2 3
mab21l2
crygn2
si:busm1-118j2.5
fabp7a
rps9
opta
cryba1l
crygmxl2
crybb1
zgc:86723
eef1g
zgc:86723
zgc:162402
cryba4
crybb1
crygm2d16
crygm2d15
crygm2d7
zgc:165347
zgc:173645
R3HDM1
vamp2
crygm2d12
crygn2
stxbp1
fabp7a
gamt
zgc:65861
rn7sk
gamt
gamt
gatm
zgc:171792
slc25a5
ccni
zgc:173645
gtpbp1
crybb1
crygm2d8
zgc:65861
crygm2d4
eef1g
crygm2d10
crygm2d3
crygm2d3
tubb5
LOC799807
crybb1
crygm2d2
eef1g
wu:fc48a12
rnf10
cryba2a
wu:fc48a12
tuba1l
tubb5
zgc:85644
slc25a5
mibp2
slc25a5
cryba1b
crybb1l2
ppia
vdac2
zgc:92006
ubn2
btbd9
zgc:173506
si:busm1-180g5.6
gpm6ab
zgc:85939
unknown
hspb15
nox1
unknown
sdcbp
zgc:174354
zgc:174354
zgc:103506
tnnl2
CR926516
wu:fd14c10
tmub1
si:busm1-180g5.6
rpl7l1
lman2la
egfl6
zgc:77366
LOC796144
stmn2a
> -2.47
< 2.47

Figure 15: Micro-array analysis of *hace1* morphants.
Heat map of upregulated and downregulated genes identified by micro-array performed on 48 hpf zebrafish embryos injected with *hace1* morpholino (1.6 mM) compared to control morpholino (1.6 mM). *cyclin G1* and *sox3* are upregulated in *hace1* morphants, whereas *gamt* is downregulated.
Provided by Dr. Stephen Lewis, Atlantic Cancer Research Institute.

Future Directions)[115]. In the interim, I undertook the alternative strategy of generating stable transgenic zebrafish lines possessing a dominant negative mutated copy of the gene of interest. Dominant negative mutations are changes in the genetic sequence that result in a gene product that acts antagonistically to the wild type allele, thereby creating a "functional knockout". Dr. Poul Sorensen's laboratory at the University of British Columbia has generated Hace1 mutant mice by disrupting the human *HACE1* gene in mouse embryonic stem cells. They created mice in which the ankyrin repeat domains of human *HACE1* are deleted[89].

We created two transgenic zebrafish lines; one line expressing a wild type human *HACE1* gene, and one line expressing a dominant negative mutated human *HACE1(C876S)* gene. This mutation at cysteine residue 876 results in loss of ubiquitin ligase activity. *β–Actin* is a cytoskeletal gene that is ubiquitously expressed in zebrafish. Transgenic zebrafish lines using the *β–actin* promoter were first described by Higashijima *et al.* in 1997 when they created a zebrafish line expressing green fluorescent protein under control of the *β–actin* promoter[123]. We decided to create *HACE1* and dominant negative *HACE1* transgenic zebrafish lines under control of the *β–actin* promoter because of the ubiquitous expression that this promoter provides. *HACE1* is widely expressed in human tissues; therefore using this well established ubiquitous promoter would provide important insight into the function of *HACE1*.

Plasmids containing either a wild type human *HACE1* or dominant negative mutated human *HACE1* gene fused to GFP (peGFP-C3-hHACE1 and peGFP-C3-C876S) were digested with Nhe1 and BamHI. Concurrently, pEC2-eGFP-4-4-Spe1-Rev was digested with Spe1 and BamH1. The 3.9 kb fragment from Nhe1/BamHI digested

peGFP-C-hHACE1 and peGFP-C-C876S were gel extracted along with the 2.8 kb vector backbone of pEC2-eGFP-4-4-Spe1-Rev. pEC2-hHACE1 and pEC2-C876S plasmids were generated by ligating the DNA fragments of wild type or dominant negative *HACE1* with the 2.8 kb pEC2-eGFP-4-4Spe1-Rev backbone. Correct clones were identified by EcoRI restriction digests.

Gateway cloning is a technique developed in Japan, now available from Invitrogen (Burlington, ON, Canada)[124]. It allows the transfer of DNA sequences between plasmids, while maintaining the proper reading frame. It works by recombination using *att* sites that flank the DNA sequence of interest. More specifically, the LR reaction uses *attL* and *attR* sites, and generates a destination vector that possesses the promoter of choice, gene of interest, and reporter gene. LR reactions were performed to generate destination vectors containing the zebrafish *β–actin* promoter, and either wild type or mutated *HACE1*. Clones were transformed into *E. coli*. Colony PCR using primers to human *HACE1* sequence identified positive clones (Figure 16A). Positive clones were verified with SacII restriction digests (Figure 16B). *β–Actin::eGFPhHACE1* clone #18 and *β–actin::eGFPC876S* clone#17 were injected into wild type zebrafish embryos. *EGFP* expression was observed in transgenic embryos at 24 hpf of development. There was germline transmission of the transgene to the F1 generation zebrafish, as evidenced by ubiquitous GFP fluorescence in embryos and confirmed by genomic PCR on adults (Figure 17). Wild type or dominant negative mutated *HACE1* adult fish 1-3 months of age were genotyped by DNA extraction from tail clipping to ensure that they expressed the transgenic sequence. Tail clippings were subjected to PCR amplification using primers that flanked the critical cysteine residue within the *HACE1*

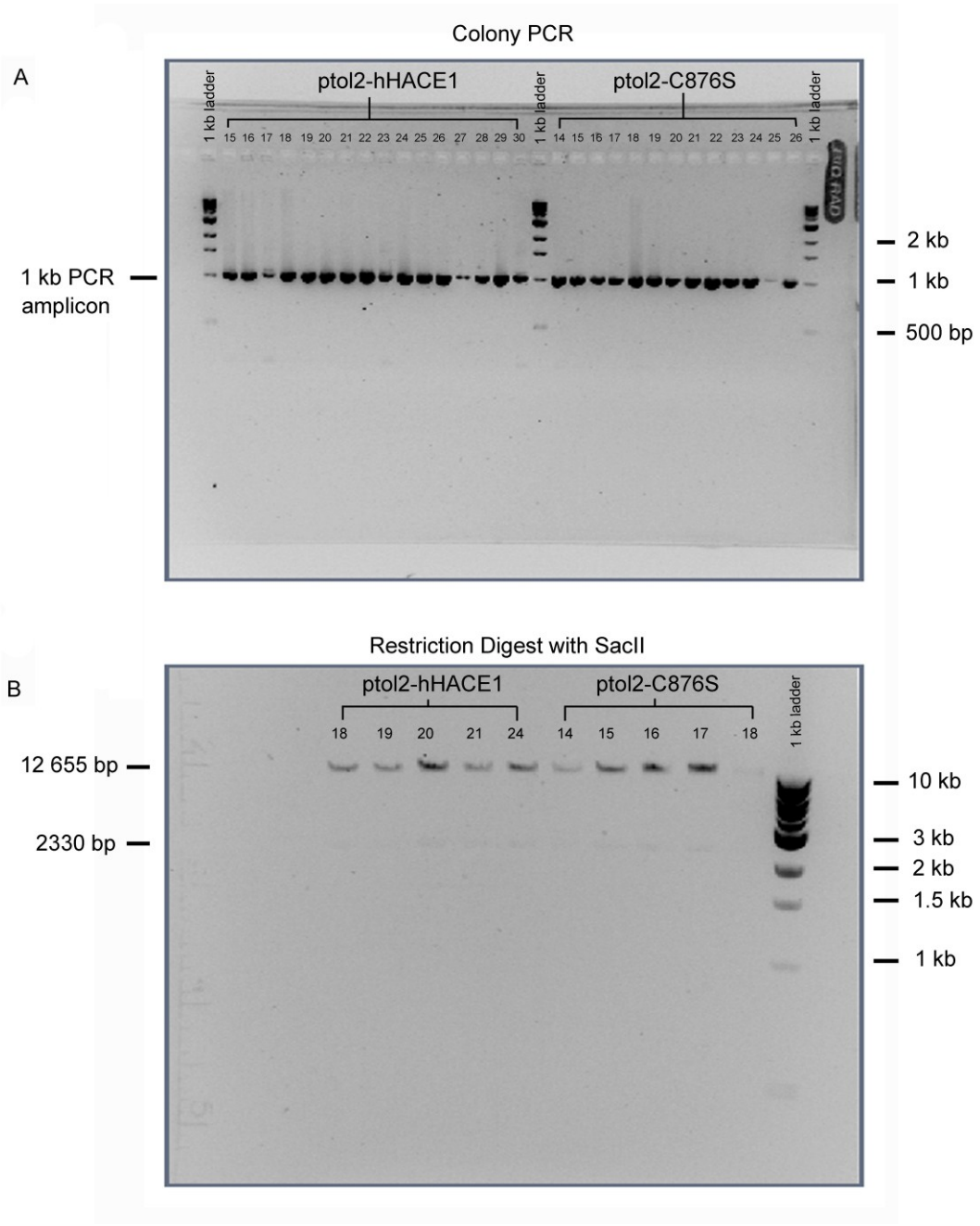

Figure 16: Agarose gels confirm creation of Gateway destination vectors.
(A) Colony PCR performed from *E. coli* colonies transformed with the Gateway LR reactions used to create ptol2-hHACE1 and ptol2-C876S. Primers were designed within human *HACE1* sequence to amplify a 1 kb amplicon.
(B) Minipreps from positive clones identified by colony PCR digested with SacII display the expected bands (12 655 bp and 2330 bp) in all digested samples.
bp = base pairs, kb = kilobase pairs.

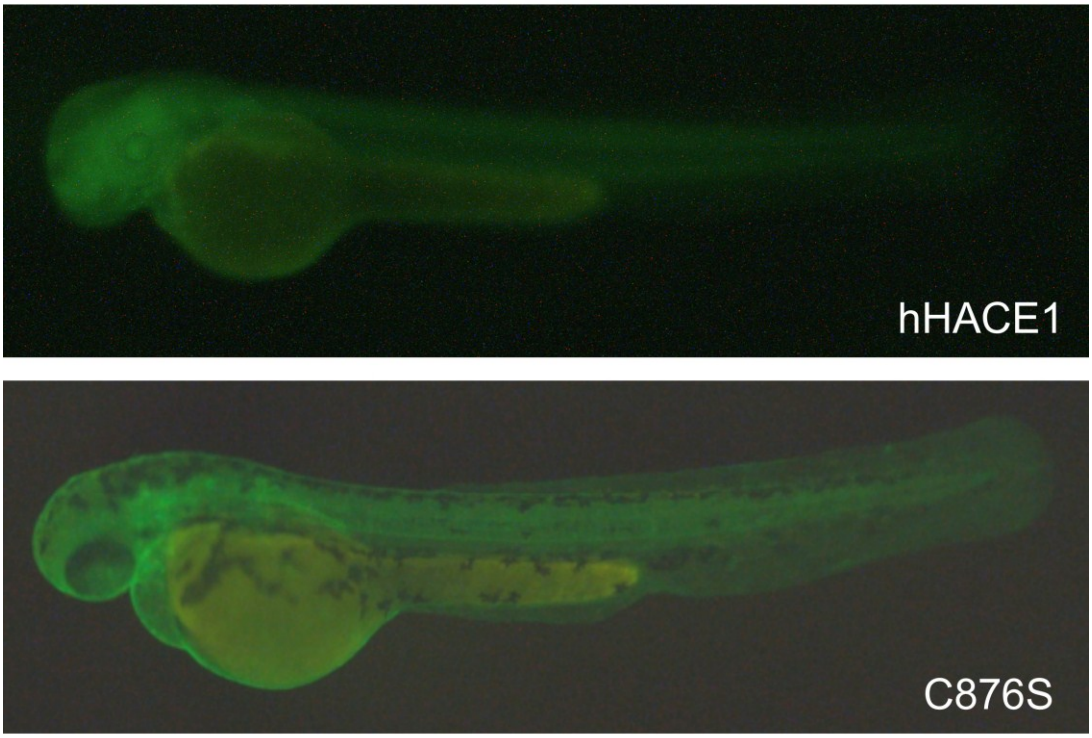

Figure 17: Stable *HACE1* and dominant negative *HACE1* transgenic zebrafish lines. Germline F2 generation transgenic zebrafish at 48 hpf expressing GFP tagged *HACEl* under control of the *β-actin* promoter (*β-actin::GFPhHACE1)* (top panel). Germline F1 generation transgenic zebrafish at 48 hpf expressing GFP tagged dominant negative *HACE1(C876S)* under control of the β-*actin* promoter (β-*actin::GFPC876S)* (bottom panel).
GFP = green fluorescent protein

gene. Six wild type (*β–actin::GFPhHACE1*) transgenic zebrafish founders and four mutated (*β–actin::GFPC876S*) founders were identified. Three of each of these lines (*hHACE1* and *C876S*) were confirmed by genotyping one fish from their F1 generation. F1 zebrafish were incrossed to generate the F2 generation (Figure 17). All experiments were performed on the embryos of the stable transgenic *HACE1* F2 generation.

3.6 Dominant Negative (*β-actin::GFPC876S*) Transgenic Zebrafish Demonstrate Increased Apoptosis

Alterations in apoptosis, and genes involved in its regulation, is instrumental in the development and progression of cancer. The ability of cancer cells to evade apoptosis is one of the fundamental hallmarks of cancer. In order to determine the effect of loss of *HACE1* function on apoptosis, an acridine orange assay was performed on transgenic embryos. Acridine orange is a well-established assay for labeling apoptotic cells in live zebrafish embryos[103,125,126]. *β–Actin::GFPhHACE1* and *β–actin::GFPC876S* transgenic zebrafish embryos (non irradiated and irradiated) were subjected to acridine orange staining at 28 hpf. Live imaging of embryos revealed an increased level of apoptosis throughout the transgenic embryos compared to wild type controls. When exposed to 16 Gy of irradiation, there were significantly increased levels of apoptosis seen in transgenic embryos compared to controls (Figure 18).

To further elucidate the mechanism underlying how *HACE1* is involved in the apoptotic pathway, an activated caspase 3 assay was performed. Caspase 3 is a member of the cysteine-aspartic acid protease family, and is an effector molecule of apoptosis.

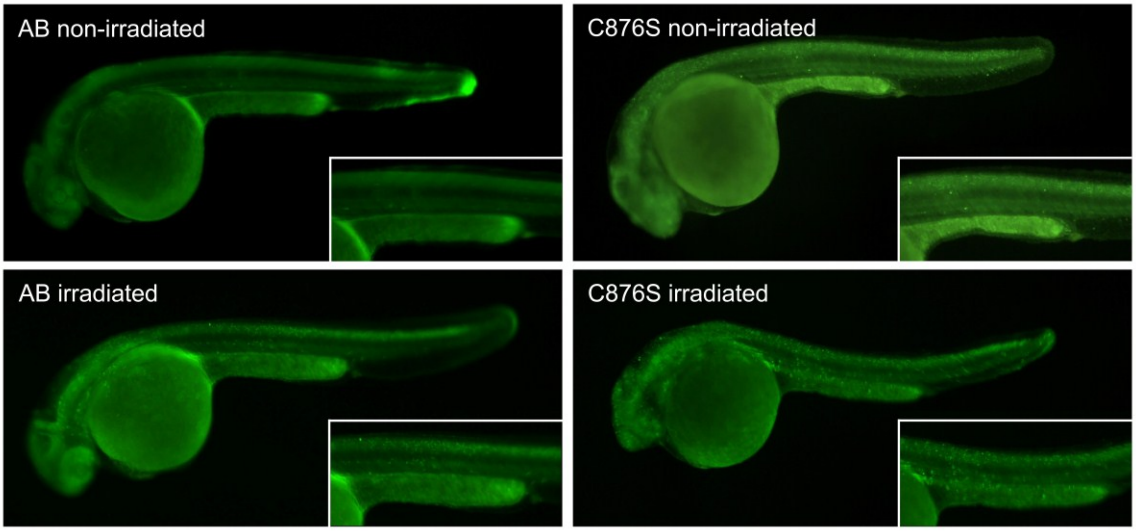

Figure 18: Dominant negative transgenic zebrafish show increased apoptosis. Acridine orange assay performed on live 28 hpf wild type and dominant negative transgenic zebrafish showing increased apoptosis in transgenic zebrafish compared to wildtype controls. Increased apoptosis is observed both prior to and following 16 Gy of gamma irradiation. Lateral view, anterior to the left, 5X objective. Inset shows magnified view of the anterior portion of the tail. hpf = hours post-fertilization, Gy = Gray.

Immunostaining with an antibody against the activated (cleaved) form of caspase 3 has been established in zebrafish literature as a measure of caspase-dependent apoptosis[127]. Preliminary results show an increase of activated caspase 3 in *β–actin::GFPC876S* transgenic embryos compared to controls (Figure 19). This assay has only been performed once due to difficulty with zebrafish breeding.

3.7 Effects of Loss of *HACE1* Function on Cell Cycle Progression

Decreased *HACE1* expression leads to a multitude of cancers in humans. Additionally, loss of *HACE1* results in a variety of malignancies in mice[89]. Cell cycle regulation is integral to normal cell proliferation, and altered regulation can lead to cellular transformation and the formation of tumours. Therefore, we were interested to examine the effects of loss of *HACE1* function on different aspects of the cell cycle using our transgenic zebrafish model. We employed 5-Bromo-2'-deoxyuridine (BrDU) to examine the S phase of the cell cycle and Phosphohistone H3 (PH3) to examine the G2/M phase of the cell cycle.

BrDU is a synthetic nucleoside that is an analogue of thymidine. BrDU is incorporated into newly synthesized DNA, and is therefore a measure of S phase of the cell cycle[128]. This assay has been well established to assess S phase of the cell cycle in zebrafish embryos, as well as adult fish[129]. *β–Actin::GFPhHACE1* and *β–actin::GFPC876S* transgenic zebrafish embryos were incubated in BrDU at 28 hpf. BrDU incorporation was assessed with a primary antibody against BrDU, followed by a fluorophore-conjugated secondary antibody. Differences in BrDU incorporation were

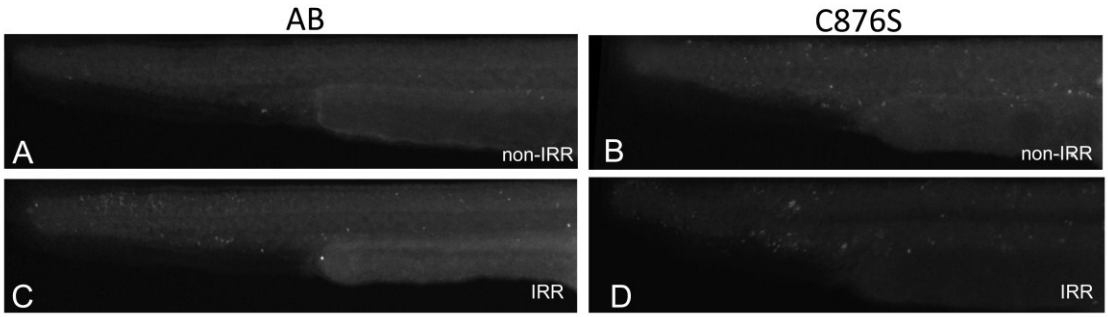

Figure 19: C876S mutants exhibit increased caspase 3 activation.
Wildtype embryos (N = 7) and dominant negative transgenic mutants (C876S) (N = 8) were irradiated at 26 hpf and stained with anti-activated caspase 3 antibody at 28 hpf. Non-irradiated embryos (wildtype (N = 6) and transgenic (N = 5)) were also stained with anti-activated caspase 3 antibody at 28 hpf. C876S mutants showed increased caspase 3 staining with or without irradiation compared to controls. Representative images shown. hpf = hours post fertilization, images lateral tail view, anterior to the right.

quantified by area fraction using ImageJ. There was no statistically significant difference in the amount of BrDU labeling when comparing transgenic zebrafish embryos to wildtype control embryos at 28 hpf, suggesting that loss of *HACE1* does not affect DNA synthesis (Figure 20).

Phosphorylation of histone H3 is a crucial step required at the onset of mitosis. An antibody has been developed against the phosphohistone H3 (PH3) protein, and has been widely used in *Drosophila* and mammalian cell lines as a marker of mitosis[130]. This assay has been adapted for use in zebrafish, thereby allowing for the assessment of cell proliferation throughout the embryo[129]. The PH3 assay was performed on wildtype and transgenic zebrafish embryos at 28 hpf, and results were quantified with ImageJ. There was no significant difference in PH3 labeling in *β–actin::GFPC876S* transgenic zebrafish embryos compared to controls at 28 hpf (Figure 21).

3.8 Transgenic Zebrafish Display Changes in Gene Expression by Micro-Array Analysis.

Micro-array analysis was used to examine the changes in gene expression in both transgenic zebrafish lines (*β–actin::GFPhHACE1* and *β–actin::GFPC876S*). Whole embryo RNA was extracted at 48 hpf from approximately 50 *β–actin::GFPhHACE1* and 50 *β–actin::GFPC876S* embryos. The RNA samples were labeled, and micro-array analysis was performed at the Atlantic Cancer Research Institute. Results were based on two sequential RNA extractions and three micro-array analyses. A heat map of upregulated and downregulated genes identified by micro-array analysis are shown in

A

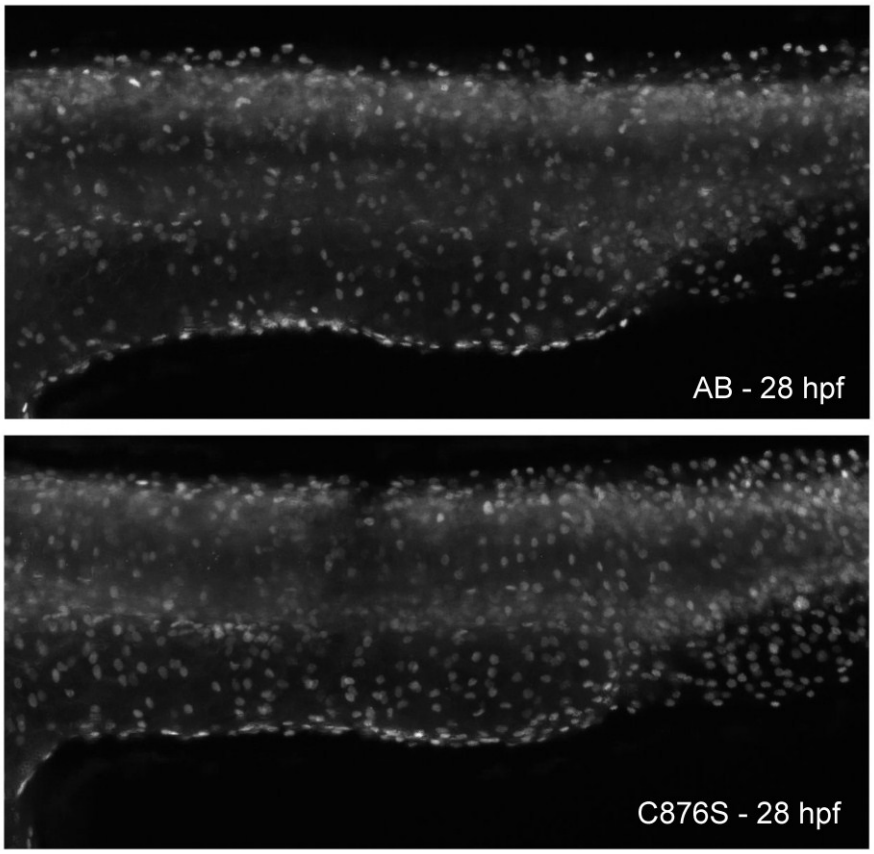
AB - 28 hpf
C876S - 28 hpf

B

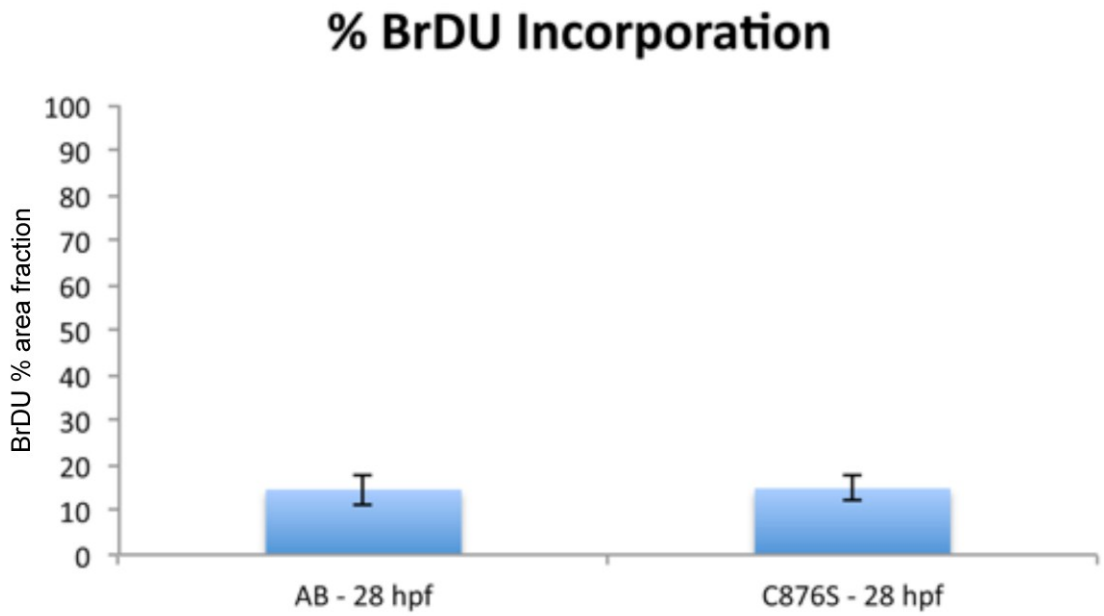
% BrDU Incorporation
BrDU % area fraction
100
90
80
70
60
50
40
30
20
10
0
AB - 28 hpf
C876S - 28 hpf

Figure 20: Dominant negative transgenic zebrafish show no difference in S phase cell proliferation.

(A) Representative image of a zebrafish tail subjected to proliferation assay performed on 28 hpf wild type or dominant negative transgenic zebrafish showing no difference in bromodeoxyuridine (BrDU) incorporation. An experiment was performed in triplicate on 7 or 8 embryos per experiment with no statistically significant difference ($p = 0.1$, $p = 0.9$, $p = 0.4$)

(B) Graphical representation of one BrDU assay showing no statistically significant difference in BrDU incorporation in dominant negative transgenic zebrafish compared to wildtype zebrafish ($N = 8$, $p = 0.9$).

hpf = hours post fertilization, images lateral tail views, anterior to the left.

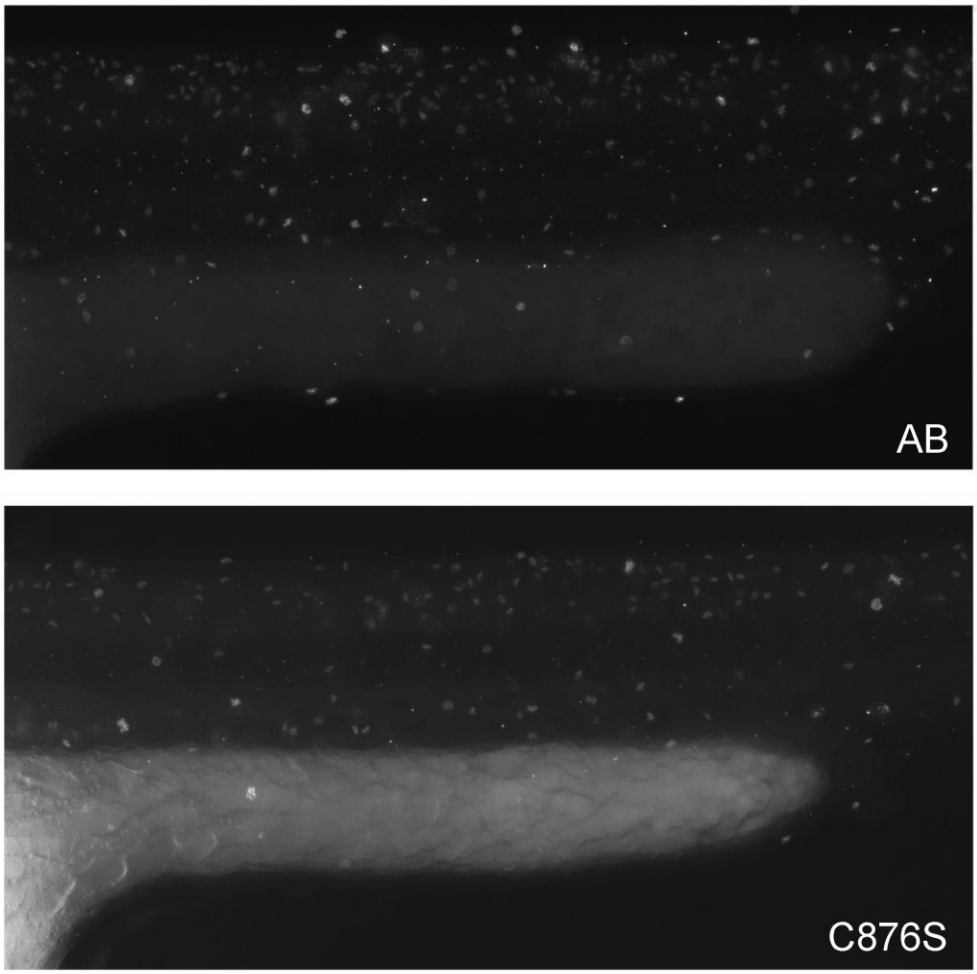

Figure 21: Dominant negative transgenic zebrafish show no difference in G2/M phase.
Representative images of wildtype and C876S transgenic mutants stained with anti-phosphohistone H3 antibody at 28 hpf. C876S mutants show no statistically significant difference in phosphohistone H3 staining compared to wildtype (1.3 ± 0.8% vs. 0.9 ±0.6%, p=0.3). Experiments were performed using 8 wildtype and 8 mutant embryos. Images lateral tail views, anterior to the left.

Figure 22. The cell cycle regulators previously identified by micro-array in *hace1* morphants have not been identified by micro-array of transgenic embyros. However, interesting genes detected include upregulation of *rbm9* and *calmodulin 3a.* *Rbm9* is highly expressed in brain (neurons), heart and skeletal muscle, and is involved in neural cell specific alternative splicing[131,132]. *Calmodulin 3a*, is a member of the calmodulin superfamily, which are involved in calcium signaling. Calmodulin is associated with neuronal potentiation, memory and learning[133].

3.9 *β-ACTIN::GFPHHACE1* AND *β-ACTIN::GFPC876S* TRANSGENIC ZEBRAFISH DEVELOP MASSES AND HAVE INCREASED MORTALITY

Transgenic fish were monitored daily for the development of tumours or for abnormal behaviour, such as unusual swimming pattern "flashing" (a fish that turns on its side and makes a rapid semicircular swimming motion) or a sick appearance. Adult fish appearing unwell or with a clinically apparent mass were euthanized, fixed and sectioned. Both transgenic zebrafish *β–actin::GFPhHACE1* and *β–actin::GFPC876S* developed to adulthood and appeared grossly normal compared to wild type zebrafish. There were a total of 59 *β–actin::GFPhHACE1* zebrafish in the laboratory (5 founders and 54 F1 generation. There were 184 *β–actin::GFPC876S* adult transgenic zebrafish in the laboratory (3 founders, 46 F1 generation and 135 F2 generation). Tables 1 and 2 summarize the transgenic zebrafish that were sacrificed. Interestingly, there were an increased number of transgenic fish (both *β–actin::GFPhHACE1* and *β–actin::GFPC876S*) that died or appeared sick compared to wildtype fish in the

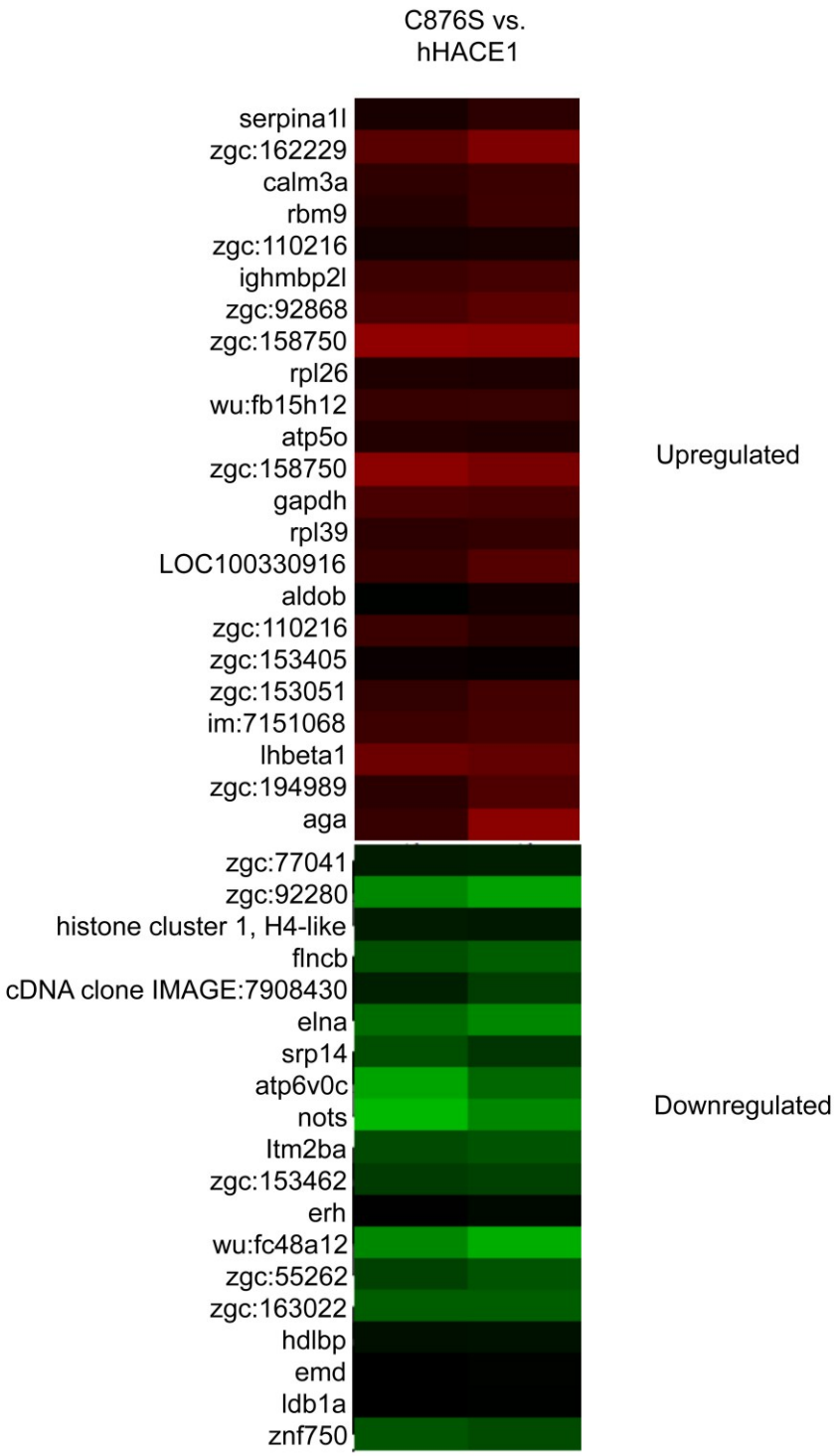
C876S vs.
hHACE1
serpina1l
zgc:162229
calm3a
rbm9
zgc:110216
ighmbp2l
zgc:92868
zgc:158750
rpl26
wu:fb15h12
atp5o
zgc:158750
gapdh
rpl39
LOC100330916
aldob
zgc:110216
zgc:153405
zgc:153051
im:7151068
lhbeta1
zgc:194989
aga
Upregulated
zgc:77041
zgc:92280
histone cluster 1, H4-like
flncb
cDNA clone IMAGE:7908430
elna
srp14
atp6v0c
nots
ltm2ba
zgc:153462
erh
wu:fc48a12
zgc:55262
zgc:163022
hdlbp
emd
ldb1a
znf750
Downregulated

Figure 22: Micro-array analysis of transgenic zebrafish embryos.
Heat map of upregulated and downregulated genes identified by micro-array performed on 48 hpf *β-actin::GFPC876S* zebrafish embryos compared to *β-actin::GFPhHACE1*. Upregulated genes include *rbm9* and *calmodulin 3a.*
Provided by Dr. Stephen Lewis, Atlantic Cancer Research Institute.

β-actin::GFPhHACE1

Age	Generation	Comment
6 months	Injected mosaic	Found dead in tank
5 months		Appeared sick
4 months		Found dead
6 months		Found dead
6 months	F1B	Found dead
3 months	F1A	Found dead
5 months	F1A	Swimming abnormal in tank
4 months	F1B	Found dead

Table 1: Summary of sacrificed adult *β-actin::GFPhHACE1* transgenic fish.
Summary of *β-actin::GFPhHACE1* transgenic zebrafish that were sacrificed because of a sick appearance in the tank, or being found dead in the tank.

β-actin::GFPC876S

Age	Generation	Comment
6 months	F1	Abnormal swimming in tank
5 months	F1	Found dead
5 months	F1B	Mass ventral anterior
3 months	F1C	Found dead
2 months	F1D	Found dead
4 months	F1A	Found dead
13 months	Injected Mosaic	Mass along abdomen
6 months	F1B	Large abdomen

Table 2: Summary of sacrificed adult *β-actin::GFPC876S* transgenic fish.
Summary of *β-actin::GFPC876S* transgenic zebrafish that were sacrificed because of a clinically apparent mass, a sick appearance in the tank, or being found dead in the tank.

laboratory. Of note, all of these fish were young (4-13 months post fertilization) in age when they appeared unwell. There were two *β–actin::GFPhC876S* fish that developed a mass (Figure 23). Both of these fish displayed green fluorescent protein when visualized under the microscope. One of these zebrafish was four months of age. The 4 month old fish was sectioned and stained with hematoxylin and eosin (H&E). Upon examination of the histological sections, the mass located on the anterior, ventral side (indicated by an arrow in Figure 23A) of the fish was its heart, which was enlarged and full of blood. There was no evidence of malignancy anywhere throughout the fish. The second fish was 13 months old and had an enlarged abdomen with some ulceration on its scales (Figure 23B). The histological sections did not reveal any evidence of malignant tissue. The remaining transgenic zebrafish in the laboratory are continuing to be monitored for the development of masses.

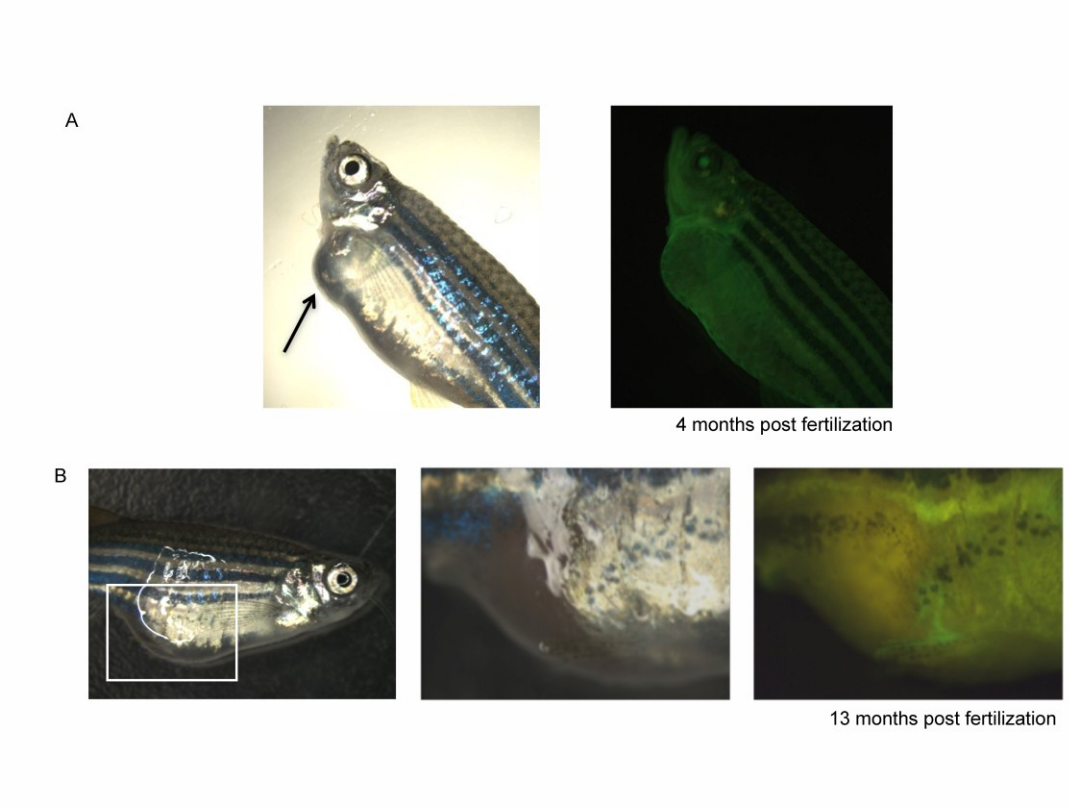

Figure 23: Dominant negative transgenic zebrafish develop masses at an early age.
(A) C876S dominant negative transgenic zebrafish with a mass located on the ventral anterior side (arrow) by 4 months post fertilization. Fluorescence imaging confirms the presence of green fluorescent protein.
(B) Mosaic injected C876S dominant negative transgenic zebrafish with a large abdomen and scale changes (middle panel) at 13 months post fertilization. Middle (brightfield) and right panel (flurorescence) are magnified views of the left panel. Fluorescence imaging confirms mosaic green fluorescent protein.

CHAPTER 4 DISCUSSION

4.1 *HACE1* EXPRESSION IS CONSERVED IN ZEBRAFISH

The use of animal models in the research and investigation of human cancers serves to identify and characterize molecular mechanisms of disease within a whole organism. Classically, *in vitro* studies set up a controlled environment, in most cases delivering optimum experimental conditions. While lacking this optimal control, *in vivo* models more closely represent the complex intracellular interactions present in the human body, thereby offering crucial insight into the multifaceted network of signalling pathways. In order to serve as a useful tool in molecular pathology research, *in vivo* animal models rely on gene homology with their human equivalents.

The zebrafish was first used by George Streisinger and colleagues to study vertebrate development in the 1960s, and has proven to be an incredibly useful model for development, disease and cancer research[97,134]. Due to their external fertilization, clutches consisting of large numbers of transparent embryos and their rapid embryonic development, zebrafish provide many technical advantages in the study of developmental processes at very early stages, providing visual data that would be extremely technically challenging to ascertain in a more traditional mammalian animal model. Furthermore, their fully sequenced genome facilitates the identification and characterization of numerous genes with critical cellular functions, not to mention oncogenes and tumour suppressing genes, with striking similarity to human counterparts. Thus, research using zebrafish has the capacity to complement knowledge gained from murine studies and will provide insight into the role of *HACE1* in human development and oncogenesis.

We have identified a *HACE1* homologue in zebrafish that shares 74.7% DNA homology, and 88.9% protein identity. Because of its high degree of sequence similarity at both the DNA and protein levels, we believe that the normal developmental functions of zebrafish *hace1* are similar to that of human *HACE1*. More importantly, zebrafish *hace1* shares the distinctive structural and functional domains that are found in the human gene (ankyrin repeat domain and HECT domain). According to the most up to date zebrafish genome sequence (Zv9), the critical cysteine residue in human *HACE1,* found at amino acid 876, is conserved in the zebrafish protein sequence (Ensembl). Previous studies using human tissue have demonstrated that there is strong *HACE1* mRNA expression in brain, heart and kidney tissue[31]. HACE1 protein is detected in fetal kidney samples, suggesting that it has a developmental role[31]. Zebrafish antibodies have been previously limited but more recently have become commercially available; however, there are no antibodies readily available against zebrafish *hace1* at the current time. Therefore, *hace1* expression data is limited to RNA expression until an antibody is raised for use in protein studies.

We hypothesized that *hace1* expression was conserved in zebrafish. In order to validate the zebrafish as a model for studying the function of *HACE1,* WISH studies were performed to demonstrate conserved *HACE1* expression. I created antisense digoxigenin-labeled probes to the zebrafish *hace1* sequence within either the ankyrin repeat domain or the HECT domain. These sequences were chosen for probes, as the plasmids possessing these sequence domains were commercially available.

Single WISH studies using the probe to the ankyrin repeat domain of *hace1* revealed relatively widespread expression throughout the zebrafish embryo. Ankyrin

repeat domains are 33 amino acid motifs consisting of two alpha helices separated by loops. They were first discovered in yeast cdc10 and *Drosophila melanogaster* Notch proteins in 1987[135]. Ankyrin repeat motifs are among the most abundant protein motifs found in nature, being present in 3608 proteins[136]. It is therefore plausible that the extensive staining visualized throughout the early zebrafish embryo is a reflection of lack of specificity of the antisense probe to zebrafish *hace1*, and binding to other RNA sequences containing ankyrin repeats.

An antisense digoxigenin RNA probe was subsequently made to the sequence from GenBank accession number CT707500, which corresponds to the HECT domain sequence of zebrafish *hace1*. A BLAST search (National Centre for Biotechnology Information, Bethesda, MD, USA) showed sequence specificity with zebrafish *hace1* and the BAC clone CH73-97E20. WISH studies performed with this probe confirmed expression at the RNA level in heart, kidney, and brain tissue, which is consistent with human *HACE1* RNA expression profiles[31]. Double *in situ* hybridization (both with single and double fluorescence) with known tissue probes again confirmed expression of *hace1* in kidney and heart tissue. Double *in situ* with the *hace1* HECT domain probe and *krox20* suggests that there is *hace1* expression in the brain. *Krox20* was used as an initial central nervous system (CNS) probe available in the Berman laboratory. It is a very specific neural probe, labeling rhombomeres 3 and 5 in the hindbrain[137]. Future studies to confirm neural *hace1* expression should be undertaken with a more ubiquitous CNS probe, such as 3-monooxygenase/tryptophan 5-monooxygenase activation protein gamma polypeptide 1 (*ywhag1*), which is expressed in the diencephalon, tegmentum and hindbrain[138]. Given the degree of homology between zebrafish and human *HACE1,* and

conserved tissue expression, these data support the use of zebrafish as a model to study the role of *HACE1*.

4.2 *HACE1* IS REQUIRED FOR CARDIAC DEVELOPMENT

Zebrafish provide an ideal organism for studying vertebrate development, as their embryos are virtually transparent, and organogenesis can easily be monitored by live visualization, as well as with whole mount *in situ* hybridization[97]. Morpholinos allow for the temporary knockdown (approximately 72 hours post fertilization) of genes within the zebrafish genome[139]. Given the technical difficulties and high cost of generating stable knockout lines in zebrafish, morpholino knockdown has been extensively used and proven to be extremely valuable for studying the role of critical early developmental genes. In this study, a morpholino was designed to a splice site located in the *hace1* transcript, in order to determine a possible role of *hace1* in zebrafish development. This splice site was chosen as it is located within the catalytically active HECT domain, and it is positioned upstream of the critical cysteine residue required for *HACE1* ubiquitin ligase function. Injection of this morpholino results in aberrant splicing, leading to loss of an exon within the HECT domain, and therefore presumed loss of function.

The zebrafish heart consists of 4 chambers in series, the sinus venosus, atrium, ventricle and bulbus arteriosus. Unlike the human heart, the zebrafish heart possesses a single atrium and single ventricle. Deoxygenated blood enters the sinus venosus, travels through the atrium and ventricle and then the bulbus arteriosus. The deoxygenated blood is then pumped to the ventral aorta, where it becomes oxygenated in the gills, and is

subsequently delivered to the zebrafish organs and tissues[117]. Valves are formed between the chambers of the zebrafish heart by 5 dpf. At 48 hpf, the heart chambers are clearly defined by a constriction between the segments, and cardiac contractions can be clearly identified with microscopy.

Initially, the *hace1* HECT domain morpholino was injected into wildtype zebrafish embryos, and the dose was titrated to the appearance of a phenotype. When injected at a concentration of 1.6 mM, by 48 hpf, *hace1* morphants displayed severely abnormal cardiac structure and function compared to embryos injected with a control morpholino. The embryos were otherwise developmentally normal appearing. To confirm specificity, I took advantage of the *cmlc2::GFP* zebrafish line, which has green fluorescent protein labeled cardiac tissue[116] and generated *hace1* morphants in this line by injecting 1.6 mM of *hace1* morpholino. It was strikingly evident that *hace1* morphants lost the defined constriction between their atrium and ventricle, resulting in a "tubular" appearance of their heart. Associated with this defect were large pericardial effusions that developed by 48 hpf. None of the *hace1* morphants survived longer than 6 dpf, suggesting that loss of *hace1* is developmentally lethal. It is unclear whether these embryos were dying secondary to an unknown cause; however, given the degree to which cardiac function is affected, it seemed likely that their functionally abnormal hearts were unable to sustain organ and tissue oxygen demand. When quantified, *hace1* morphants had a statistically significant increase in cardiac abnormalities compared with the control morpholino group ($p=0.0007$). Additionally, there was a significantly higher mortality rate observed in *hace1* morphants. Therefore, the number of cardiac defects observed may be underestimated, as embryos alive at 48 hpf were analyzed for developmental cardiac

defects. These results also confirm that *hace1* is required for zebrafish development, as none of the morphants survived past the first week of life.

In order to further elucidate specifically how cardiac development is altered by loss of *hace1* function, we are collaborating with Dr. Ian Scott at the University of Toronto. In Dr. Scott's laboratory, *hace1* morphants were subjected to WISH at 24 hpf and 48 hpf with probes to different structures within the forming heart. WISH using the probe to *cmlc2* shows that cardiomyocyte bulk is not significantly affected, however more sophisticated methods are required to examine this in more detail (Figure 24). WISH was also performed on *hace1* morphants with the following battery of probes:

vmhc – heart ventricle

amhc – heart atrium

tbx2b – atrioventricular canal

nppa – heart inner and outer curvature

The results of WISH studies using these probes are shown in Figure 24. The ventricle was unchanged at 24 hpf; however, it was morphologically altered by 48 hpf, whereby ventricle remains located in the midline of the zebrafish embryo. It was similarly apparent that the heart remained midline in the WISH studies performed using the probe to *cmlc2*. This observation is termed a "looping defect". The WISH using the *tbx2b* probe did not appear to be stained optimally, and should be repeated to better examine the atrioventricular canal in *hace1* morphants. Further studies are needed to confirm the role of *HACE1* in cardiac development. Co-injection of *hace1* morpholino with human *HACE1* mRNA should be performed to assess whether human *HACE1* mRNA is able to rescue the cardiac phenotype that is observed in *hace1* morphants. This

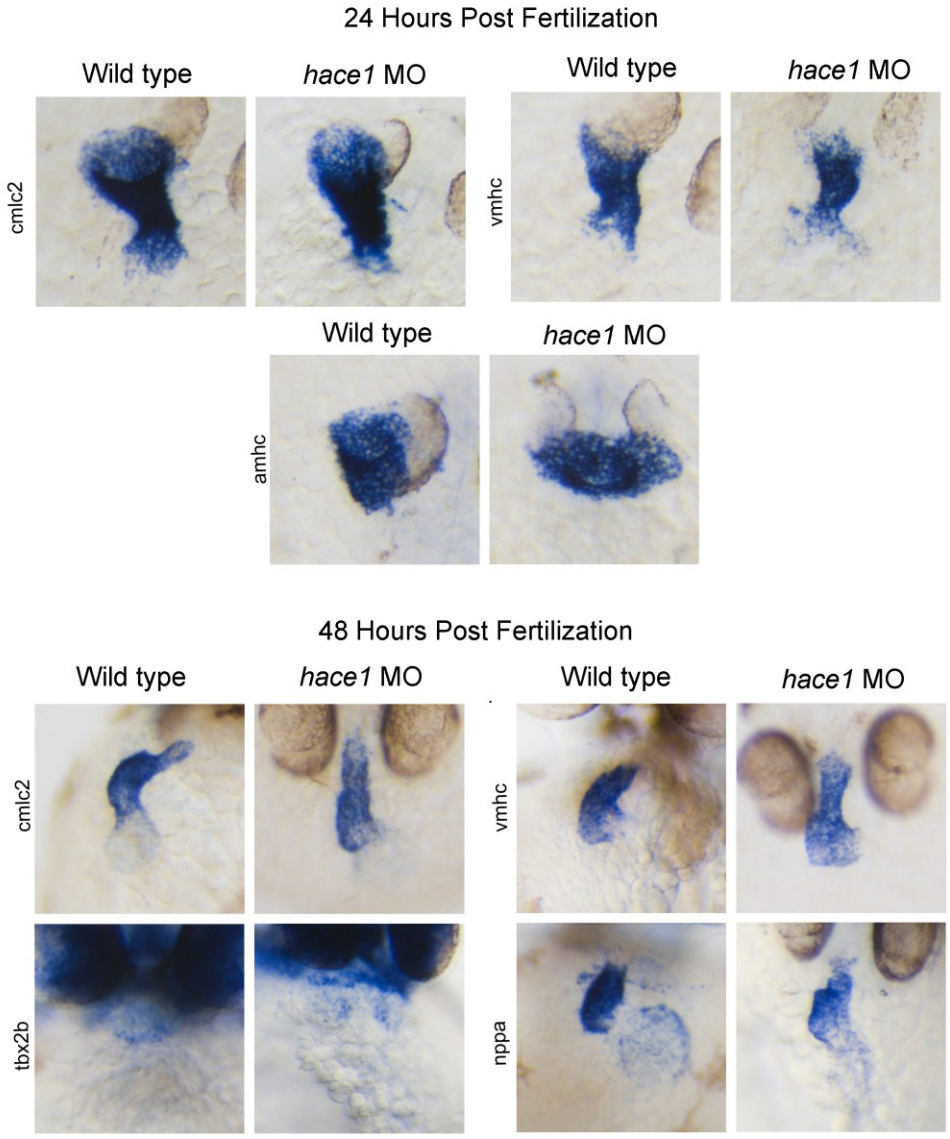

Figure 25: *hace1* morphants display a cardiac "looping defect"
Whole mount *in situ* hybridization (WISH) of *hace1* morphants and wildtype embryos at 24 hpf and 48 hpf using specific cardiac probes. Knockdown of *hace1* by morpholino injection results in abnormal ventricle morphology at 48 hpf. The developing hearts in *hace1* morphants remain in the midline (looping defect) compared to wildtype control embryos at 48 hpf.
hpf = hours post fertilization.
Provided by Dr. Ian Scott, University of Toronto.

would suggest that the cardiac abnormalities seen in *hace1* morphants are caused by *hace1* knockdown, and not the result of an off-target morpholino effect, thereby strengthening the evidence that *HACE1* is involved in cardiac development.

The cardiac defect observed in *hace1* morphants may be akin to human atrioventricular canal defects in that the definition between the atrium and ventricle is abolished. Interestingly, when the term "atrioventricular canal defect" is searched in the OMIM database, there are results that map to chromosome 6q21, the *HACE1* locus. Future research could assess for *HACE1* deletions or mutations using blood samples or buccal swabs from children diagnosed with congenital cardiac defects, and may discover a new gene involved in genesis of congenital heart defects.

4.3 *HACE1* AFFECTS VASCULATURE DEVELOPMENT

Following the finding that loss of *hace1* function by morpholino injection leads to aberrant cardiac development, we wondered if this was limited to the heart tissue, or if there may be a more global defect in the zebrafish vasculature development. A close relationship exists between heart development and vasculogenesis. Throughout mammalian development, the heart forms initially as a paired tube. Regions within the mesoderm differentiate into blood vessels and fetal red blood cells. These vessels then connect to the heart tube[140]. Therefore, we used the *fli1::GFP* zebrafish line, which has green fluorescent protein expression in the endothelium, thereby labeling blood vessels throughout the organism. Preliminary results showed that *hace1* morphants had a more disorganized vasculature throughout the length of the zebrafish tail compared to controls

(Figure 14). The intersomitic vessels in control embryos arborize in a very orderly fashion. In contrast, *hace1* morphants lack the normal defined vascular architecture, and have a more disorganized appearance. This experiment has only been performed once, and has not been quantified for statistical significance; however, it provides preliminary data suggesting that *hace1* may play a role in the formation of blood vessels. The tails of these *hace1* morphants are slightly more curved in the lateral direction than control embryos, which might be a reflection of inadequate blood flow to the forming tail tissue. However, it is also possible that loss of *hace1* function results in an abnormal tail morphology, and as a result, subsequent disorganized vasculature. As in mammals, vasculogenesis in the zebrafish involves the differentiation of hemangioblasts from the mesoderm, with subsequent differentiation of angioblasts and endothelial cells[141].

Additional studies are required to dissect this effect further, including repeating experiments to better characterize the abnormal vascular structure. Angiogenesis is an integral part of tumour growth and maintenance. It involves the generation of new blood vessels within tumour tissue, and allows for delivery of adequate blood flow and oxygen. Key mediators of angiogenesis include vascular endothelial growth factor (VEGF), platelet-derived growth factor, fibroblast growth factor and their receptor tyrosine kinases[10,11,142]. Angiogenesis has become a key focus in cancer research and many antiangiogenic chemotherapeutic agents are currently being tested in clinical trials[143]. The abnormal vasculature observed in *hace1* morphants suggests a possible role for *HACE1* in angiogenesis. Tumours in *hace1-/- Tp53-/+* mice grew to enormous size in a short time period[89]. It is possible that this rapid tumour growth was accompanied by angiogenesis. Future work in the zebrafish focusing on angiogenesis mediators may

provide insight into the mechanism by which downregulation of *HACE1* results in tumour formation and rapid growth.

4.4 *HACE1* Transgenic Zebrafish Provide a Model for Studying Cancer

In order to assess the mechanism by which *HACE1* is involved in cellular transformation, and malignancy, I generated a transgenic zebrafish line harbouring either the wildtype human *HACE1* gene, or a dominant negative mutated human *HACE1* gene. These genes were introduced into the zebrafish genome under control of the ubiquitous β–actin promoter, in order to mimic the known diffuse expression of human *HACE1*. Zebrafish with *HACE1* integration were identified by the presence of green fluorescent protein. As mentioned previously, it has been difficult to develop knockout lines in zebrafish, which is standard practice in mammalian research. Therefore, dominant negative mutations are used to create a loss of function phenotype. These transgenic can be studied for embryonic/developmental phenotypes, as well as grown to adult age, and monitored for the onset of malignancy.

I generated six stable transgenic zebrafish lines expressing wildtype human *HACE1 (β–actin::GFPhHACE1)*. These transgenic fish may represent a model of overexpression of *HACE1,* as *HACE1* expression is ubiquitous in these fish. Prior to my creation of *β–actin::GFPhHACE1* transgenic zebrafish, there were no *in vivo* studies with overexpression of *HACE1* reported in the literature. *β–Actin::GFPhHACE1* fish appear grossly normal during embryonic development and continue to have a normal appearance

through to adulthood. Therefore, *HACE1* overexpression appears to not be severely toxic to zebrafish, and does not convey a lethal phenotype. They began breeding at approximately 3 months of age, consistent with wildtype zebrafish, suggesting that they reach sexual maturity at the usual developmental time point. However, there has been some difficulty mating these transgenic fish, suggesting that *HACE1* might be somehow harmful to the zebrafish sperm or eggs. As a result, the *β–actin::GFPhHACE1* zebrafish could not be used in apoptosis and cell cycle studies because of the lack of embryo numbers. Conducting apoptosis and cell cycle studies in the *β–actin::GFPhHACE1* line would enable the evaluation of the effect of overexpression of *HACE1* on cell cycle regulation and apoptosis.

I created four stable transgenic zebrafish lines expressing a dominant mutated human *HACE1 (β–actin::GFPC876S).* This line was then used to assess the effect of loss of *HACE1* at different points within the cell cycle, as well as the effect on apoptosis. Using this transgenic zebrafish model, I have shown that dominant negative mutated *HACE1* results in increased apoptosis compared to wildtype control zebrafish. This result was consistent in non-irradiated embryos, as well as embryos exposed to 16 Gy of radiation. Given that *HACE1* functions as a tumour suppressor, it was hypothesized that loss of *HACE1* function would lead to decreased apoptosis. My results show the opposite, with increased apoptosis observed by acridine orange assay. Additionally, preliminary results using an activated caspase 3 assay support this phenotype of increased apoptosis, although this assay needs to be repeated for validation. It is possible that loss of *HACE1* on its own is insufficient for cells to evade apoptosis. The ability to evade apoptosis is a common phenotype of many human cancers[2]. It is possible that under

other stress conditions (i.e. oxidative stress), loss of *HACE1* promotes cell survival. Homozygous *Hace1* mutant mice with a single mutant p53 allele display greatly increased tumour incidence, suggesting cooperativity between *HACE1* and p53[89]. I attempted to assess whether this association between *HACE1* and p53 would lead to decreased apoptosis and increased cell survival. Unfortunately, I was unable to generate a sufficient number of *β–actin::GFPC876S* crossed with mutant p53 zebrafish to complete an acridine orange or activated caspase 3 assay. An additional mechanism by which this could be studied is by injection of *β–actin::GFPC876S* transgenic zebrafish embryos with a p53 morpholino. Future work should investigate the effect of mutant *HACE1* and p53 on apoptosis pathways.

Another hallmark of cancer is increased cell proliferation. This phenotype is accomplished in several cancers by dysregulation at cell cycle checkpoints. Using dominant negative mutated *HACE1* zebrafish, I examined the effect of loss of *HACE1* function on different aspects of the cell cycle. I started by examining the S phase of the cell cycle using a BrDU incorporation assay[129]. This was chosen as a starting point, as this assay is well established in the Berman lab. I have shown that there was no difference in S phase of the cell cycle by BrDU incorporation. It is possible that loss of *HACE1* function is insufficient on its own for increased proliferation. It is also possible that DNA replication is not affected by *HACE1,* but that *HACE1* exerts its function at different points in the cell cycle. *In vitro* studies have shown that overexpression of *HACE1* results in decreased cyclin D1, suggesting that *HACE1* may modulate its malignant potential at the G1/S phase transition[89]. There was, however, no change in cyclin D1 with expression of ligase-dead C876S *HACE1*. It might be expected that

dominant negative *HACE1 (C876S)* would result in an increase in cyclin D1, and thus increased progression to S phase; however, *in vitro* studies with expression of mutated *HACE1 (C876S)* show no difference in cyclin D1 compared to vector alone. *In vivo* assessment of S phase of the cell cycle in zebrafish harbouring *HACE1 (C876S)* reflect the results from *in vitro* studies.

Phosphohistone H3 is a marker of mitosis and marks the G2 to M transition in the cell cycle. This assay is also well established in the Berman laboratory. Dominant negative transgenic *HACE1 (C876S)* zebrafish were subjected to a phosphohistone H3 assay at 28 hpf. Compared to wildtype control fish, there was no difference in phosphohistone H3 staining, suggesting that both transgenic and wildtype fish had similar rates of mitosis. Once again, there was insufficient numbers of *β–actin::GFPhHACE1* to include in this assay. It would be interesting to examine the effect of overexpression of *HACE1* on mitosis. The lack of a change in cell division suggests that *HACE1* does not affect the G2/M phase of the cell cycle. Subjecting these dominant negative mutated fish to additional genetic mutations, such as p53, may be required to result in increased cell division.

Ultimately, we anticipated that the *HACE1* transgenic zebrafish would develop clinically apparent malignancies. To date, two dominant negative fish have displayed masses, and were sacrificed and sectioned. To date, we have not identified any malignant tissue in either of these fish; although, further sectioning is currently being performed at the University of British Columbia. Both transgenic fish expressing wildtype human *HACE1,* and those fish expressing dominant negative *HACE1* have significantly increased mortality over wildtype fish in the laboratory. Alteration of *HACE1* expression

(overexpression or loss of function) appears to affect the zebrafish, leading to increased mortality; however, the underlying etiology remains uncertain. The fish that have been sacrificed or found dead do not display any evidence of infection. Further pathological investigation of these and other dying transgenic fish may reveal a cause of death in these fish.

4.5 Micro-Array Analysis Reveals Changes in Cell Cycle Genes and Developmental Genes

Zebrafish micro-array chips are now commercially available. In collaboration with Dr. Stephen Lewis at the Atlantic Cancer Research Institute, micro-array analysis of *hace1* morphants identified an upregulation of *cyclin G1,* and in one of the experiments, identified *cyclin D1*, both of which are involved in cell cycle regulation. As mentioned previously, *in vitro* studies showed a decrease in *cyclin D1* with overexpression of *HACE1*. Our *in vivo* results in *hace1* morphants compliment this data, as one would expect that with knockdown of *HACE1,* that *cyclin D1* might be upregulated. These results suggest that downregulation of *HACE1* allows increased cell cycle progression through the G1/S phase transition. Cell cycle assays performed on dominant negative mutated *HACE1 (C876S)* transgenic embryos demonstrated no difference in S phase of the cell cycle by BrDU incorporation. *In vitro* studies of overexpressed *HACE1* identified a decrease in *cyclin D1*; however, loss of function by dominant negative mutation did not reveal any changes in *cyclin D1* expression [89]. The similar rates of S phase by BrDU incorporation in transgenic zebrafish are consistent with *in vitro* studies,

suggesting a similar transition of cells into S phase. *Hace1* morphants resulted in upregulation of *cyclin D1*. It is possible that use of a morpholino is a more robust knockdown of *hace1* function. Cyclin G1 is a p53-dependent cyclin, induced in response to DNA damage, and may play a role in G2/M phase arrest[144]. The upregulation of *cyclin G1* in *hace1* morphants that we identified is interesting, given that *HACE1* knockout mice display increased tumours when p53 is mutated[89]. Also, this suggests a possible mechanism through which *HACE1* results in cell survival. Cells may arrest at the G2/M phase transition, leading to increased cell survival. However, there was no statistically significant difference at the G2/M phase transition by PH3 assay using C876S transgenic zebrafish embryos.

Micro-array analysis of *hace1* morphants also identified an upregulation of *sox3*. Sox3 is a member of the SRY box proteins, and is involved in neural development. Sox3 maintains a stem cell like state, and inhibits neuronal differentiation[145]. As *HACE1* has strong expression in brain tissue, this supports a role for *HACE1* in neuronal development[31]. Downregulated genes identified by micro-array analysis of *hace1* morphants include guanidinoacetate N-methyltransferase (*gamt*), and ELAV-like 3 protein. GAMT is involved in creatine biosynthesis, which is important to cardiomyocytes. Knockdown of *hace1* by morpholino resulted in altered cardiac structure, potentially implicating *gamt* in this altered cardiac phenotype, although, mouse models of *gamt* deficiency do not show changes in cardiac structure of function[146]. However, *gamt* deficiency has been implicated in epilepsy and extrapyramidal movement disorders, linking downregulation of *gamt* with neural phenotypes[147]. ELAV-like protein

3 is a neural specific RNA binding protein[148]. Micro-array results once again suggest a neural phenotype in *hace1* morphants by downregulation of ELAV like protein 3.

Micro-array analysis using transgenic zebrafish failed to identify some of the same genes as *hace1* morphants. *β–Actin::GFPC876S* fish were compared to *β–actin::GFPhHACE1* fish, and therefore may not be a true representation of loss of *HACE1* function compared to wildtype controls. Overexpresion of *hace1* may alter signaling pathways, and therefore may not identify the true changes in gene expression caused by loss of *hace1* function by the dominant negative mutation. A micro-array should be performed comparing *β–actin::GFPC876S* RNA to wildtype RNA.

4.6 CONCLUSIONS

In summary, this work has shown that *HACE1* expression is conserved in zebrafish, validating the use of zebrafish as a model system to study the role of the *HACE1* tumour suppressor. *HACE1* expression at early embryonic time points (24 hpf – 7 dpf) reflects the expression pattern in humans, as there is evidence of *HACE1* expression in fetal development. It also suggests that *hace1* possesses a key developmental role. The developmental role of *HACE1* was assessed in zebrafish by knockdown of *hace1* using a morpholino targeting a *hace1* splice site within its catalytic domain. *Hace1* morphants show severe cardiac abnormalities, implicating *hace1* in cardiac development.

I have established transgenic zebrafish lines expressing dominant negative mutated human *HACE1* and wildtype human *HACE1,* which serve as a platform to

investigate the effect of *HACE1* on tumourigenesis. Initial studies show that loss of *HACE1* function results in increased apoptosis, but no change in S phase or G2/M phase transition of the cell cycle. There is currently no prior published literature on the effect of *HACE1* at these cell cycle timepoints.

Micro-array analysis of *hace1* morphants, as well as transgenic zebrafish embryos, identified upregulated and downregulated genes, including genes involved in cell cycle progression and neural development. *In vitro* studies have implicated cyclin D1 as a potential *HACE1* mediator of cell proliferation. Microarray analysis of *hace1* morphants has identified *cyclin D1* as an upregulated gene. This finding supports a proliferation phenotype with loss of *hace1,* by increased G1/S phase transition via upregulated *cyclin D1*. These microarray results provide an interesting framework for future studies using zebrafish.

4.7 FUTURE DIRECTIONS

These studies have established the zebrafish as a model for investigating the role of *HACE1* in normal development and tumourigenesis. Future experiments are required to validate *hace1* expression in neural tissue. Since genes involved in neural development have been identified by micro-array analysis, and there is strong *HACE1* expression in brain tissue, it will be important to confirm that zebrafish express *hace1* in neural tissue. This can be accomplished by double *in situ* hybridization with neural specific probes.

Knockdown of *hace1* using a morpholino results in aberrant cardiac structure. Studies are underway by our collaborators in Dr. Ian Scott's laboratory at the University of Toronto to further dissect out the specific cardiac abnormality. *In situ* hybridization of *hace1* morphants suggests a looping defect present by 48 hpf. It will be essential to show rescue with co-injection of morpholino with *HACE1* mRNA to confirm specificity of this cardiac phenotype. We hypothesize that the addition of wildtype human *HACE1* mRNA will rescue the cardiac phenotype. Additionally, studies can be undertaken using blood samples or buccal swabs from children with cardiac defects. Genetic screening of chromosome 6q21 may reveal mutations within the *HACE1* gene, and may potentially identify HACE1 as a novel gene involved in congenital heart defects.

I have established transgenic zebrafish lines to be used as a cancer research model. This approach utilizes a dominant negative mutation, as knockout zebrafish have been difficult to create. Activated caspase 3 and phosphohistone H3 assays will need to be repeated in order to validate the results that I have reported. Additionally, the cooperativity between *HACE1* and p53 should be investigated by breeding these transgenic zebrafish with p53 mutants. Acridine orange and activated caspase 3 assays, as well as cell cycle (BrDU and phosphohistone H3) assays can be performed to elucidate how *HACE1* and p53 may interact to form tumours. Additionally, RNA from these fish, or transgenic fish injected with p53 morpholino can be subjected to micro-array analysis in order to investigate what downstream targets are affected. In order to assess the effect of DNA damage on loss of *hace1* function, *hace1* morphants or dominant negative transgenic zebrafish embryos can be irradiated. Micro-array analysis of these irradiated embryos may provide insight into the downstream genes involved in cell transformation.

Surveillance of transgenic zebrafish is ongoing, and will continue. Zebrafish displaying masses or tumours or appearing sick will be sacrificed and sectioned. In collaboration with Dr. Poul Sorensen at the University of British Columbia, these fish will be analyzed for tumour formation.

Until recently, the zebrafish community has relied on the use of zebrafish lines with dominant negative mutations in order to study loss of gene function. A recent technique for gene inactivation in zebrafish is the use of zinc finger nucleases. Zinc finger nucleases recognize a specific DNA sequence, and upon binding, cause a double strand break. This break is then repaired by nonhomologous recombination, which frequently leads to small insertions or deletions[99]. This technique enables site directed mutagenesis of a particular gene of interest. Generation of zinc finger nucleases has been hindered by the lack of publicly available methods for engineering zinc finger arrays. Context dependent assembly (CoDA) is a publicly available set of reagents and software, making this technology more accessible[115]. The National Institutes of Health (NIH) is supporting an initiative to generate mutated zebrafish lines using zinc finger nucleases. We submitted *HACE1* as a potential gene for NIH to target in their efforts. *HACE1* was selected, and will therefore be targeted for mutagenesis. This generated zebrafish line will be utilized to dissect the effect of *hace1* on cell cycle regulation, and can be subjected to micro-array analysis in order to determine downstream targets of *hace1*. This will be an extremely valuable tool for studying *HACE1* in the zebrafish.

REFERENCES

1. Hanahan, D. & Weinberg, R.A. The hallmarks of cancer. *Cell* **100**, 57-70 (2000).

2. Hanahan, D. & Weinberg, R.A. Hallmarks of cancer: the next generation. *Cell* **144**, 646-674 (2011).

3. Nicholson, R.I.*, et al.* Growth factor signalling in endocrine and anti-growth factor resistant breast cancer. *Rev Endocr Metab Disord* **8**, 241-253 (2007).

4. Knudson, A.G., Jr., Hethcote, H.W. & Brown, B.W. Mutation and childhood cancer: a probabilistic model for the incidence of retinoblastoma. *Proc Natl Acad Sci U S A* **72**, 5116-5120 (1975).

5. Huang, L., Frampton, G., Liang, L.J. & Demorrow, S. Aberrant DNA methylation profile in cholangiocarcinoma. *World J Gastrointest Pathophysiol* **1**, 23-29 (2010).

6. Chou, R.H., Lin, S.C., Wen, H.C., Wu, C.W. & Chang, W.S. Epigenetic activation of human kallikrein 13 enhances malignancy of lung adenocarcinoma by promoting N-cadherin expression and laminin degradation. *Biochem Biophys Res Commun* (2011).

7. Meng, Y.*, et al.* Epigenetic Inactivation of the SFRP1 Gene in Esophageal Squamous Cell Carcinoma. *Dig Dis Sci* (2011).

8. Hanahan, D. & Folkman, J. Patterns and emerging mechanisms of the angiogenic switch during tumorigenesis. *Cell* **86**, 353-364 (1996).

9. Nagy, J.A., Chang, S.H., Shih, S.C., Dvorak, A.M. & Dvorak, H.F. Heterogeneity of the tumor vasculature. *Semin Thromb Hemost* **36**, 321-331 (2010).

10. Andrae, J., Gallini, R. & Betsholtz, C. Role of platelet-derived growth factors in physiology and medicine. *Genes Dev* **22**, 1276-1312 (2008).

11. Ferrara, N. Role of vascular endothelial growth factor in the regulation of angiogenesis. *Kidney Int* **56**, 794-814 (1999).

12. Van Meter, M.E. & Kim, E.S. Bevacizumab: current updates in treatment. *Curr Opin Oncol* **22**, 586-591 (2010).

13. Fidler, I.J. The pathogenesis of cancer metastasis: the 'seed and soil' hypothesis revisited. *Nat Rev Cancer* **3**, 453-458 (2003).

14. Yilmaz, M. & Christofori, G. Mechanisms of motility in metastasizing cells. *Mol Cancer Res* **8**, 629-642 (2010).

15. Zavadil, J. & Bottinger, E.P. TGF-beta and epithelial-to-mesenchymal transitions. *Oncogene* **24**, 5764-5774 (2005).

16. Savagner, P., Yamada, K.M. & Thiery, J.P. The zinc-finger protein slug causes desmosome dissociation, an initial and necessary step for growth factor-induced epithelial-mesenchymal transition. *J Cell Biol* **137**, 1403-1419 (1997).

17. Graham, T.R.*, et al.* Insulin-like growth factor-I-dependent up-regulation of ZEB1 drives epithelial-to-mesenchymal transition in human prostate cancer cells. *Cancer Res* **68**, 2479-2488 (2008).

18. Gupta, G.P. & Massague, J. Cancer metastasis: building a framework. *Cell* **127**, 679-695 (2006).

19. Rous, P. A Sarcoma of the Fowl Transmissible by an Agent Separable from the Tumor Cells. *J Exp Med* **13**, 397-411 (1911).

20. Martin, G.S. The hunting of the Src. *Nat Rev Mol Cell Biol* **2**, 467-475 (2001).

21. Fero, M.L.*, et al.* A syndrome of multiorgan hyperplasia with features of gigantism, tumorigenesis, and female sterility in p27(Kip1)-deficient mice. *Cell* **85**, 733-744 (1996).

22. Fero, M.L., Randel, E., Gurley, K.E., Roberts, J.M. & Kemp, C.J. The murine gene p27Kip1 is haplo-insufficient for tumour suppression. *Nature* **396**, 177-180 (1998).

23. Payne, S.R. & Kemp, C.J. Tumor suppressor genetics. *Carcinogenesis* **26**, 2031-2045 (2005).

24. Lee, S.B. & Haber, D.A. Wilms tumor and the WT1 gene. *Exp Cell Res* **264**, 74-99 (2001).

25. Muller, P.A., Vousden, K.H. & Norman, J.C. p53 and its mutants in tumor cell migration and invasion. *J Cell Biol* **192**, 209-218 (2011).

26. Viadiu, H. Molecular architecture of tumor suppressor p53. *Curr Top Med Chem* **8**, 1327-1334 (2008).

27. Goh, A.M., Coffill, C.R. & Lane, D.P. The role of mutant p53 in human cancer. *J Pathol* **223**, 116-126 (2011).

28. Hollstein, M., Sidransky, D., Vogelstein, B. & Harris, C.C. p53 mutations in human cancers. *Science* **253**, 49-53 (1991).

29. Morton, J.P.*, et al.* Mutant p53 drives metastasis and overcomes growth arrest/senescence in pancreatic cancer. *Proc Natl Acad Sci U S A* **107**, 246-251 (2010).

30. Dittmer, D.*, et al.* Gain of function mutations in p53. *Nat Genet* **4**, 42-46 (1993).

31. Anglesio, M.S.*, et al.* Differential expression of a novel ankyrin containing E3 ubiquitin-protein ligase, Hace1, in sporadic Wilms' tumor versus normal kidney. *Hum Mol Genet* **13**, 2061-2074 (2004).

32. Pardee, A.B. G1 events and regulation of cell proliferation. *Science* **246**, 603-608 (1989).

33. Alberts B, J.A., Lewis J, Raff M, Roberts K and Walter P. *Molecular Biology of the Cell*, (Garland Science, New York, NY, 2002).

34. Evans, T., Rosenthal, E.T., Youngblom, J., Distel, D. & Hunt, T. Cyclin: a protein specified by maternal mRNA in sea urchin eggs that is destroyed at each cleavage division. *Cell* **33**, 389-396 (1983).

35. Harper, J.V. & Brooks, G. The mammalian cell cycle: an overview. *Methods Mol Biol* **296**, 113-153 (2005).

36. Wu, C.L., Zukerberg, L.R., Ngwu, C., Harlow, E. & Lees, J.A. In vivo association of E2F and DP family proteins. *Mol Cell Biol* **15**, 2536-2546 (1995).

37. Hoffmann, I., Draetta, G. & Karsenti, E. Activation of the phosphatase activity of human cdc25A by a cdk2-cyclin E dependent phosphorylation at the G1/S transition. *EMBO J* **13**, 4302-4310 (1994).

38. Neganova, I. & Lako, M. G1 to S phase cell cycle transition in somatic and embryonic stem cells. *J Anat* **213**, 30-44 (2008).

39. Lavoie, J.N., L'Allemain, G., Brunet, A., Muller, R. & Pouyssegur, J. Cyclin D1 expression is regulated positively by the p42/p44MAPK and negatively by the p38/HOGMAPK pathway. *J Biol Chem* **271**, 20608-20616 (1996).

40. Lundgren, K.*, et al.* mik1 and wee1 cooperate in the inhibitory tyrosine phosphorylation of cdc2. *Cell* **64**, 1111-1122 (1991).

41. Parker, L.L. & Piwnica-Worms, H. Inactivation of the p34cdc2-cyclin B complex by the human WEE1 tyrosine kinase. *Science* **257**, 1955-1957 (1992).

42. Pavletich, N.P. Mechanisms of cyclin-dependent kinase regulation: structures of Cdks, their cyclin activators, and Cip and INK4 inhibitors. *J Mol Biol* **287**, 821-828 (1999).

43. Ewen, M.E. p53-dependent repression of cdk4 synthesis in transforming growth factor-beta-induced G1 cell cycle arrest. *J Lab Clin Med* **128**, 355-360 (1996).

44. Porter, P.L.*, et al.* Expression of cell-cycle regulators p27Kip1 and cyclin E, alone and in combination, correlate with survival in young breast cancer patients. *Nat Med* **3**, 222-225 (1997).

45. Kerr, J.F., Wyllie, A.H. & Currie, A.R. Apoptosis: a basic biological phenomenon with wide-ranging implications in tissue kinetics. *Br J Cancer* **26**, 239-257 (1972).

46. Martinet, W., Schrijvers, D.M. & De Meyer, G.R. Necrotic cell death in atherosclerosis. *Basic Res Cardiol* (2011).

47. Boatright, K.M. & Salvesen, G.S. Mechanisms of caspase activation. *Curr Opin Cell Biol* **15**, 725-731 (2003).

48. Green, D.R. Apoptotic pathways: ten minutes to dead. *Cell* **121**, 671-674 (2005).

49. Creagh, E.M. & Martin, S.J. Caspases: cellular demolition experts. *Biochem Soc Trans* **29**, 696-702 (2001).

50. Liu, J.J., Lin, M., Yu, J.Y., Liu, B. & Bao, J.K. Targeting apoptotic and autophagic pathways for cancer therapeutics. *Cancer Lett* **300**, 105-114 (2011).

51. Portt, L., Norman, G., Clapp, C., Greenwood, M. & Greenwood, M.T. Anti-apoptosis and cell survival: a review. *Biochim Biophys Acta* **1813**, 238-259 (2011).

52. Jurgensmeier, J.M.*, et al.* Bax directly induces release of cytochrome c from isolated mitochondria. *Proc Natl Acad Sci U S A* **95**, 4997-5002 (1998).

53. Luo, X., Budihardjo, I., Zou, H., Slaughter, C. & Wang, X. Bid, a Bcl2 interacting protein, mediates cytochrome c release from mitochondria in response to activation of cell surface death receptors. *Cell* **94**, 481-490 (1998).

54. Shore, G.C., Papa, F.R. & Oakes, S.A. Signaling cell death from the endoplasmic reticulum stress response. *Curr Opin Cell Biol* **23**, 143-149 (2011).

55. Marciniak, S.J.*, et al.* CHOP induces death by promoting protein synthesis and oxidation in the stressed endoplasmic reticulum. *Genes Dev* **18**, 3066-3077 (2004).

56. Todd, D.J., Lee, A.H. & Glimcher, L.H. The endoplasmic reticulum stress response in immunity and autoimmunity. *Nat Rev Immunol* **8**, 663-674 (2008).

57. Adams, J.M. & Cory, S. The Bcl-2 apoptotic switch in cancer development and therapy. *Oncogene* **26**, 1324-1337 (2007).

58. Ramakrishna, S., Suresh, B. & Baek, K.H. The role of deubiquitinating enzymes in apoptosis. *Cell Mol Life Sci* **68**, 15-26 (2011).

59. van Wijk, S.J. & Timmers, H.T. The family of ubiquitin-conjugating enzymes (E2s): deciding between life and death of proteins. *FASEB J* **24**, 981-993 (2010).

60. Rotin, D. & Kumar, S. Physiological functions of the HECT family of ubiquitin ligases. *Nat Rev Mol Cell Biol* **10**, 398-409 (2009).

61. Scheffner, M. & Staub, O. HECT E3s and human disease. *BMC Biochem* **8 Suppl 1**, S6 (2007).

62. Huibregtse, J.M., Scheffner, M. & Howley, P.M. A cellular protein mediates association of p53 with the E6 oncoprotein of human papillomavirus types 16 or 18. *Embo J* **10**, 4129-4135 (1991).

63. Bernassola, F., Karin, M., Ciechanover, A. & Melino, G. The HECT family of E3 ubiquitin ligases: multiple players in cancer development. *Cancer Cell* **14**, 10-21 (2008).

64. Chen, D.*, et al.* ARF-BP1/Mule is a critical mediator of the ARF tumor suppressor. *Cell* **121**, 1071-1083 (2005).

65. Zhong, Q., Gao, W., Du, F. & Wang, X. Mule/ARF-BP1, a BH3-only E3 ubiquitin ligase, catalyzes the polyubiquitination of Mcl-1 and regulates apoptosis. *Cell* **121**, 1085-1095 (2005).

66. Fouladkou, F.*, et al.* The ubiquitin ligase Nedd4-1 is dispensable for the regulation of PTEN stability and localization. *Proc Natl Acad Sci U S A* **105**, 8585-8590 (2008).

67. Wang, X.*, et al.* NEDD4-1 is a proto-oncogenic ubiquitin ligase for PTEN. *Cell* **128**, 129-139 (2007).

68. Almond, J.B. & Cohen, G.M. The proteasome: a novel target for cancer chemotherapy. *Leukemia* **16**, 433-443 (2002).

69. Solis, V., Pritchard, J. & Cowell, J.K. Cytogenetic changes in Wilms' tumors. *Cancer Genet Cytogenet* **34**, 223-234 (1988).

70. Bernstein L, L.M., Smith M *et al.* Renal Tumors. National Cancer Institute SEER Program. (ed. Health, N.I.o.) (Bethesda, MD, 1999).

71. Davidoff, A.M. Wilms' tumor. *Curr Opin Pediatr* **21**, 357-364 (2009).

72. Sonn, G. & Shortliffe, L.M. Management of Wilms tumor: current standard of care. *Nat Clin Pract Urol* **5**, 551-560 (2008).

73. D'Angio, G.J.*, et al.* The treatment of Wilms' tumor: Results of the national Wilms' tumor study. *Cancer* **38**, 633-646 (1976).

74. D'Angio, G.J.*, et al.* The treatment of Wilms' tumor: results of the Second National Wilms' Tumor Study. *Cancer* **47**, 2302-2311 (1981).

75. D'Angio, G.J.*, et al.* Treatment of Wilms' tumor. Results of the Third National Wilms' Tumor Study. *Cancer* **64**, 349-360 (1989).

76. Green, D.M.*, et al.* Comparison between single-dose and divided-dose administration of dactinomycin and doxorubicin for patients with Wilms' tumor: a report from the National Wilms' Tumor Study Group. *J Clin Oncol* **16**, 237-245 (1998).

77. Shamberger, R.C.*, et al.* Surgery-related factors and local recurrence of Wilms tumor in National Wilms Tumor Study 4. *Ann Surg* **229**, 292-297 (1999).

78. Grundy, P.E.*, et al.* Loss of heterozygosity for chromosomes 1p and 16q is an adverse prognostic factor in favorable-histology Wilms tumor: a report from the National Wilms Tumor Study Group. *J Clin Oncol* **23**, 7312-7321 (2005).

79. Green, D.M.*, et al.* Treatment with nephrectomy only for small, stage I/favorable histology Wilms' tumor: a report from the National Wilms' Tumor Study Group. *J Clin Oncol* **19**, 3719-3724 (2001).

80. Huff, V. Wilms' tumours: about tumour suppressor genes, an oncogene and a chameleon gene. *Nat Rev Cancer* **11**, 111-121 (2011).

81. Brown, K.W. & Malik, K.T. The molecular biology of Wilms tumour. *Expert Rev Mol Med* **2001**, 1-16 (2001).

82. Coppes, M.J. & Pritchard-Jones, K. Principles of Wilms' tumor biology. *Urol Clin North Am* **27**, 423-433, viii (2000).

83. Dekel, B.*, et al.* Engraftment and differentiation of human metanephroi into functional mature nephrons after transplantation into mice is accompanied by a profile of gene expression similar to normal human kidney development. *J Am Soc Nephrol* **13**, 977-990 (2002).

84. Li, C.M.*, et al.* Gene expression in Wilms' tumor mimics the earliest committed stage in the metanephric mesenchymal-epithelial transition. *Am J Pathol* **160**, 2181-2190 (2002).

85. Pritchard-Jones, K.*, et al.* The candidate Wilms' tumour gene is involved in genitourinary development. *Nature* **346**, 194-197 (1990).

86. Huff, V. Wilms tumor genetics. *Am J Med Genet* **79**, 260-267 (1998).

87. Ruteshouser, E.C., Robinson, S.M. & Huff, V. Wilms tumor genetics: mutations in WT1, WTX, and CTNNB1 account for only about one-third of tumors. *Genes Chromosomes Cancer* **47**, 461-470 (2008).

88. Fernandez, C.V., Lestou, V.S., Wildish, J., Lee, C.L. & Sorensen, P.H. Detection of a novel t(6;15)(q21;q21) in a pediatric Wilms tumor. *Cancer Genet Cytogenet* **129**, 165-167 (2001).

89. Zhang, L.*, et al.* The E3 ligase HACE1 is a critical chromosome 6q21 tumor suppressor involved in multiple cancers. *Nat Med* **13**, 1060-1069 (2007).

90. Hibi, K.*, et al.* Aberrant methylation of the HACE1 gene is frequently detected in advanced colorectal cancer. *Anticancer Res* **28**, 1581-1584 (2008).

91. Thelander, E.F.*, et al.* Characterization of 6q deletions in mature B cell lymphomas and childhood acute lymphoblastic leukemia. *Leuk Lymphoma* **49**, 477-487 (2008).

92. Olivier, M., Hollstein, M. & Hainaut, P. TP53 mutations in human cancers: origins, consequences, and clinical use. *Cold Spring Harb Perspect Biol* **2**, a001008 (2010).

93. Langenau, D.M.*, et al.* Cre/lox-regulated transgenic zebrafish model with conditional myc-induced T cell acute lymphoblastic leukemia. *Proc Natl Acad Sci U S A* **102**, 6068-6073 (2005).

94. Langenau, D.M.*, et al.* Effects of RAS on the genesis of embryonal rhabdomyosarcoma. *Genes Dev* **21**, 1382-1395 (2007).

95. Langenau, D.M.*, et al.* Myc-induced T cell leukemia in transgenic zebrafish. *Science* **299**, 887-890 (2003).

96. Patton, E.E.*, et al.* BRAF mutations are sufficient to promote nevi formation and cooperate with p53 in the genesis of melanoma. *Curr Biol* **15**, 249-254 (2005).

97. Berman, J., Hsu, K. & Look, A.T. Zebrafish as a model organism for blood diseases. *Br J Haematol* **123**, 568-576 (2003).

98. Amatruda, J.F., Shepard, J.L., Stern, H.M. & Zon, L.I. Zebrafish as a cancer model system. *Cancer Cell* **1**, 229-231 (2002).

99. Liu, S. & Leach, S.D. Zebrafish models for cancer. *Annu Rev Pathol* **6**, 71-93 (2011).

100. Chakraborty, C., Hsu, C.H., Wen, Z.H., Lin, C.S. & Agoramoorthy, G. Zebrafish: a complete animal model for in vivo drug discovery and development. *Curr Drug Metab* **10**, 116-124 (2009).

101. Hong, C.C. Large-scale small-molecule screen using zebrafish embryos. *Methods Mol Biol* **486**, 43-55 (2009).

102. Murphey, R.D., Stern, H.M., Straub, C.T. & Zon, L.I. A chemical genetic screen for cell cycle inhibitors in zebrafish embryos. *Chem Biol Drug Des* **68**, 213-219 (2006).

103. Tucker, B. & Lardelli, M. A rapid apoptosis assay measuring relative acridine orange fluorescence in zebrafish embryos. *Zebrafish* **4**, 113-116 (2007).

104. van Ham, T.J., Mapes, J., Kokel, D. & Peterson, R.T. Live imaging of apoptotic cells in zebrafish. *FASEB J* **24**, 4336-4342 (2010).

105. Verduzco, D. & Amatruda, J.F. Analysis of cell proliferation, senescence, and cell death in zebrafish embryos. *Methods Cell Biol* **101**, 19-38 (2011).

106. Berghmans, S.*, et al.* tp53 mutant zebrafish develop malignant peripheral nerve sheath tumors. *Proc Natl Acad Sci U S A* **102**, 407-412 (2005).

107. Davies, H.*, et al.* Mutations of the BRAF gene in human cancer. *Nature* **417**, 949-954 (2002).

108. Dobson, J.T.*, et al.* Carboxypeptidase A5 identifies a novel mast cell lineage in the zebrafish providing new insight into mast cell fate determination. *Blood* **112**, 2969-2972 (2008).

109. Da'as, S.*, et al.* Zebrafish mast cells possess an FcεRI-like receptor and participate in innate and adaptive immune responses. *Dev Comp Immunol* **35**, 125-134 (2011).

110. Westerfield, M. *The Zebrafish Book*, (University of Oregon Press, Eugene, OR, 1995).

111. Horsfield, J.*, et al.* Cadherin-17 is required to maintain pronephric duct integrity during zebrafish development. *Mech Dev* **115**, 15-26 (2002).

112. Yelon, D., Horne, S.A. & Stainier, D.Y. Restricted expression of cardiac myosin genes reveals regulated aspects of heart tube assembly in zebrafish. *Dev Biol* **214**, 23-37 (1999).

113. Stull, J.T., Nunnally, M.H., Moore, R.L. & Blumenthal, D.K. Myosin light chain kinases and myosin phosphorylation in skeletal muscle. *Adv Enzyme Regul* **23**, 123-140 (1985).

114. Silver, P.J., Buja, L.M. & Stull, J.T. Frequency-dependent myosin light chain phosphorylation in isolated myocardium. *J Mol Cell Cardiol* **18**, 31-37 (1986).

115. Sander, J.D.*, et al.* Selection-free zinc-finger-nuclease engineering by context-dependent assembly (CoDA). *Nat Methods* **8**, 67-69 (2011).

116. Huang, C.J., Tu, C.T., Hsiao, C.D., Hsieh, F.J. & Tsai, H.J. Germ-line transmission of a myocardium-specific GFP transgene reveals critical regulatory elements in the cardiac myosin light chain 2 promoter of zebrafish. *Dev Dyn* **228**, 30-40 (2003).

117. Hu, N., Sedmera, D., Yost, H.J. & Clark, E.B. Structure and function of the developing zebrafish heart. *Anat Rec* **260**, 148-157 (2000).

118. Thompson, M.A.*, et al.* The cloche and spadetail genes differentially affect hematopoiesis and vasculogenesis. *Dev Biol* **197**, 248-269 (1998).

119. Lawson, N.D. & Weinstein, B.M. In vivo imaging of embryonic vascular development using transgenic zebrafish. *Dev Biol* **248**, 307-318 (2002).

120. Folger, K.R., Wong, E.A., Wahl, G. & Capecchi, M.R. Patterns of integration of DNA microinjected into cultured mammalian cells: evidence for homologous recombination between injected plasmid DNA molecules. *Mol Cell Biol* **2**, 1372-1387 (1982).

121. Mansour, S.L., Thomas, K.R. & Capecchi, M.R. Disruption of the proto-oncogene int-2 in mouse embryo-derived stem cells: a general strategy for targeting mutations to non-selectable genes. *Nature* **336**, 348-352 (1988).

122. Meng, X., Noyes, M.B., Zhu, L.J., Lawson, N.D. & Wolfe, S.A. Targeted gene inactivation in zebrafish using engineered zinc-finger nucleases. *Nat Biotechnol* **26**, 695-701 (2008).

123. Higashijima, S., Okamoto, H., Ueno, N., Hotta, Y. & Eguchi, G. High-frequency generation of transgenic zebrafish which reliably express GFP in whole muscles or the whole body by using promoters of zebrafish origin. *Dev Biol* **192**, 289-299 (1997).

124. Sasaki, Y.*, et al.* Evidence for high specificity and efficiency of multiple recombination signals in mixed DNA cloning by the Multisite Gateway system. *J Biotechnol* **107**, 233-243 (2004).

125. Abrams, J.M., White, K., Fessler, L.I. & Steller, H. Programmed cell death during Drosophila embryogenesis. *Development* **117**, 29-43 (1993).

126. Durrieu, F.*, et al.* Synthesis of Bcl-2 in response to anthracycline treatment may contribute to an apoptosis-resistant phenotype in leukemic cell lines. *Cytometry* **36**, 140-149 (1999).

127. Eimon, P.M.*, et al.* Delineation of the cell-extrinsic apoptosis pathway in the zebrafish. *Cell Death Differ* **13**, 1619-1630 (2006).

128. Meyn, R.E., Hewitt, R.R. & Humphrey, R.M. Evaluation of S phase synchronization by analysis of DNA replication in 5-bromodeoxyuridine. *Exp Cell Res* **82**, 137-142 (1973).

129. Shepard, J.L., Stern, H.M., Pfaff, K.L. & Amatruda, J.F. Analysis of the cell cycle in zebrafish embryos. *Methods Cell Biol* **76**, 109-125 (2004).

130. Hendzel, M.J.*, et al.* Mitosis-specific phosphorylation of histone H3 initiates primarily within pericentromeric heterochromatin during G2 and spreads in an ordered fashion coincident with mitotic chromosome condensation. *Chromosoma* **106**, 348-360 (1997).

131. Zhang, C.*, et al.* Defining the regulatory network of the tissue-specific splicing factors Fox-1 and Fox-2. *Genes Dev* **22**, 2550-2563 (2008).

132. Underwood, J.G., Boutz, P.L., Dougherty, J.D., Stoilov, P. & Black, D.L. Homologues of the Caenorhabditis elegans Fox-1 protein are neuronal splicing regulators in mammals. *Mol Cell Biol* **25**, 10005-10016 (2005).

133. Friedberg, F. & Rhoads, A.R. Evolutionary aspects of calmodulin. *IUBMB Life* **51**, 215-221 (2001).

134. Streisinger, G., Walker, C., Dower, N., Knauber, D. & Singer, F. Production of clones of homozygous diploid zebra fish (Brachydanio rerio). *Nature* **291**, 293-296 (1981).

135. Breeden, L. & Nasmyth, K. Similarity between cell-cycle genes of budding yeast and fission yeast and the Notch gene of Drosophila. *Nature* **329**, 651-654 (1987).

136. Mosavi, L.K., Cammett, T.J., Desrosiers, D.C. & Peng, Z.Y. The ankyrin repeat as molecular architecture for protein recognition. *Protein Sci* **13**, 1435-1448 (2004).

137. Sun, Z., Shi, K., Su, Y. & Meng, A. A novel zinc finger transcription factor resembles krox-20 in structure and in expression pattern in zebrafish. *Mech Dev* **114**, 133-135 (2002).

138. Komoike, Y.*, et al.* Zebrafish gene knockdowns imply roles for human YWHAG in infantile spasms and cardiomegaly. *Genesis* **48**, 233-243 (2010).

139. Summerton, J.E. Morpholino, siRNA, and S-DNA compared: impact of structure and mechanism of action on off-target effects and sequence specificity. *Curr Top Med Chem* **7**, 651-660 (2007).

140. Francois, M., Koopman, P. & Beltrame, M. SoxF genes: Key players in the development of the cardio-vascular system. *Int J Biochem Cell Biol* **42**, 445-448 (2010).

141. Fouquet, B., Weinstein, B.M., Serluca, F.C. & Fishman, M.C. Vessel patterning in the embryo of the zebrafish: guidance by notochord. *Dev Biol* **183**, 37-48 (1997).

142. Nissen, L.J.*, et al.* Angiogenic factors FGF2 and PDGF-BB synergistically promote murine tumor neovascularization and metastasis. *J Clin Invest* **117**, 2766-2777 (2007).

143. Reck, M. Examining the safety profile of angiogenesis inhibitors: implications for clinical practice. *Target Oncol* **5**, 257-267 (2010).

144. Kimura, S.H., Ikawa, M., Ito, A., Okabe, M. & Nojima, H. Cyclin G1 is involved in G2/M arrest in response to DNA damage and in growth control after damage recovery. *Oncogene* **20**, 3290-3300 (2001).

145. Wegner, M. Secrets to a healthy Sox life: lessons for melanocytes. *Pigment Cell Res* **18**, 74-85 (2005).

146. Schneider, J.E.*, et al.* Cardiac structure and function during ageing in energetically compromised Guanidinoacetate N-methyltransferase (GAMT)-knockout mice - a one year longitudinal MRI study. *J Cardiovasc Magn Reson* **10**, 9 (2008).

147. Ensenauer, R., *et al.* Guanidinoacetate methyltransferase deficiency: differences of creatine uptake in human brain and muscle. *Mol Genet Metab* **82**, 208-213 (2004).

148. Van Tine, B.A., *et al.* Localization of HuC (ELAVL3) to chromosome 19p13.2 by fluorescence in situ hybridization utilizing a novel tyramide labeling technique. *Genomics* **53**, 296-299 (1998).